MIXING OF JET IN A STREAM

By

RIMA DEVI

APPLIED MECHANICS DEPARTMENT

Submitted

in fulfilment of the requirement of the degree of
Doctor of Philosophy

to the

Indian Institute of Technology, Delhi.

October, 1976

M.E

CERTIFICATE

This is to certify that the thesis entitled, 'Mixing of Jet in a Stream', which is being submitted by Mrs. Reena Devi to the Indian Institute of Technology, Delhi for the award of the degree of Doctor of Philosophy, is a bonafide research work carried out by her under my guidance.

The results contained in this thesis have not been submitted, in part or full, to any other university or institution for the award of any degree or diploma.

(M.C. Chaturvedi)
Professor
Applied Mechanics Department
Indian Institute of Technology
New Delhi-110029.

ACKNOWLEDGEMENT

The author is extremely grateful to Dr. M.C. Chaturvedi, Professor, Applied Mechanics Department, Indian Institute of Technology, Delhi for suggesting this interesting field of research. His continued guidance, help and encouragement at every stage has enabled this investigation to acquire its present form.

Rema devi
(Mrs. Rema Devi)

ME

ABSTRACT

Jet and stream combinations are used and can further be used for a variety of practical applications. The wall jet, defined as a jet the spread on one side of which is inhibited due to the presence of a boundary, has been investigated in this context by a large number of research workers. Yet, in almost all cases the wall jets investigated had zero degree inclination. Oblique wall jets, which can have several practical applications have not been investigated.

A weak oblique wall jet in a uniform stream is investigated experimentally in the present work for five ratios of jet to stream velocity and two angles of inclination, one normal and one partly opposing the main flow. The issues of interest are, (i) the development of flow characteristics along space, (ii) the applicability of a few models of turbulence and (iii) the possible use of such a flow combination as an energy dissipation arrangement. The study with the large number of velocity ratios investigated is expected to help in the formulation of a working model of turbulence for real life application.

TABLE OF CONTENTS

List of Figures

...

LIST NOTATIONS

A	Calibration constant for hot wire
B	Calibration constant for hot wire; Also, a function of η in diffusion term, as given by Bradshaw
a	Bradshaw parameter - $\overline{u'v'}/q^2$; also exponent in velocity scale where specifically mentioned
b	Slot width, also exponent in length scale where specifically mentioned
c	Exponent in hot wire equation
c_1, c_2, c_3	Constants
c_μ	Constant in Prandtl-Kolmogorov mixing length
$c_f/2$	Skin friction coefficient
d	Depth of tunnel
H	Shape factor, $\frac{\delta^*}{\theta}$
i,j	Usual tensor notation
K	Proportionality constant of instantaneous spatial gradients of instantaneous fluctuations
k	Constant in hot wire calibration
l_1	Prandtl mixing length
l_2	Prandtl-Kolmogorov mixing length
p_a	Atmospheric pressure
p_b	Static pressure at base

p_0	Static pressure
p'	Instantaneous pressure fluctuation
$q^2/2$	Mean turbulent energy
A	Surface
S_w	Shear work integral
u, v, w	Instantaneous velocities in x,y,z direction (Chapter 3 and Appendix) mean velocity in other Chapters and graphs
$\bar{u},\bar{v},\bar{w}$	Mean velocity components in x,y,z direction
u',v',w'	Instantaneous fluctuations in x,y,z direction
$-\rho\overline{u'v'}$	Turbulent shear stress
V_0	Net mean velocity
v'^2	Net turbulent x velocity
V_1	Mean voltage anemometer
x_r	Reattachment distance
u_+	A non-dimensional velocity u/u_τ
u_τ	Shear velocity $\sqrt{(\tau_0/\rho)}$
y_+	$\frac{u_\tau y}{\nu}$
u_j	Jet velocity
u_s	Stream velocity
u_m	Maximum or maximum excess velocity
ΔU_m	Half maximum or half maximum excess velocity

δ, y_g	Boundary layer thickness
δ_1	Distance from wall to point of maximum velocity
δ_2	Distance from wall to point of half maximum velocity in the outer layer
θ	Momentum thickness
δ^*	Displacement thickness
ρ	Density of air
ν	Kinematic viscosity of air
μ	Molecular viscosity of air
μ_{eff}	Effective viscosity
ϵ	Dissipation
η	Ratio of y to δ_2
τ_o	Wall shear
ϕ_c, ϕ_D	Inclination of hot wire

CHAPTER-I

INTRODUCTION

The combination flow of a jet and a stream find a wide number of applications in the field of fluid mechanics. For instance, one of the most common methods of boundary layer control is by blowing high velocity fluid into it. The jet in such a case is inclined to the main flow and is not generally off set from the stream boundary. A practical example of such a combination of inclined jet and stream flow is the jet flap. In some other fluidic devices, the jet may be parallel to the flow itself. At times, the flow situation which exists may be of a jet and stream combination type. The exhaust jet from a vertical take-off air craft may be cited as an example. All these jets have one point in common — the spread on one side is inhibited by the presence of a solid boundary.

Compared to the extent to which the flow combination has already been used, the structure of flow properties of the combination is not adequately known. While going through the literature on wall jets - that is, jets the spread on one side of which is inhibited by the presence of a solid boundary - one point stands out clearly. Almost all the cases investigated are for zero degree wall jets. It

may be said that a zero degree wall jet has been almost thoroughly investigated. The effect of pressure gradient, laminar and turbulent jet, radial and plane jet have all been investigated for jet to stream velocity ratios greater than two. Flow with a large ratio of jet to stream velocity can be, to some extent, theoretically analyzed because of self-similarity of velocity profiles. Yet, the word almost is used in this context, because a ratio of jet to stream velocity of less than unity has been investigated by only one set of investigators - Maher and Whitelaw (18,19). A number of applications of flow combination fall in this category. For example, in blowing through slots on jet flaps, the ratio of jet to stream velocity is nearly one. Such wall jet or rather wall wake flows need more investigations.

Somehow, the real analysis of an oblique wall jet for any ratio of jet to stream velocity has not beentaken up for study except for the length of separation bubble. One factor which perhaps stood in the way of investigations is the separation bubble itself, which makes a mathematical analysis almost impossible. The oblique wall jet mainly differs from a zero degree wall jet because of the comparatively large size of separation bubble. The effect of this separation bubble cannot be neglected as in the case of thin

lipped zero degree wall jet. Also, the turbulence is non-homogeneous and anisotropic and being of a localised nature similarity in turbulence scale cannot be assumed. The edge of the standing eddy serves as a production mill for turbulence. A thick lipped zero degree wall jet for ratios of jet to stream velocity less than unity by Kacker and Whitelaw (18,19) is the only work which is of a remotely similar type.

Since the oblique wall jet (wake) type of flow is of practical importance, a knowledge of the development of flow properties is called for. For example, in some applications the requirement of the flow combination may have to be achieved with minimum energy dissipation where as in some case the objective may be dissipation of energy itself. Since such extreme demands may be made on the flow, unless an idea of the flow development in all its aspects is obtained, the design of the combination flow is of a hit and trial type.

With a large volume of research available on turbulence characteristics of different types of flow, mathematical turbulence models are available for many types of flow. These models are based on experimental verifications of similar types of flow by many authors and once perfected

for a particular type of flow are very useful in predicting the flow characteristics of any similar flow. These are not exact solutions but are working models which, being computer oriented, give solutions in a short time in a more economical way, within acceptable limits of accuracy for practical designs. Such working models of turbulence are of particular relevance to cases where an exact or even an approximate theoretical analysis is not possible. To form such a model a large volume of experimental data is required. As research is done on any problem the existing turbulence models can be tested with the help of measured data to ascertain whether any of the models are applicable to the particular case in part or full.

The present work on oblique wall jets in a stream was undertaken keeping the above issues in view. The objective of the present work could thus stated to be (i) an experimental verification of the flow (since a theoretical analysis is not possible), (ii) to check with the help of measured data how far the existing models of turbulence are applicable and, (iii) as a practical case of application whether the flow combination can be used as an energy dissipation device.

The angles of injection were chosen to be; (i) normal to the flow and, (ii) opposing the flow from considerations of energy dissipation. Five different jet to stream velocity ratios were considered so as to form a base work for formulating a turbulence model. The formulation part itself being a hard task, is not done in the present work. Only a checking of the applicability of some existing models of turbulence is done at present. The velocity ratios are taken on either side of unity as in the practical application envisaged for energy dissipation the jet is to be obtained from the stream itself. The practical application, envisaged is the energy dissipation at the foot of the spill way. Another practical application anticipated is that of aeration for environmental management.

Considering the high levels of turbulence reached, an accurate quantitative determination of mean velocity and static pressure itself is difficult. Hence the accuracy of the measured quantities are first verified through balancing of mass, momentum and mean energy for the flow. Once the accuracy is thus established the data is used for the evaluation of turbulent energy equation of which some terms are negligible, while others are measurable in some form. Only the diffusion term remains not measurable. The diffusion term is evaluated from turbulent energy equation as

the balancing quantity. This method is reliable only if other terms, particularly dissipation term are evaluated accurately. All terms except dissipation term are checked by means of momentum and mean energy equation.

X The results obtained are expressed non-dimensionally. Also the results have been arranged graphically to give at a glance the stationwise development of the flow properties as functions of velocity ratios. Although analytical techniques cannot be applied, the field development is tried to be interpreted in terms of basic factors.

...

CHAPTER 2

LITERATURE SURVEY

The present study can be classified under wall jets since after the reattachment zone one side of the jet remains in contact with the base. A wall jet has the spread on one side inhibited by the presence of a solid boundary. The separation zone of an oblique wall jet is much larger than that of a thick lipped 0° wall jet, yet the separation bubble is small compared to the flow field. Hence, the literature survey on an oblique jet should start with the zero degree wall jet and must essentially contain the large volume of work on the zero degree wall jet. The literature survey is not exhaustive but attempts to review [illegible] of the important contributions.

The term wall jet was first used by Glauert (12) who defined it as a jet which strikes a surface at angles between 0° and 90° and spreads over it. Wall jets can be radial as in the case of a downward directed jet of a vertical take-off aircraft spreading over the ground or plane as in the case of two sections of a canal separated by a slightly raised slope. Other examples of wall jets are, a jet of water falling into

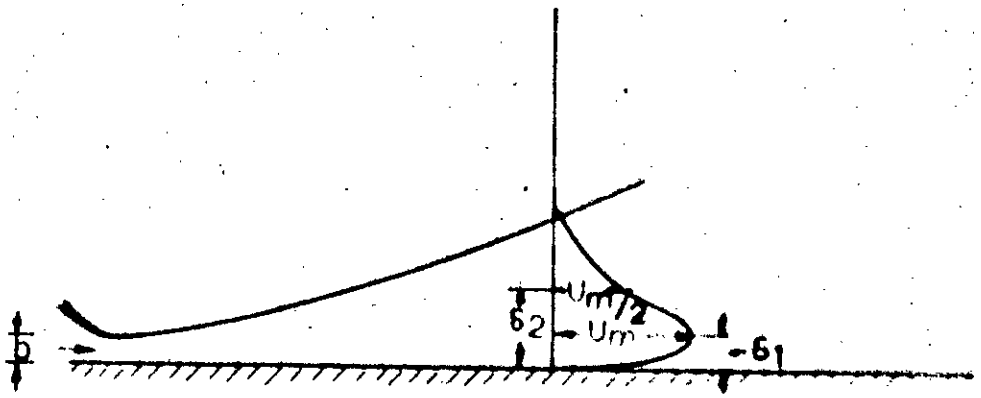

(a) ZERO DEGREE WALL JET IN STILL AIR

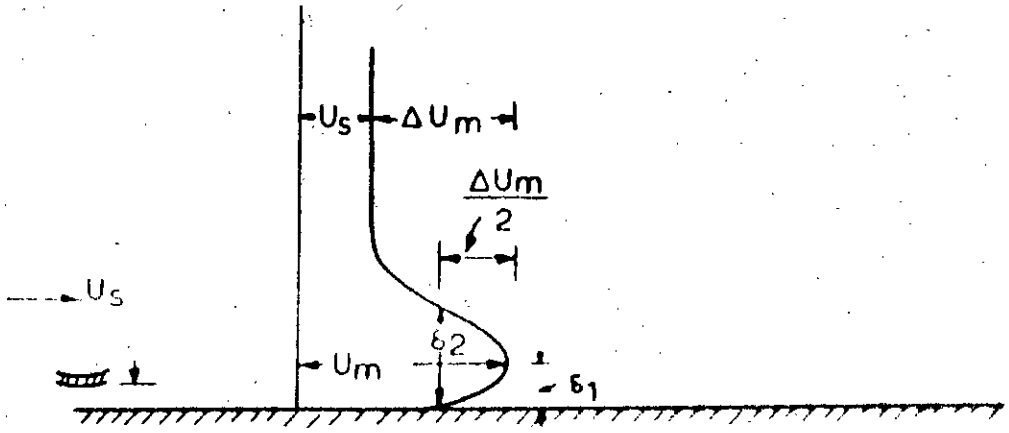

(b) ZERO DEGREE WALL JET IN A UNIFORM STREAM

FIG. 2.1: DEFINITION SKETCH

a partially filled sink and spreading over the bottom; jets of air issuing through slots (radial and plane) in aeroplane wings; a plane jet impinging over a flat plate kept parallel to the flow resulting in two wall jets one on each side of the plate.

Wall jets of zero degree inclination have been studied extensively under diverse conditions by a large number of research workers. Examples of some conditions are, zero pressure gradients and adverse pressure gradients; for large and small ratios of jet to stream velocities; laminar and turbulent flows; and radial and plane sections.

The general approach of analysis of a wall jet can be classified into following groups. One, where the flow is treated in a semi empirical form with self preservation assumed and the constants involved are determined by experiments. Second, where the flow is treated as an ideal fluid flow. The largest number of investigations on wall jets belong to the first group while most of the oblique jet studies are in the latter group. In both cases, the zone of separation is neglected. Some studies of a reattaching flow are however available, wherein the field of investigation is limited to the reattaching zone case only. A still another approach now available is the turbulence scale models, which are evolved from the large number of experi-

mental studies available.

The earliest available work on plane wall jets is by Forthmann (10). This was part of a general investigation of turbulent mixing of free and confined jets. The jet studied issue into still air. A characteristic Reynolds number for the flow was defined on the maximum velocity in the jet and the distance from the wall to the point of half maximum velocity in the free zone, δ_2 as shown in Fig. (2.1). The investigations were done in the range of Reynolds number 91,000 to 1,13,000 and between 20 to 33 slot widths downstream. The conclusions arrived at were (i) the wall jet is self-preserving in nature, (ii) the boundary layer thickness varied linearly with x, where x is the distance downstream from jet exit, (iii) U_m, the maximum velocity, varied inversely as the half-power of x, (iv) the velocity in the inner layer varied as the one seventh power of distance from the wall, (v) the virtual origin of the flow was downstream of the slot, (vii) the angle of jet spread was approximately 4.7^0 and (viii) the similarity profile is $u/U_m = x^a f(y/x^b)$ where u is the velocity at y, x and y are longitudinal and transverse distance from origin, and a and b are constants depending on the type of flow.

A detailed theoretical analysis of the wall jet,

laminar and turbulent, radial and plane, was carried out by Glauert (12). The basic assumption made was that since the wall jet comprised of a boundary layer flow near the wall and a free mixing flow, there could not be a unique solution for the flow as a whole. Accordingly, he divided the flow into two regions, an inner layer near the wall, where the eddy viscosity distribution was consistent with the Blasius power law velocity profile and a constant eddy viscosity in the outer region. Complete similarity of the flow at all distances from the origin was found impossible as the eddy viscosities in the inner and outer parts of the flow varied differently with y. That is, if the maximum velocity u_m and jet width δ_2 are expressed as functions of x, it was found that the exponents themselves were functions of x, although the variation is so slow as to be undetectable experimentally. The ratio of the eddy viscosities in the inner and outer parts of the flow varies only as the fourth root of slowly changing Reynolds number. Solutions were obtained for each region and were matched at the point of maximum velocity. His assumption of constant eddy viscosity implies zero shear stress at the velocity maximum.

An experimental investigation of Glauert's theoretical analysis was carried out by Bakke (1) for a round turbu-

lent wall jet. Sigalla (30) studied a tangential plane wall jet and correlated the existing data on wall jets. The distance investigated down stream was 150 nozzle widths. About 15 to 20 nozzle widths downstream of the jet exit, the wall jet was found unaffected by the local discharge conditions. In the developed part of the wall jet, the maximum velocity could be expressed as $u_m / u_j = 3.45\ (b/x)^{\frac{1}{2}}$ where u_j is the jet exit velocity and b is the nozzle width. The corresponding expression given by Zerbe and Selna (33) is $2.0\ (b/x)^{\frac{1}{2}}$. The half maximum velocity point δ_2 was found to lie on a plane inclined at 3.7° to the wall and passing through the centre of the jet axis. δ_1, the distance from the wall to the point of maximum velocity, was deduced as $\delta_1 = 0.182\ x/(u_m\ x/\nu)^{1/8}$ from skin friction measurements (valid between $x/b = 25$ and Reynolds numbers between 2.4×10^4 and 5.2×10^4). For x/b greater than 30, the velocity profile was found to be similar and of the form given by Forthmann.

Glauert's (12) deduction that similarity does not exist over the entire section, but the inner and outer velocity profiles are respectively similar was also substantiated by Sigalla's experiments (30). For a hot wall jet where the wall temperature, is maintained near the ambient temperature, the decay of maximum temperature was

found to be a function x/b and θ where θ is a non-dimensional function of the maximum temperature T_1 at any section, jet exit temperature T_j and ambient temperature T_o. This function is similar to that of decay of velocity maximum. Zerbe and Selna's data (33) gave $\theta = 2.93(b/x)^{\frac{1}{2}}$, whereas Jacob et al (17) give $\theta = 3.30(b/x)^{\frac{1}{2}}$. The difference between the two is attributed to different nozzle discharge conditions.

For $x/b > 30$, the skin friction coefficient C_f is represented by $C_f = 0.0865\ (u_m\ x/\nu)^{-0.2}$ and when x/b is less than 5, $C_f = 0.592\ (u_m\ x/\nu)^{-0.2}$. It was found easier to express C_f in terms x rather than δ_1, since δ_1 itself is difficult to determine accurately.

The Reynold's number range of 10^4 to 4×10^4 for a wall jet was investigated by Schwarz and Cosart (29). Measurements were taken upto 70 slots widths. The main conclusions were as follows. The velocity profiles in the inner layer varied as $1/4 \pm 1$ power of the distance from the wall rather than $1/7$ given by Forthmann, Glauert etc. The virtual origin was found to depend on individual systems. The length scale varied as x^b and the velocity scale as x^a where $b = 1$ and $a = -0.555$ assuming that mean velocity and turbulent fluctuating quantities were self

preserving with the same scale. The viscous stresses are negligible and hence turbulent boundary layer approximations are applicable. Near the velocity maximum in the outer layer the velocity profile is considerably different from that of a free jet due to the effect of the inner layer.

The works mentioned so far were of wall jets issuing into still air. A more practical situation would be a wall jet issuing into a stream moving in the same direction, as in the case of aerodynamic flaps etc. Eskinasi and Kruka (9) studied wall jets discharging into a uniform stream. The jet to stream velocity ratios were 2.06, 3.65 and 18.4. Both the jet and stream velocities were adjustable. In addition to mean velocity, static pressure, and skin friction, turbulent shear stresses were also measured for a much larger range of distance, namely 3 to 400 slot widths. It was found that the outer layer shows similarity in velocity profile whereas the inner layer does not. Hence the inner and the outer layers were treated separately and a better agreement of similarity in velocity profile was achieved. Similarly it was seen that the jet opening angle is 4.2° for the entire flow, 0.57° for the inner flow and 3.18° for the outer part. This indicates a rapid jet like diffusion in the outer layers and boundary layer flow

results only for down stream. A characteristic width δ_2, was derived of the form $\delta_2 = C_1 x_s^b$ by Schwarz and Cosart (29), where x_s is the distance travelled by the jet relative to the stream and b = 1, C_1 is a dimensional proportionality constant and δ_2 is the distance from the wall to the point of half maximum excess velocity. The value of C_1 obtained was -.0737 as against 0.0678 of Schwarz and Cosart (29). The value of b = 1 agreed with Schwarz and Cosart's and Förthmann's (10) evaluation. The excess maximum velocity, Δu_m is given by $C_2 x_s^a$ where a is found to depend on u_j / u_s and for large ratios of jet to stream velocity approaches the value obtained by Förthmann for stream velocity, $u_s = 0$; a was obtained as a function of Reynolds number based on Δu_m, b and x_s and C_1, 'a' = [(ln R - ln C_3 / ln x_s] - b where $C_3 = C_1 C_2 / \nu$ and $R = \Delta u_m \delta_2 / \nu$ and other terms are as already defined. Eskinasi and Kruka (9) were the first group of investigators who measured shear stress in the combined flow with the help of hot wire anemometer. The wall shear stress were measured with a pre-calibrated Pitot tube.

The assumption of similarity for shear stress by Schwarz and Cosart (29) $\overline{u'v'} = u_m^2 g(y/\delta_2)$ was found not substantiated, but τ/τ_{max} could be expressed as $f(y/\delta_2)$

and agreed with Forthmann's computed values. The applicability of Blasius assumption of skin friction coefficient being proportional to $R^{1/4}$ was verified and found valid if the Reynold's number is based on the maximum values of boundary layer. But the proportionality constant was found to vary from experiment to experiment.

The ratio of jet to stream velocity was much greater than one in all previous studies. Eriksen and Whitelaw[18] carried out detailed measurements of the mean and fluctuating properties of a two-dimensional constant property, plane turbulent wall jet in a moving stream. The quantities involve $\overline{u'^2}, \overline{v'^2}, \overline{w'^2}, \overline{u'v'}$ mean velocity, total and static pressure. The assumption of zero pressure gradient was found invalid for distance less than 100 slot hights though the error in assuming so is negligible after 20 slot heights. The momentum defect caused by a finite lip thickness was traceable to a considerable distance. The shapes of the velocity profiles at 150 slot heights were considerably different for jet and wake like flows. A logarithmic region existed for the wall jet especially for x/b in excess of 50. The wake flows tended to exhibit a logarithmic region close to the jet exit. For the jet to stream velocity ratio of 1.33 the momentum thickness Reynold's number passed through zero. For the

lower values of velocity ratio, the shape factor tended to 1.35, the usual value for a plate boundary layer.

For a wake like flow, the kinetic energy initially decreased with x and far down stream began to increase, where it resembled that of a flat plate boundary layer. The jet like flow also showed a decrease initially but from 50 to 150 slot heights the total kinetic energy remained almost constant.

Turbulence length scale obtained through correlation measurements showed that in the plane of the slot the scale of turbulence in the free stream was greater than that in the slot. By eighty slot heights, the turbulence scale attained a constant value of 0.15 y_g for wake like flows, where y_g is the distance from the wall to the point where the velocity is 99 percent of free stream velocity.

The turbulent shear stress profiles passed through zero for all values of x/b in the case of jet like flows and for low values of x/b for wake like flows. The zero shear stress and zero velocity gradient points did not coincide and the zero shear stress point is nearer to the boundary. For wake like flows the shear stress profile is similar to that of a flat plate boundary layer in zero pressure gradient.

The suggestion by Phillips (24) that at the edge of a turbulent flow $\overline{u'^2}$ is proportional to $(y-y_o)^4$ was found satisfied except that the constant of proportionality varied with the particular flow configuration. Here y_o is the apparent origin of irrotational fluctuations.

While the turbulence models were not tested directly, since they are not directly suitable to cases with velocity maxima, some aspects of the models are compared with the experimental results. Thus Bradshaw's parameter a, which is $-\overline{u'v'}/q^2$ was verified and was found to be not a constant for small values of x/b. The values are negative when velocity maximum is present against 0.15 adopted by Bradshaw (5).

The mixing length profiles did not show any similarity. Starting with a measured velocity profile at x/b of 20 the Patankar - Spalding procedure (22) predicted velocity profiles which were in agreement with the measured profiles except that of u_j/u_s of 0.58.

The point of minimum kinetic energy and point of zero shear stress coincided. On the whole it is seen that a wake like flow behaves like a flat plate boundary layer, in zero pressure gradient downstream of 150 slot heights.

A second paper by the same authors, Maher and Whitelaw (19) compares the effect of lip thickness on the flow. A zero degree necessarilly involves a nozzle projecting into one side of the stream. The nozzle body would produce a wake, the size of the wake depending on the size of the nozzle. Moreover except in their own earlier work, all the wall jet and stream combinations had a very high jet velocity, two to eighteen times that of the stream. Hence this paper alongwith the earlier paper opens fresh areas of investigation of a wall jet. The measurements are much more in detail, and most of the measureable turbulent quantities were measured. The velocity ratios were 0.75, 0.91, 1.33 and 2.3 and thickness ratios t/b were 0.126 and 1.14. The range of down stream distance investigated was between zero and 150 slot heights. Measurements of $\overline{u'^2}$, $\overline{v'^2}$, $\overline{w'^2}$, $\overline{u'v'}$ and turbulent energy spectra were made.

Their deductions could be summarised as follows. The static pressure in the stream was not uniform along the flow. In the region down stream of the slot the static pressure rose considerably. This rise was particularly significant for the large value of lip thickness. For smaller values of u_j/u_s and high values of t/b the high pressure region was more significant which suggests

a tendency to form a region of separated flow. The boundary layer equations are applicable only after 90 slot heights downstream. For small values of t/b the equations are satisfactory for x/b greater than 20. The large wake caused by a thick lip which is very obvious at x/b of zero became less obvious by x/b of 10. Thus the effect of thick lip was to cause the velocity minimum to be located at large values of y/y_s where y_s is the distance upto the point where u is 99 percent of freestream velocity u_s. The thick lip resulted in a more rapid initial decay of velocity maximum than the thin lip. That is, the larger region of separated flow and the larger momentum defect behind the slot lip caused a substantially increased mixing scale. Even at $x/b = 150$ the velocity maximum existed for both the lips, for higher ratio of velocity of u_j/u_s of 2.3. For $x/b > 20$, a logarithmic velocity region existed for all velocity ratios and for both the thick and thin lips. The logarithmic region could be well represented by the law of the wall and Patel's [23] equation. For all velocity ratios the Reynolds numbers based on momentum thickness is significantly larger for thick lips. The shape factor H was significantly large for low values of u_j/u_s ($x/b < 20$) for the thicklip case, where as no significant difference between the thick and thin lip was found for large velocity ratios for any x/b.

For the thick lip, the skin friction coefficient was always much smaller, the difference being considerable for small values of u_j/u_s. This was attributed to the separated region to the slot.

The thick lip caused near isotropy of turbulent velocities for small values of x/b. As x/b increased the tendency to isotropy disappeared. Turbulent fluctuations were very high near the slot. At a distance of 150 slot heights, the distribution of fluctuating quantities resembled that of a turbulent boundary layer, which was also found in the earlier case of thin lips. Thus the fluctuating components of velocity were found to be less dependant on the lip thickness than on velocity ratio.

It was seen that the turbulent kinetic energy is higher for thick lips for x/b of 10 whereas at x/b of 150, the turbulent kinetic energy is more dependent on velocity ratio than on lip thickness. The shear stress crossed zero in all cases except u_j/u_s of 0.75 at x/b of 10. The crossing is close to the wall, than the point of zero velocity gradient. For all cases at x/b of 150 only three shear stress curves crossed zero, that of u_j/u_s of 2.33 for both the lips and u_j/u_s of 1.33 for the thin lip. For u_j/u_s of 2.33, y values of maximum velocity and shear stress diverged as x/b increases. The minimum kinetic

energy is between maximum velocity and zero shear stress, but closer to the maximum velocity location for thick lip and nearer to zero shear stress location for the s thin lip.

The turbulent energy spectra measurements were carried out to determine the periodicity of flow if any due to the thick lip and resulting separated region. Also, with this measurement turbulent energy dissipation could be estimated. The maximum energy peaks existed corresponding to the corners of the lower and upper lips. The peaks existed at a frequency of 600 Hz against a shedding frequency of 100 Hz. The energy contained within the peaks represented less than 25 percent of the energy bounded by a smooth curve. The transition wave frequencies agreed well with the contention by Bloor (2) that inthe flow around a cylinder the transition wave frequency is proportional to $u_j^{3/2}$. The only modification to be made here was u_j had to be replaced by $(u_j+u_s)/2$., Bloor (2) has shown that shedding frequencies are 4 to 20 times transition wave frequency and this part of Bloor's findings was also confirmed. No peaks existed in the spectra for x/b of 150 and the spectra resembled a zero pressure gradient, turbulent boundary layer. Close to the wall more energy is contained at the higher frequencies. Away from the wall

-5/3 law is valid over a greater region of the spectra than close to the wall.

From the U-spectra measurements the scale of turbulence is obtained. The turbulent energy balance is obtained through the secondary flow equation containing advection, production, diffusion and dissipation, in the same order as given below

$$\left[\frac{1}{2}\frac{\partial\overline{q^2}}{\partial x}+\frac{v}{2}\frac{\partial\overline{q^2}}{\partial y}\right]+\left[\overline{u'v'}\frac{\partial u}{\partial y}+\overline{u'v'}\frac{\partial v}{\partial x}+(u^{-2}-v^{-2})\frac{\partial u v}{\partial x}\right]$$

$$+\frac{\partial}{\partial x}\left(\overline{u'\left(\frac{p}{\rho}+\frac{q^2}{2}\right)}\right)+\frac{\partial}{\partial y}\left(\overline{v'\left(\frac{p}{\rho}+\frac{q^2}{2}\right)}\right)-\frac{\nu}{2}\left(\frac{\partial^2\overline{q^2}}{\partial x^2}+\frac{\partial^2\overline{q^2}}{\partial y^2}\right)$$

$$+\epsilon=0 \qquad (1)$$

The dissipation term ϵ was measured in terms of $\overline{\left(\frac{\partial u'}{\partial t}\right)^2}$. All terms except diffusion are measurable, hence the diffusion term is evaluated. The dissipation from spectra measurements and through differentiation of u' did not agree well. Production was high near the wall and in the wake of slot lip. In the outer flow it was low. Advection was negative mostly and in the wake and was of the same order as production itself. For higher velocity ratios, the production was large in the wake. Advection and dissipation were small and of the same magnitude at low velocity ratios. Thus the production is matched by diffusion.

The Prandtl mixing length ℓ_1, and Prandtl-Kolomogorov turbulent length scale ℓ_s were calculated and it is seen that their distributions are not similar. The Bradshaw parameter, a, (5) also was evaluated and it was found to be not a constant, but far downstream, $x/b > 150$, it could be taken as 0.15.

Wall jet in an external stream with adverse pressure gradients was investigated in detail by Irwin (16). The measurements by Irwin are the most elaborate available on wall jets. The measured quantities include, skin friction, mean velocity profiles, turbulence shear stress intensities, spectra, dissipation rate through differentiation, single point triple and quadruple velocity correlations and intermittency. The pressure-velocity correlation is the only term left not measured, but the pressure velocity gradient correlations are obtained with the assumption of local isotropy. A velocity ratio of u_j/u_s of 2.65 was chosen. The jet Reynold's number was 2.8×10^4 and the range of measurements was 60 to 260 slot heights.

The slot was 6.73 mm high and the lip thickness was 3.18 mm. The working section was 2.30 m long and 0.432 m high. The turbulence of stream was 0.5 percent at the working speed. On comparison of the measured skin friction with the expressions given by many earlier research workers, it

was found that the results of different authors did not agree with each other, but the agreement with Patel's (23) data for a zero pressure gradient is fairly good. That is, pressure-gradient has little influence on skin friction.

Mean velocity profiles obtained by hotwire and pilot tube are fairly in agreement. Choosing a coordinate system of y/δ_2 and $(u-u_s)/\Delta u_s$ the mean velocity data for different x/b could be collapsed onto one single plot. In the inner layer for a given y/δ_2, $u-u_s/\Delta u_s$ increases slightly as x/b increases. The logarithmic law applies in a limited range of $30 < y < 150$ where $y_+ = u_\tau\, y/\nu$ and u_τ is the shear velocity.

The measurements showed that the turbulence was almost in self preserving state except for the point of zero shear stress, which occured at lower values of η as x increased, when η, here stands for y/δ_2. The measured range of skin friction was in agreement with $\overline{u'v'}$ data. The shear stress calculated from the mean momentum equation agreed very well with the measured data except near the velocity maximum. The turbulent quantities $\overline{u'^2}, \overline{v'^2}, \overline{w'^2}$ all reached their maximum values at about the same point as maximum shear stress. The term $\overline{v'^2}$ was almost constant in the inner layer and, rose to a maximum a near the

point of zero shear and then decreased. $\overline{u'^2}$ was the largest of the three except for $\eta = 2.0$ where $\overline{v'^2}$ was slightly larger. The maximum intensity of turbulence $\sqrt{\overline{u'^2}}/u$ was 20 percent at η of about 1.3 (The graph supplied show that maximum intensity of turbulence is $\eta = 1.0$).

All triple velocity correlations passed through zero in the range of $0.7 < \eta < 0.8$ which was nearer the wall than the point of maximum shear ($\eta = 1$). The agreement with the models of Hanjalic and Launder (15) was pretty good for some cases of $\overline{v'^2 w'^2}$, $\overline{v'^3}$, $\overline{v'^2 u'^2}$ while for the remaining cases of triple velocity correlation the model value and measured values did not agree in magnitude though the general shape of the curves was similar to that predicted by Hanjalic and Launder for the case of asymmetric channel flow.

The fourth order correlation showed that the flatness factors of u', v', w' were close to the Gaussian value of 3 for the fully turbulent region, but rose in the outer region. The fluctuating component $\overline{u'^2}$ was independent of $\overline{w'^2}$, but $\overline{v'^2}$ was correlated to $\overline{v'^2}$ as seen by the correlation $\overline{u'^2 v'^2}$, $\overline{u'^2 w'^2}$ and $\overline{v'^2 w'^2}$.

The dissipation quantity was measured through spectra and also as time differentiation of u' as by Taylor's hypothesis for isotropic turbulence. The two values did not agree well. The dissipation obtained by differentiation was within 25 percent of that by the -5/3 law. The micro scale and dissipation length were also calculated.

Since all the terms of the turbulent energy balance equation are measured the curves for advection, production, diffusion and dissipation were plotted and compared with the models of Hangalic and Launder. The measured diffusion was found quite close to the diffusion obtained by difference. Yet a conclusion of the negligible magnitude of pressure diffusion could not be arrived at as the accuracy of the dissipation term is in doubt.

The dissipation was almost equal to the production every where except in the region of velocity maximum. The pressure velocity gradient correlation models, proposed by Hanjalic and Launder, are compared with the measured data.

The position of zero shear stress always remained closer to the wall than the point of maximum velocity. At the velocity maximum $\overline{u'v'}$ was positive.

As mentioned earlier this work contains the most elaborate measurements in a wall jet and the paper shows that it is possible to obtain a self-preserving wall jet by adjusting the pressure gradient.

The works mentioned so far dealt with wall jets in an empirical or semi empirical fashion. The second category of works on wall jets is when the flow is treated as ideal. When the flow is treated as an ideal flow the jet chosen is mostly an oblique one, where the jet and stream total pressure are very nearly equal. As far as the present problem of mixing of an inclined jet is considered, these analysis are not very helpful. Yet, since they are of the same problem a few references are given below.

Ehrich (8) considered an offset oblique jet introduced into a stream where both the jet and the stream had the same total pressure and density. Using Helm holtz - Kirchoff method of a series of conformal transformation, the penetration of the jet normal to the stream was obtained.

An analytical solution for an oblique jet introduced into a stream had also been obtained by Gold Stein and Braun (13). The jet was treated as inviscid to make it amenable to mathematical treatment. The total pressure of jet and the stream were assumed to be very nearly equal.

The jet was off set and the introduction in the upstream, downstream and normal directions were considered. It is shown that a small difference in total pressure caused a large change in penetration and thickness. And this effect increases as the angle increased. When the jet faced the stream, the flow configuration was found to be extremely sensitive to the difference of total pressures and the perturbation analysis was bound to break down. For a fixed orifice angle the velocity was bound to increase both at the upstream and downstream end of the slipline with increasing total pressure difference. For negative angles (downstream injection) velocity tended to be constant along slipline. For non-negative angles, there was a definite peak in the velocity profiles which became more marked as the orifice angle was increased.

The re-circulation zone is an integral part of a wall jet, particularly when it is an oblique jet. Yet, the number of investigation on the reattachment zone is very limited. Reattachment of a plane jet to an adjacent plate was dealt by Bourque and Newman (3). This analysis was a further development of Dodd's (7) analysis of reattachment of a jet to a plate off set from and parallel to a plate. For separation bubble to exist a steady two dimensional flow is absolutely essential. The analysis is made on the

assumption of (i) in compressible two dimensional flow (ii) uniform exit velocity, (iii) pressure in the seperation bubble being uniform, (iv) the centre line of the jet in the reattaching zone is an arc of a circle (v) the jet entrains fluid as if it were a free jet and hence its momentum is conserved, (vi) where the entrainment ceased the jet centre line intersected the plate, (vii) the forces due to skin friction are negligible near the reattachment and the flow is independent of viscosity at high Reynolds numbers. Through the momentum theory on the above assumptions, an expression for reattachment distance is obtained.

The authors investigated through experiments the pressure on the wall and the reattachment for off set and inclined plates. A hysteresis in reattachment angle was observed, the pressure inside the seperation bubble was found to be far from uniform and the analysis has been compared with experimental results.

Newman and Wygnaski (32) tried to find out the reattachment length when an oblique jet is introduced into a stream. An approach similar to dimensional analysis was followed to find out the parameters on which the reattachment distance depends. The kind of dependence on the parameters were obtained through experiments on 60° and 70°

incompressible jets. The effect of some possible parameters like pressure-gradient, skin friction were obtained by suitably modifying the experimental set up. As in the earlier case, it seems that if the Reynolds number exceeded a certain minimum value the reattachment distance is independent of jet momentum. Also, it was seen that if the plate length was sufficient, the reattachment was independent of skin friction. For an adverse pressure gradient, the non-dimensional reattachment distance could not be collapsed on to a single curve, while it was possible for zero pressure gradient. It was also observed if the jet angle is greater than 70° no reattachment takes place.

The above three groups show the method of attack so far developed in a wall jet. The study being of a semi-empirical type where no self-preservation is expected, the basic theory required for an experimental study is based on the fundamental equation of fluid mechanics. The equations of momentum, energy are modified to measurable quantities as suggested by Rouse (25, 26, 27). A survey of the applications of this method is a formidable task. A number of investigators under Rouse himself have adopted this method for their research work. A few of them are Rao , Nagaratnam (26) and Chaturvedi (6).

Also the work on wall jets by Kacker and Whitelaw and Irwin also use this method to some extent.

A glance on the above works on wall jets show that the wake type formation (a weak jet) has been investigated only by Kacker and Whitelaw and oblique wall jet has not been, in fact, investigated except for the reattachment distance.

The present work was undertaken with the hope of filling the gap, where the oblique jet as a real flow was left out. Also a turbulence model for such a flow is as yet not available even for zero degree wall jet. It is hoped that the work would be useful in this respect also.

CHAPTER 3

THEORETICAL BACKGROUND

3.1

The previous chapter gives a glimpse of most of the available works on two dimensional wall jets right from Forthmann to Irwin. As mentioned in that chapter the research papers on wall jets fall into three groups- (i) where a semiempirical treatment is given to the flow, (ii) where the flow is treated as potential flow, and (iii) where only the reattaching zone is considered.

Going through the group where semiempirical treatment is given, the following point show why such a treatment cannot be taken up in the present study. The flow is treated as self-preserving except for a small initial distance. This condition is satisfied only if the jet flow is much stronger than the stream, which is not the case taken up. All the papers show jet to stream velocity considered was more than 3. The work by Hacker and Whitelaw is an exception to this case. Here there is no similarity profile even at large distances down stream (x/b of 150). Nor there is a theoretical analysis except the applications of the basic equations of fluid mechanics.

The similarity profile assumes that the flow can be split into an inner layer behaving like a turbulent boundary

layer and an outer layer similar to that of a stream. The applications of boundary layer equations imply a a tranverse pressure gradient which is negligible. At least for distances upto x/b of 96 this is not the situation that exists as is evident from the static pressure measurements. That is, boundary layer equations are not applicable upto x/b of 48. All the above papers deal with zero degree wall jet, where when the jet is strong and lip thickness is small, the separation zone is extremely small or non existent. The thick lip case of a weak jet [Elsner and Whitelaw (19)] does produce a separated zone, but it is much smaller than in the case of an oblique jet. The edge of the standing eddy is a zone of turbulence production, from where the turbulence gets transported. While some of the above papers have compared the various parameters of turbulence models, the comparison does not have a direct significance since the models are based on boundary layer equations.

The second group of ideal flow treatment is altogether not helpful. Since the flow does not take into account the viscosity and turbulence effects. Similarly the third set of papers are not infact papers on wall jets as the only factor investigated is the reattachment length.

Considering all these factors, the suitable approach to be adopted appears to be that suggested by Pouse.(27). The basic theoretical equations are modified to such forms, that all the terms, involved would contain either only measurable quantities or quantities which are very small so as to be negligible. These equations are then integrated over pre-chosen control volumes. The state of system is measured and decided through the application of the basic equations. Finally, the true state of the system in terms of the various components of the fluid dynamic balance are identified. Further more, through analysis of the interacting integrated form, the dynamics of the flow is tried to be understood.

3.2 Equations of Motion

The basic fluid mechanics equations valid for any flow are (i) the equation of continuity and (ii) the equation of motion.

The equation of continuity is the application of conservation of mass and the equations of motion are obtained on applying Newton's second law to the flow concerned. The derivations of these equations are available in all text books of fluid mechanics and hence are not reproduced here.

The equation of continuity is

$$\frac{\partial u}{\partial x} + \frac{\partial v}{\partial y} + \frac{\partial w}{\partial z} = 0 \qquad (3.1)$$

when the flow is steady and incompressible. Here Here u, v and w are the velocities in the x, y and z directions. The equation of motion in the x-direction for the same case is,

$$\frac{Du}{Dt} = X - \frac{1}{\rho}\frac{\partial p}{\partial x} + \frac{\mu}{\rho} \nabla^2 u \qquad (3.2)$$

where ρ, p, μ and X are the density, pressure, dynamic viscosity and external force respectively. Similarly, the equations of motion for y and z directions can be written.

The above equations of motion, known as the Navier-Stokes equation can be modified for turbulent flows by assuming that these equations are valid for instantaneous as well as mean conditions of flow. The resulting equations of motion are known as Reynolds equations. The same approach can be adopted for modifying the equation of continuity. Thus each instantaneous flow characteristic is assumed to be a combination of a mean and a fluctuating part $u = \bar{u} + u'$, $v = \bar{v} + v'$, $p = \bar{p} + p'$ etc. The dash quantities stand for fluctuations and bar quantities for time-averaged mean.

The equations of continuity, for two dimensional turbulent flow are

$$\frac{\partial \bar{u}}{\partial x} + \frac{\partial \bar{v}}{\partial y} = 0 \qquad (3.3a)$$

and

$$\frac{\partial u'}{\partial x} + \frac{\partial v'}{\partial y} = 0 \qquad (3.3b)$$

Similarly the equation of motion can be simplified and summarised to

$$\frac{\partial \bar{u}_i \bar{u}_j}{\partial x_j} + \frac{\partial \overline{u_i' u_j'}}{\partial x_j} = -\frac{1}{\rho}\frac{\partial \bar{p}}{\partial x_i} + \frac{\mu}{\rho}\frac{\partial^2 \bar{u}_i}{\partial x_j \partial x_j} \qquad (3.4)$$

where i, j, refers to the usual tensor notation.

3.3 The Energy Equation

The instantaneous energy equation can be derived from the momentum equation by multiplying the momentum equations with the corresponding velocities and adding all the three resulting equations together. Taking the time average of the resulting equation gives the total work energy equation. The total work energy equation thus obtained is,

$$\bar{u}_j \frac{\partial\left(\bar{v}_t^2 + \overline{v'^2}\right)}{\partial x_j} + u_j' \frac{\partial(v'^2/2)}{\partial x_j} + \frac{\partial}{\partial x_j}\left(\overline{u u_i' u_j'}\right)$$

$$= -\frac{1}{\rho}\bar{u}_i \frac{\partial \bar{p}}{\partial x_i} - \frac{1}{\rho}\overline{u_i' \frac{\partial p'}{\partial x_i}} + \frac{\mu}{\rho}\bar{u}_i \frac{\partial^2 \bar{u}_i}{\partial x_j \partial x_j} + \overline{u_i' \frac{\partial^2 u_i'}{\partial x_j \partial x_j}} \qquad (3.5)$$

where $V_t^2 = u^2 + v^2 + w^2$ and $V'^2 = u'^2 + v'^2 + w'^2$

The terms of this equation can be grouped into work energy equation for mean flow and for the fluctuating flow.

The work-energy equation for mean flow is,

$$\bar{u}_j \frac{\partial \overline{V_t^2}}{\partial x_j} + \bar{u}_i \frac{\partial \overline{u_i' u_j'}}{\partial x_j} = -\frac{1}{\rho} \bar{u}_i \frac{\partial \bar{p}}{\partial x_i} + \frac{\mu}{\rho} \bar{u}_i \frac{\partial^2 \bar{u}_i}{\partial x_j \partial x_j} \quad (3.6)$$

and for the turbulent fluctuations,

$$u_j \frac{\partial}{\partial x_j} \left(\frac{\overline{V'^2}}{2} \right) + \overline{u_j' \frac{\partial}{\partial x_j} \left(\frac{V'^2}{2} \right)} + \overline{u_i' u_j'} \frac{\partial \bar{u}_i}{\partial x_j}$$

$$= -\frac{1}{\rho} \overline{u_i' \frac{\partial p'}{\partial x_i}} + \frac{\mu}{\rho} \overline{u_i' \frac{\partial^2 u_i'}{\partial x_j \partial x_j}} \quad (3.7)$$

These equations of continuity, momentum and work-energy for mean flow and fluctuating quantities can be utilised to investigate the mixing of jet in a stream. These equations require to be broken up into terms which are directly measurable. Unfortunately all the terms are not yet directly measurable. Yet, it has been observed that some of the non-measurable quantities are negligible, while some other terms can be deducted from the above equations. Thus this set of equations serve as the theoretical background for the experimental study. The non-negligible terms of

both the energy equations are obtained either directly or by derivation from momentum equation. Hence a check by substituting in the momentum equation gives the degree of accuracy of the measured terms. Once the accuracy is established, the non-measurable terms can be evaluated as the balancing quantity.

3.4 Adaption of the Equations

These equations can be integrated over a control volume using Gauss's theorem connecting volume integrals to surface integrals. Taking the momentum equation and integrating over the control volume,

$$\int_V \frac{\partial}{\partial x_j}(\bar{u}_i \bar{u}_j)dV \int_V \frac{\partial \overline{u_i' u_j'}}{\partial x_j} dV = -\frac{1}{\rho} \int_V \frac{\partial \bar{p}}{\partial x_i} dV + \int_V \frac{\mu}{\rho} \frac{\partial^2 \bar{u}_i}{\partial x_j \partial x_j} dV \quad (3.8)$$

Reducing the volume integral to surface integral by Gauss's theorem,

$$\int_S \bar{u}_i \bar{u}_j \frac{\partial x_j}{\partial n} dS + \int_S \overline{u_i' u_j'} \frac{\partial x_j}{\partial n} dS = -\frac{1}{\rho} \int_S \bar{p} \frac{\partial x_i}{\partial n} dS + \int_S \frac{\mu}{\rho} \frac{\partial \bar{u}_i}{\partial x_j} \frac{\partial x_j}{\partial n} dS \quad (3.9)$$

The integral has value only when j and n coincide. Making term by term and reducing it to the control volume, the momentum equation in the X-direction g reduces

$$\int_0^d \bar{u}^2\,dy + \int_0^d \overline{u'^2}\,dy = -\frac{1}{\rho}\int_0^d \bar{p}\,dy + \int_0^d \frac{\mu}{\rho}\frac{\partial \bar{u}}{\partial x}\,dy \qquad (3.10)$$

for the entrance and exit sections of the control volume. Similarly an equation can be obtained for the y-direction

$$\int_0^d \bar{v}\bar{u}\,dy + \int \overline{v'u'}\,dy = -\frac{1}{\rho}\int_0^x \bar{p}\,dx + \frac{\mu}{\rho}\int_0^x \frac{\partial \bar{v}}{\partial y}\,dx \qquad (3.11)$$

The work-energy equation (3.6) when similarly integrated and simplified reduces to

$$\int_0^d \bar{u}\,\frac{\overline{v^2}}{2}\,dy + \int_0^d \bar{u}\overline{u'^2} + \bar{v}\,\overline{u'v'} + \int_0^d (\bar{u}\,\overline{u'^2} + \bar{v}\,\overline{u'v'})dy$$

$$-\int_0^d\int_0^x \left[\,\overline{u'v'}\left(\frac{\partial \bar{u}}{\partial y} + \frac{\partial \bar{v}}{\partial x}\right) + \left(\overline{u'^2} - \overline{v'^2}\right)\frac{\partial \bar{u}}{\partial x}\,\right]dx\,dy$$

$$= -\frac{1}{\rho}\int_0^d \bar{u}\,\bar{p}\,dy + \frac{\mu}{\rho}\int_0^d \left[\,2\bar{u}\frac{\partial \bar{u}}{\partial x} + \left(\frac{\partial \bar{u}}{\partial x} + \frac{\partial \bar{u}}{\partial y}\right)\bar{v}\,\right]dy$$

$$-\frac{\mu}{\rho}\int_0^d\int_0^x \left[\,\left(\frac{\partial \bar{u}}{\partial y} + \frac{\partial \bar{v}}{\partial x}\right)^2 + 4\left(\frac{\partial \bar{u}}{\partial x}\right)^2\,\right]dx\,dy. \qquad (3.12)$$

Similarly the energy equation for turbulent flow reduces to

$$\int_0^d \frac{\overline{v'^2}}{2}\bar{u}\,dy + \int_0^d \frac{\overline{v'^2u'}}{2}\,dy = \Big[-\frac{1}{\rho}\int \overline{p'u'}\,dy +$$

$$\frac{\mu}{\rho}\int_0^d \frac{\partial}{\partial x}\left(\frac{\overline{v'^2}}{2} + \overline{u'^2}\right) + \frac{\partial \overline{u'v'}}{\partial y}\Big]\,dy$$

$$-\frac{1}{\rho}\int_0^d\int_0^x \Big[\,\overline{u'v'}\left(\frac{\partial \bar{u}}{\partial y} + \frac{\partial \bar{v}}{\partial x}\right) + \left(\overline{u'^2} - \overline{v'^2}\right)\frac{\partial \bar{u}}{\partial x}\Big]\,dxdy$$

$$-\frac{\mu}{\rho}\int_0^d\int_0^x K\,\overline{\left(\frac{\partial u'}{\partial x}\right)^2}\,dxdy \qquad (3.13)$$

In all the above equations d stand for the depth of the flow. The terms are positive when the outside normal to the surface is in the positive co-ordinate direction.

Many of the terms of the equation 3.13 can be grouped together and interpreted as different aspects of turbulence. The first two terms $\int_0^d \frac{\overline{v'^2}}{2}\bar{u}\,dy$ and $\int_0^d \frac{\overline{v'^2}}{2}u'\,dy$ represent the net fluxof kinetic energy out of the section by convection (by mean flow) and diffusion (by turbulence). The term $\int_0^d\int_0^x \Big[\,\overline{u'v'}\left(\frac{\partial \bar{u}}{\partial y} + \frac{\partial \bar{v}}{\partial x}\right) + \left(\overline{u'^2} - \overline{v'^2}\right)\frac{\partial \bar{u}}{\partial x}\Big]dxdy$ is the quantity representing production of turbulence. This interpretation can be easily understood since the same term exists in the energy equation for mean flow, but with a negative sign. Hence as far as main flow is considered it is a loss, but it

is a gain (production) term for the secondary flow. The term $\int_0^d \overline{p'u'}\, dy$ is the rate at which work is done is externally by the fluctuating pressure. The terms containing μ represent the rates att which work is done by the viscous stresses over the surface of the region and through out the interior of the $\int_0^d \int_0^x \mu \overline{(\frac{\partial u'}{\partial x})^2}\, dxdy$ is dissipative. The dissipation term can be simplified for isotropic turbulence by Taylor hypothesis. By this hypothesis, the dissipation, $\epsilon = \frac{15}{U^2} \overline{(\frac{\partial u'}{\partial t})^2}$. Thus the dissipation involving $\overline{(\frac{\partial u'}{\partial x})^2}$ can be measured through a differentiator.

These above equations and interpretations serve as the theoretical basis for the present work. Detailed derivations of all the equations are given in the appendix.

...

CHAPTER 4

EXPERIMENTAL PROGRAMME

4.1 Equipment

The experimental programme involved the measurement of static pressure, total pressure and fluctuating quantities. The experimental set up needed a stream and a jet and the instruments for measurement of various quantities.

The equipment used in the experimental program is shown in Fig. 4.1a,b,c,d. The uniform stream was provided by a blower-type open wind tunnel. The power section consisted of two contra-rotating fans each driven by a 7.5 h.p. motor operating on 440 volts. The contra-rotation reduced the tendency of the flow to swirl. The tunnel was originally of a suction type providing a stream velocity of 30 m/sec. By reversing the power connection of the motor the fans were made blower type, but with some loss of efficiency. Each fan could be independently operated and a velocity range upto 20 m/sec could be obtained. The size of the power section was 0.50 m dia and 1.05 m long.

The power section was preceded by a control section and a noise reducer of size 0.60 m(dia) by 0.76 m. The noise

reducer consisted of a 5 cm wide annular space packed with glass wool and the inner plate was of perforated sheet. The noise reducer was not efficient for a blower type of tunnel. The control of flow was by a flap valve which could be adjusted as desired. The power section was connected to a circular to rectangular transition. To reduce the wake effect of the motor of the fan a coarse G.I. screen was fitted between the power section and the transition section. Next to the rectangular end of the section, a 10 cm. deep honey comb section was provided to straighten the flow. The connection between the control section and honey comb was of flexible leather, sewed to shape to reduce vibration effects. The flow thus straightened by the honey comb section entered a settling chamber of size 0.43 m by 0.43 m. The settling chamber was fitted with three fine nylon screens spaced 6.5 cms apart. These fine screens reduced the size of eddies to a very small size which get dissipated soon. The settling chamber was connected to the working section through a well designed contraction cone. The working section was 0.297 m by 0.307 m in section and 2 m long. One side of the working section was made of perspex and the other of wood. Part of the perpex side was made removable for fitting the nozzle properly. The floor of the working section was fitted with a number of static taps. The centre to centre distance

of these taps varied from 3.5 mm near jet exit to 5 cms at the last section. The working section ended at a bend to which a diffuser was connected. The diffuser was later on dispensed with.

The jet was supplied by a centrifugal blower run by a 5 h.p. motor. The rectangular exit of the fan was connected to a 7.5 cm. pipe through a transition piece 15 cms long. A three way gatevalve provided the controlling mechanism. The bleed line was directed away from the experimental set up. From the gate valve the pipe line was straight for 6 m. A static tap was fitted on to one side of the pipe and an adjustable 16 gauge Pitot tube was provided at the same section as the static tap itself. One meter downstream of the pitot-static fitting a bend was provided in the supply line. The bend was connected to a settling chamber by a short pipe length and a nearly two metre piece of flexible tubing.

The settling chamber was 0.95 m by 0.95 m and was fitted with three fine Nylon screens to distribute the flow evenly in the chamber and to reduce the size of eddies. To one side of the chamber, opposite the side through which air entered, a 7.5 cm by 30 cm conduit was connected at an angle of 45°. The conduit ended with a flange section to fit the required nozzle. The nozzle

pieces were either of G.I. or M.S. 7.5 cm by 30 cm at one end and were provided with flanges on all sides. The exit end of the nozzle was sharpened to a thin lime. The nozzles were designed for angles of 90° and 127°. A large contraction of 7.5 cm to 7 cm was effected in about 20 cms. The length of flexible tubing and the adjustable foot screws supporting the settling chamber gave the nozzle some freedom of movement in any required direction.

4.2 Instrumentation

To introduce the instruments vertically, holes were drilled on the roof and fitted with well fitting caps. A central longitudinal slot 15 cm long was made onthe roof of the tunnel at jet exit. The lid for this slot was made of four interchangeable pieces, each of which was provided with a central hole to introduce instruments. Thus, for the recirculation bubble a velocity transverse could be made under any central hole by taking Pitot and static traverses from the two flanking holes. The central hole could be used for directly evaluating the centre of the eddy by means of tuft and hot wire anemometer. At the jet exit a large slot was made on the wooden side also. The slot could be closed with two sliding panels which moved through groves a made on the sides of the slot. The two parts of the lid when joined together closed perfectly

except for a small hole at the centre. This facilitated the introduction of the Pitot tube at any height and at any angle in a vertical plane. At each of the sections x/b = 48, 96, 144 and 192 a similar slot was made (but of 2 cm width) at the sides and also a central roof hole was made.

A small section of the base was cut at an angle. The size of slot thus made was slightly larger than the nozzle. The nozzle piece was introduced through this slot and adjusted to level position with the help of foot screws. The fitting was made semi-permanent by Duco putty, which was later sand papered to a level finish.

The measuring system consisted of the traverse system and the instruments. A set of lead screws with central holes of different sizes could be fitted on the roof for vertical introduction of the instruments. The least reading was 0.1 mm. Pitot tube, static tube, hot wire probe, eddy tube etc. could be introduced through these lead screws and adjusted to any point on the vertical. Also rotation of the instrument in the horizontal plane was possible. For horizontal introduction, a holder and clamp arrangement fitted to a sliding piece which moved over a vertical scale, was used. The vertical scale could be

rotated about the vertical axis, the holder about a horizontal axis and also the lead screw clamped to the holder. could be moved in a to and fro fashion. Thus, the probe could be adjusted to any required position. An adjustable indicator on the probe body made angle measurements possible.

The total head was measured by a Pitot tube 1.6 mm dia and the static head by a 1.4 mm dia static tube. Except very near the jet, the Pitot and static heads were measured with vertical introduction. For the jet size of 7 mm these tubes were considered too large. A 22 gauge Pitot tube and static tube combination was used for jet exit velocity. The Pitot tube length was matched to the length upto the static holes, to get the velocity at the same points.

For measuring the inclination of the flow a modified Pitot tube was used. It consisted of two stainless steel tubes of 1.6 mm dia bent like a Pitot tube and held together by a think film of adhesive. The tubes were cut to 45° at the ends facing the flow. When thereadings from the two tubes were the same the tube was aligned in the direction of flow. A back to back Pitot tube was made for measuremonts in eddy. It was later on abandoned for lack of consistency. The eddy centre was decided with the help of a freely swinging woolen tuft and also by hot wire probe. The hot wire anemometer reading is the least at the centre

of the eddies.

The turbulence quantities were measured by a hot wire probe and a Disa 55 D01 constant temperature hot wire anemometer set. The probe was introduced through a lead screw which could be fitted on to the stand mentioned bove. An L shaped mirror checked the original setting of the wire normal to the flow. The 45° and 135° inclinations then could be adjusted.

For measurements of reattachment distance, paper tufts, 3.5 mm wide and 1.5 cm long were pasted on the floor. The tuft which fluttered in both directions equally was considered to be at the reattaching point. Betz micro manometer was used for measurement of pressure.

4.3 Calibrations

Calibrations of Pitot and static tubes were done with the help of NPL Pitot-static tube in a turbulence free stream. The coefficient was found to be 1.005.

Hot wire probe was calibrated with respect to the Pitot and static tubes, when the velocity was more than 4 m/sec. The calibration was done for a range of 4 to 20 m/sec in another wind tunnel, where the turbulence was less than 0.5 percent for the range of 0 to 4 m/sec, where

Pitot tube is not accurate enough, a special calibration tank was fabricated.

The special calibration tank was made of 10 cm pipe line, 1½ m long and held vertically with the help of a stand. To the top of the pipe line a fitting lid was welded. At the threaded bottom side an orifice plate with a centrally placed orifice of 5 mm diameter could be fitted. The tank thus provided was fitted with an inlet near the top, glass tube on side. To one side of the tank, near the top, a 1 cm perspex tube, 1 m long was fitted with the help of proper supports. The orifice could be closed and opened as desired.

The principle of this calibration tank is as follows. Once the orifice is opened, water level goes down in the tank. The change in water level in a known time gives the volume of air that has entered. Since the tank is sealed except for the perspex tube the average velocity with which air moves in the perspex tube is known. Th flow is laminar and hence the central velocity is twice the average velocity. So, if a hot wire is introduced at th centre a calibration of the hot wire can be done for very small ranges of velocities. The hot wire could be introduced either vertically or horizontally. Details of calculation are shown inthe chapter of results and analysis.

For measurements of turbulent quantities, a DISA constant-temperature hot wire anemometer was used alongwith its accessories of linearizer, RMS meter and digital voltmeter. These units were calibrated as instructed in their manuals and the calibrations were checked once in while. As the line voltage tended to go below the range of the instruments, each instrument was connected to a voltage stabilizer. The probe used was of a single wire type DISA 55 F 31. $\overline{u'v'}$ measurements were also taken with the same probe. The hot wire was calibrated at the beginning and end of the traverse in the working tunnel itself, upstream of the jet exit. In addition the Pitot tube traverse helped in checking the accuracy of hot wire readings.

For measuring the dissipation term in the turbulent energy equations, the space derivatives were assumed as functions of time derivative as shown in the next chapter. A differentiator was fabricated and calibrated with the help of a known wave form. A circuit diagram of the differentiator is shown (Fig. 4.3).

Once all the instruments were calibrated, the stream and jet remained to be calibrated. The stream was calibrated for the working velocity and the jet required calibration for every setting.

The calibration of the stream was done in detail at the jet exit with the jet exit closed and also a centre line traverse was taken at the last station. A total head and static head traverse was made at every nodal point of a 2 cm grid. These tubes were introduced horizontally. The angle of flow at these nodal points were checked by the angle measuring Pitot tube. At no nodal point the angle was more than $\pm 0.5^{\circ}$, in the vertical direction. A freely swinging tuft fixed to a 4 mm rod also introduced horizontally gave an indication of the total angle of the flow. With these traverses, the velocity distribution was found satisfactory. A detailed centre line traverse with the Pitot tube and static tube introduced vertically gave the boundary layer characteristics at the beginning and end of the working section. A traverse with a hot wire probe was taken along the centre line to determine the turbulence level of the tunnel. The turbulence level was found to be slightly more than 0.75 percent. The static pressure measurements along the centre line of the tunnel showed a very small decrease towards the down stream direction. The static head at the jet exit showed uniform pressure distribution when no stream was present.

The stream velocity was unaltered from the value of 14.5 m/sec. The different velocity ratios were adjusted by adjusting the jet velocity alone.

The jet exit angle was checked with the help of a tuft, with the stream being absent. The width at the exit end was checked at 2 cm intervals and the difference was found to be less than 2 percent. For each jet velocity, velocity traverse was done along the centre line of the jet, and on two lines, one on either side of the centre line. The jet could be taken as a uniform one. The asurements were taken in the core, just above the plane of exit. The Pitot sm tube used was a pre-calibrated 22 gauge tube. The static and Pitot tube lengths were matched to give the velocity on the same line. The two were mounted together with a gap of 2 cms. A Pitot tube and static tap in the 7.5 cms supply line of the jet were connected always to a Betz micro manometer providing an instant check on the jet setting at any time.

4.4 Programme of Measurement

Four main stations were chosen along the length of the flow at x/b of 48, 96, 144 and 192. In addition two station were chosen within the reattachment length at x b of 4 and 12, where mean velocity and static pressure were only measured.

A traverse by tuft was done at first to check the orientation of the flow. It was found that upto x/b of

48 a small reach of flow near the base was inclined to the horizontal. The flow at all other locations was in the x-direction.

Static pressure measurements at any section included base pressure and a traverse along a vertical. For base pressure, the static taps fitted into the floor was used. The base pressure was found to be negative for some distance from the jet exit but much before x/b of 48 the base pressure remained positive. The static pressure, traverse (vertical) at different x b sections were taken at different intervals varying from 5 mm to 2 cms. The traverses showed nearly uniform pressure distribution after x/b of 48. For the stations within the reattachment zone, the pressure distribution was taken with the tube facing the flow at any point.

The total head measurement were taken at graded intervals of 0.5 mm to 1 cm from boundary to mid stream. Also, for the reattachment zone the Pitot tubes faced the flow at any point, except for the slight inclination of the flow.

The hot wire probe support was inserted horizontally so as to take $\overline{u'^2}$, $\overline{u'v'}$ and vertically for $\overline{\omega'^2}$. The intervals of hot wire readings were based on the readings

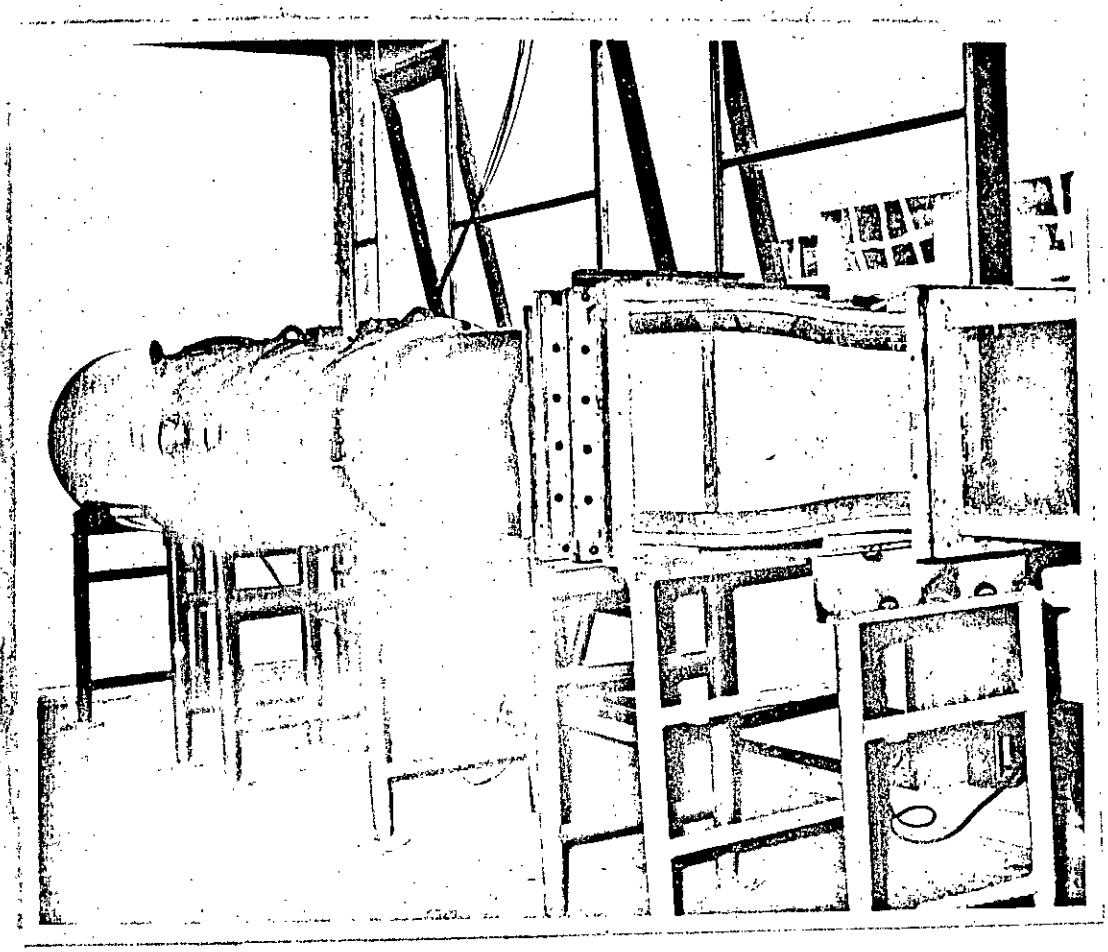

FIG. 4.1a: WIND TUNNEL

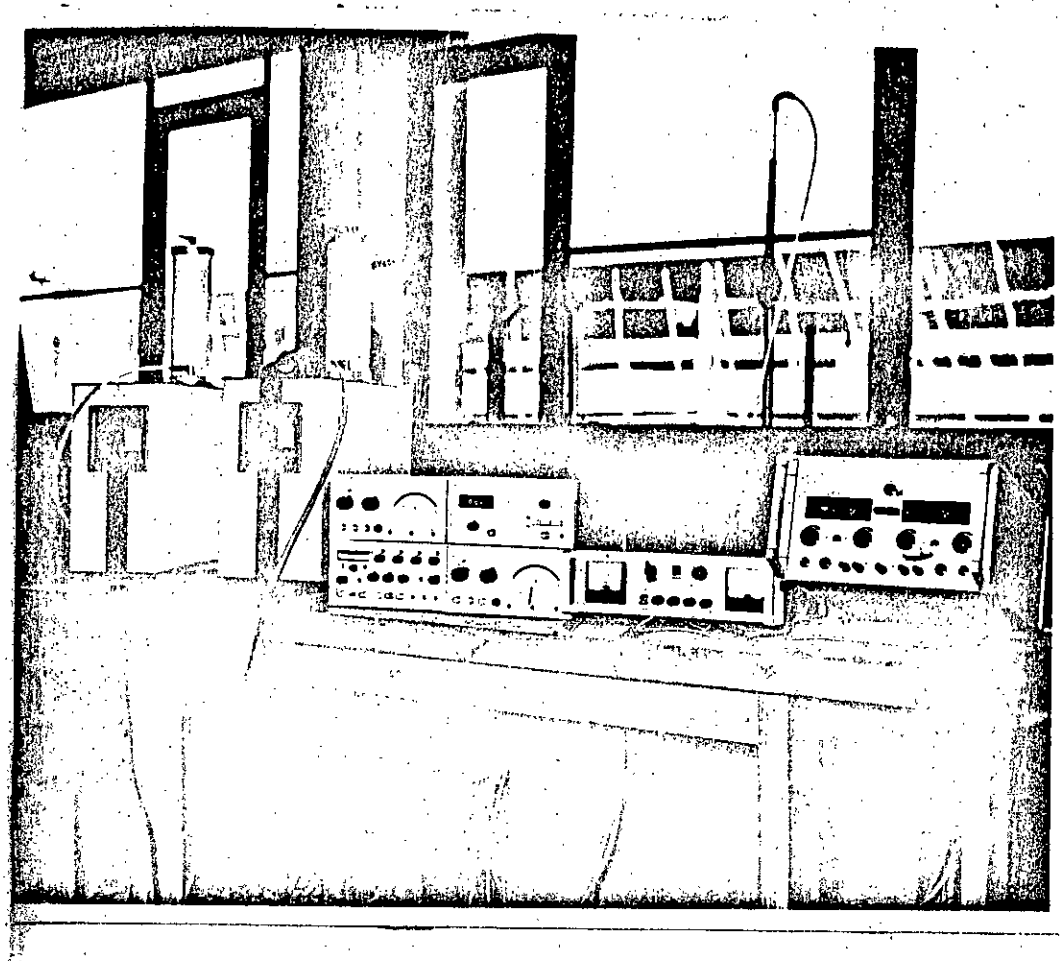

FIG. 4.16: INSTRUMENT ASSEMBLY

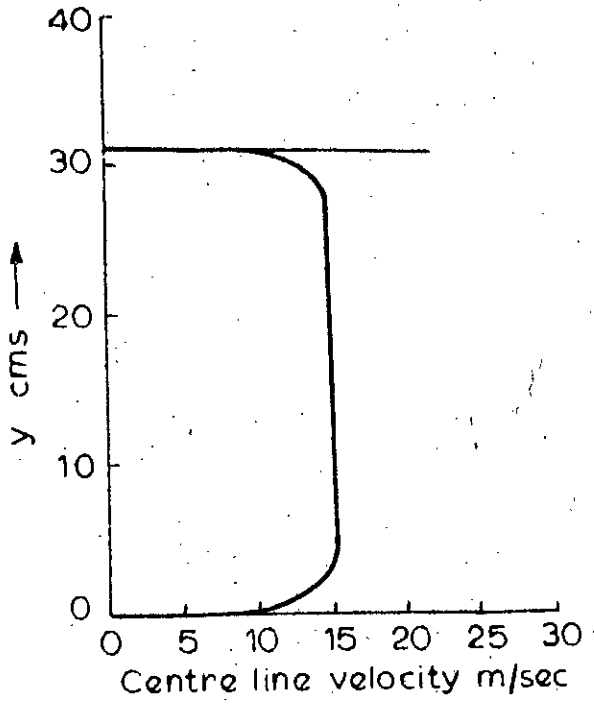

FIG. 4.2: VELOCITY DISTRIBUTION μ/S OF JET EXIT

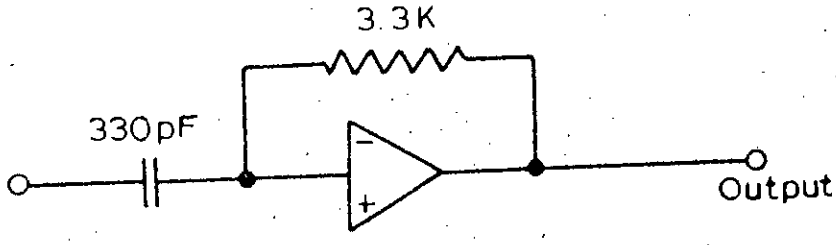

FIG. 4.3: DIFFERENTIATOR CIRCUIT

on the RMS meter, being very small for large values and about 1 cm where RMS meter did not show much variation.

Skin friction measurements were based on the Pitot tube readings at the first setting over the boundary.

The temperature difference between the stream and jet was only 0.5 degree hence no special arrangement was required to adjust the jet temperature to that of the stream.

The calibration charts for the stream are shown in Fig. 4.2a,b.

...

CHAPTER 5

RESULTS AND ANALYSIS

5.1 Evaluation of Measured Data

The general procedure for correction of measured data involved correction for scatter and correction for measuring conditions which at times were different from calibration conditions. The correction for scatter was done by considering variables as continuous functions in space. Thus a simultaneous plotting of the variables in the X and Y directions eliminated discontinuous gradients.

The second type of correction for the Pitot tube and static tube involved correction for angularity and turbulence. The angles of the stream lines were extremely small except in the vicinity of the reattaching bubble. Hence the corrections were made by successively plotting the measured velocities and plotting the streamlines. Based on the inclination of the streamlines, the angular correction was applied. The actual mean velocity was calculated from the measured total and static pressure using the formula

$$\frac{\bar{u}}{U_{uncorr}} = 1 - \frac{1}{2}\left(\frac{\overline{u'^2} + \overline{v'^2} - \overline{w'^2}}{U^2}\right)_{uncorr} \qquad (5.1)$$

where $U_{u\,nc}$ stands for the velocity based on measured readings.

The skin friction was calculated on the assumption of logarithmic velocity distribution. The calibration of hot wire before and after each traverse, eliminated many a correction from the hot wire reading. Also the traverse by the Pitot tube checked the accuracy of the hot wire readings. The calibration of hot wire for the range of less than 4m/sec was done by using the calibration tank described in Chapter-4. The formula used for evaluation was

$$u = 4 \left(\frac{D}{d}\right)^2 \frac{h_{max}}{t_{max}} \sqrt{\frac{h}{h_{max}}} \qquad (5.2)$$

where u is the velocity at the probe, D, the inner diameter of the tank, d, the diameter of the orifice, tmax is the time in seconds required to bring down the water level through a depth of h_{max}. The fluctuating quantities were evaluated on the basis of the formula,

$$\frac{V_1^2 - A}{R(u - Ra)} = B\,\rho U^c \left[(\sin^2\phi + k^2 \cos^2\phi)\right]^{c/2} \qquad (5.3)$$

where B, c, and A are calibration constants, u is the velocity, V_1 is the voltage reading of the anemometer, ϕ is the inclination of the x wire, R and Ra are the

operating resistances of the wire. Here the constant k^2 is usually taken as 0.04.

5.2 Analysis of Mean Flow

The static pressure distribution along Y was far from uniform, especially at stations nearer to the jet exit. The pressure distribution inside the separation was also far from uniform. The non-uniformity of lateral pressure existed till far down stream, though to a much smaller extent.

A small longitudinal pressure gradient also existed, which was of the same order as that of the stream when the jet was absent. The base pressure showed negative values till about the reattachment point, after which it remained more or less of the same as the pressure in the mid-stream. This lateral pressure gradient implies that the x-directional and Y-directional equations are to be considered for solution. The base pressure is shown in Fig. 5.2.

Mean Velocity Profile

The mean velocity profiles at x/b of 4 and 12 show that the velocity profile consists of a re-circulating flow and the flow in the general direction (Fig. 5.1). Yet

after x/b of 48, no velocity maximum is present. This could be attributed to the intense production of turbulence along the edge of the standing eddy and consequent intense mixing. A logarithmic distribution of velocity is found to exist after a distance of x/b of 48 (Fig. 5.8). The velocities measured by Pitot and hot wire are in fairly good agreement as seen in Fig. (5.3).

The corrected quantities of mean pressure and mean velocity and turbulent fluctuations are used to evaluate continuity, momentum and energy integrals. The continuity equation is satisfied with an error range less than 1.5 percent. The momentum equation and energy equation are satisfied with error ranges not exceeding 3 percent and 5 percent respectively. The terms of the momentum equation are termed A,B,C and shown in Fig.(5.5). Similarly the terms of the mean energy equations are plotted in Fig.(5.6). The first term which represents the flux of the kinetic energy is combined with the second term, which represents the work done by Reynolds stress, and is shown as A in Fig. (5.6). The second term alone is shown in Fig. (5.6) as A, but with a base of zero. The third term is represented by C and the last term by D. The last term represents the production of turbulence, which is a loss to the mean energy field. Hence it is a dissipation term. The substi-

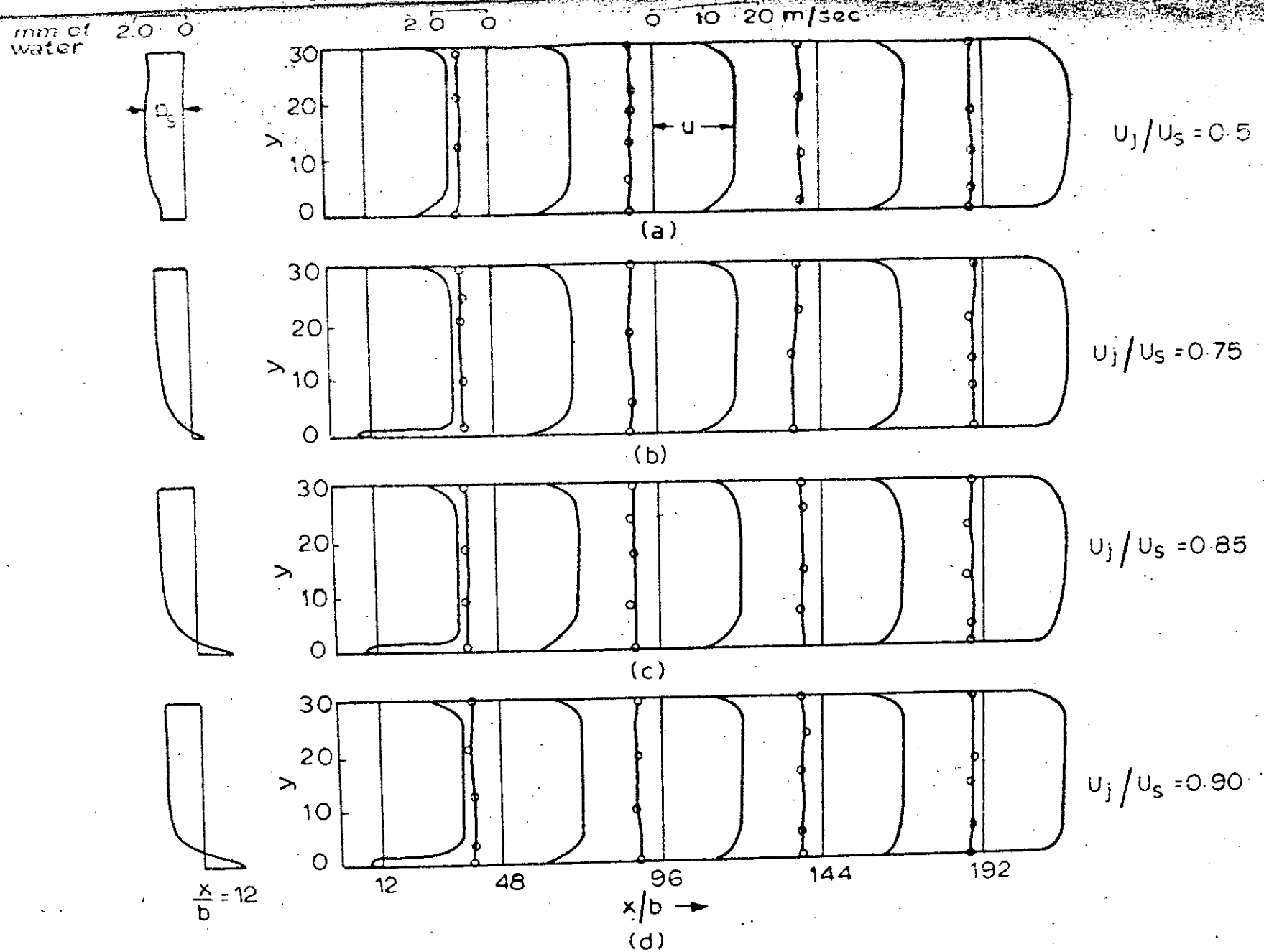

FIG. 5.1: MEASURED VELOCITY AND STATIC PRESSURE FOR 90° INJECTION

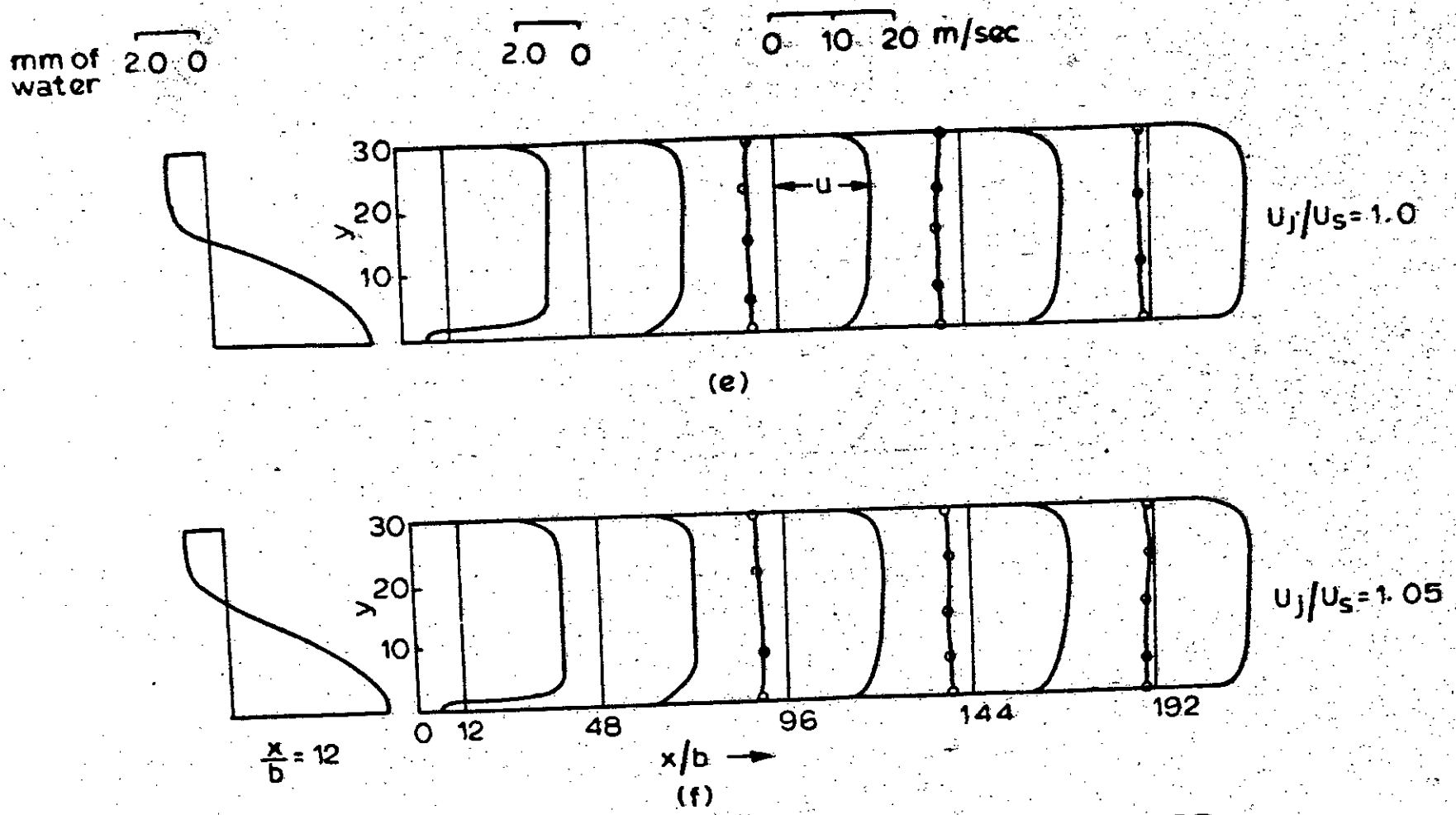

FIG.5.1: MEASURED VELOCITY AND STATIC PRESSURE FOR 90° INJECTION

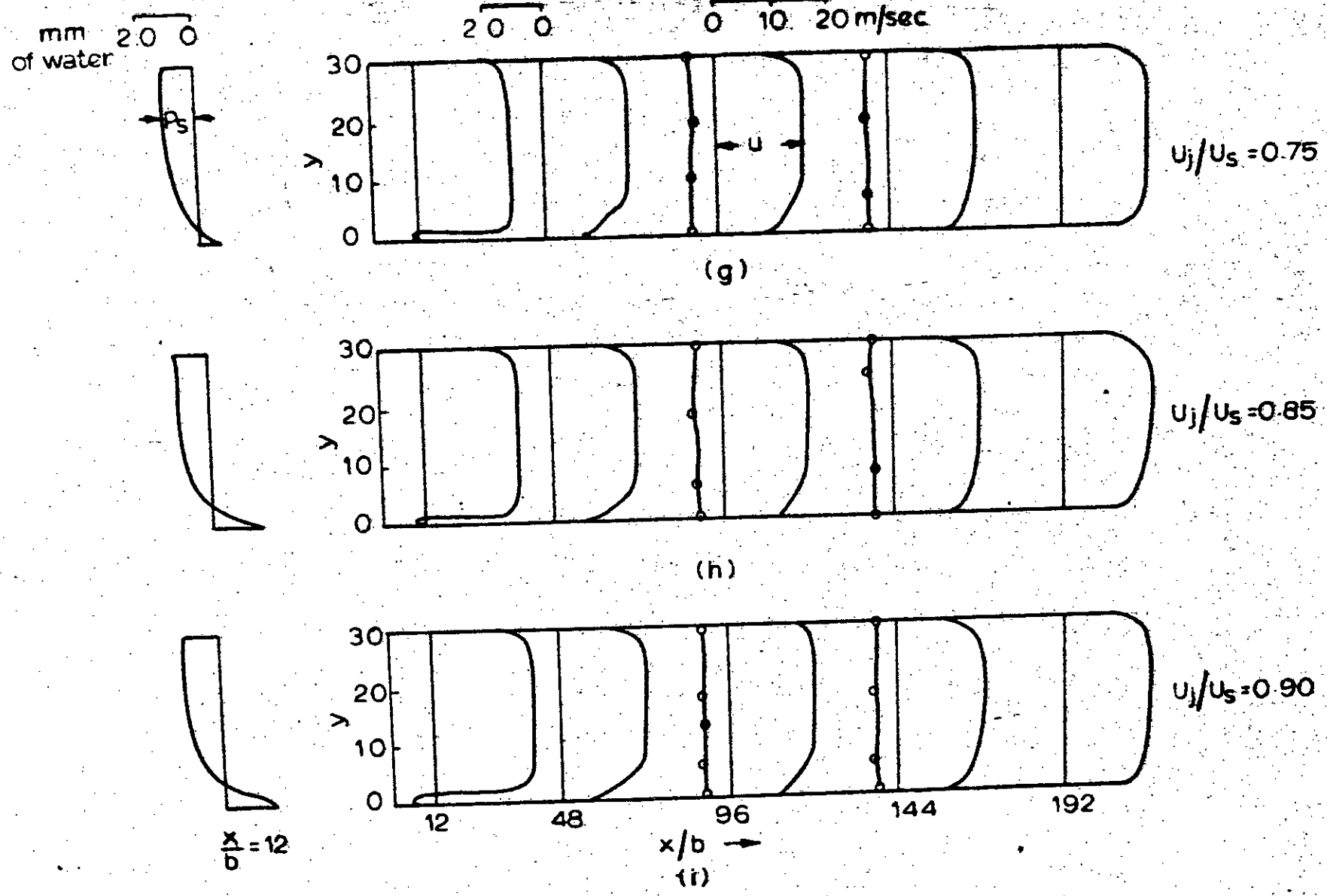

FIG. 5.1: MEASURED VELOCITY AND STATIC PRESSURE FOR 127° INJECTION

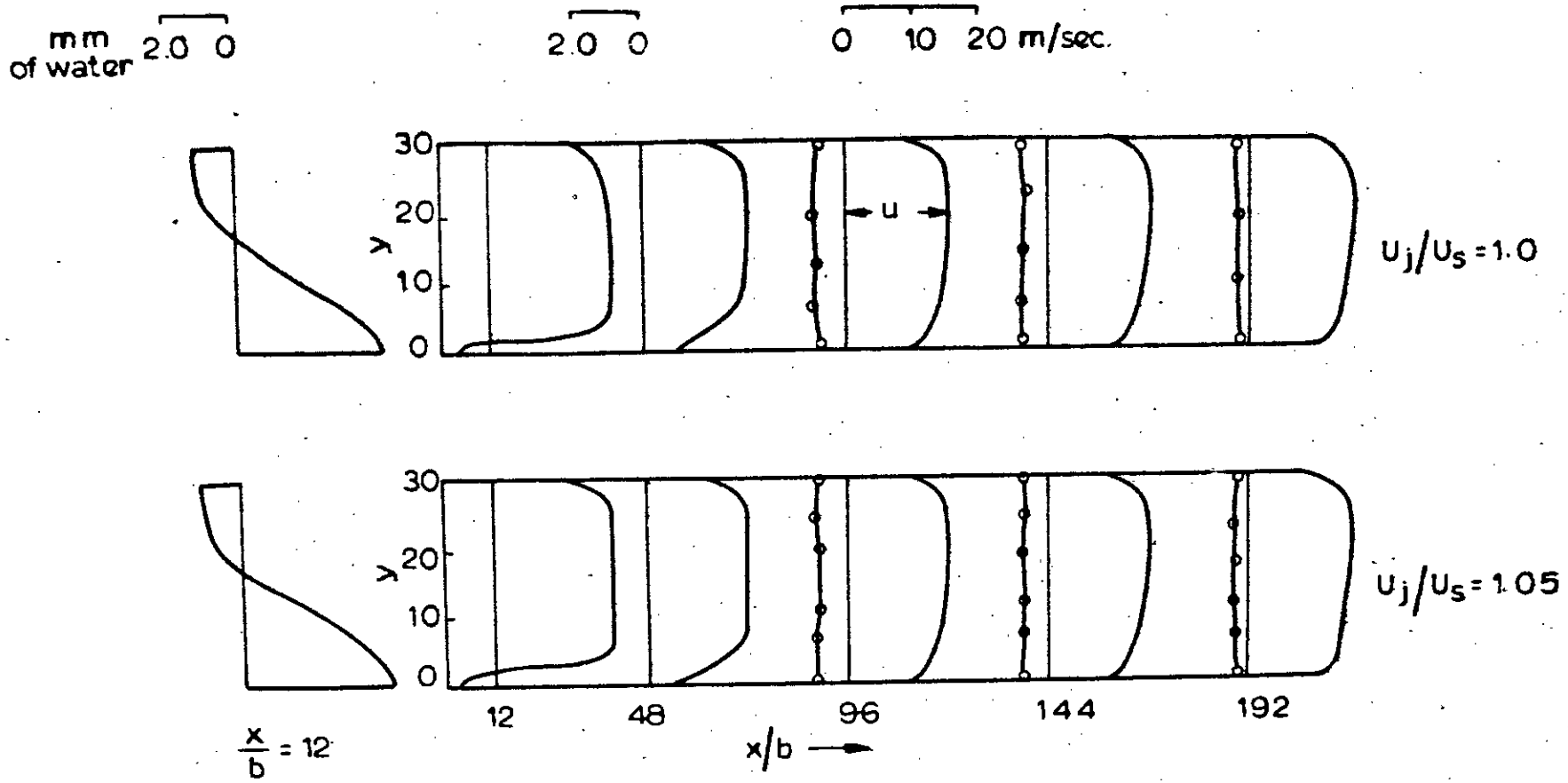

FIG. 5.1: MEASURED VELOCITY AND STATIC PRESSURE FOR 127° INJECTION

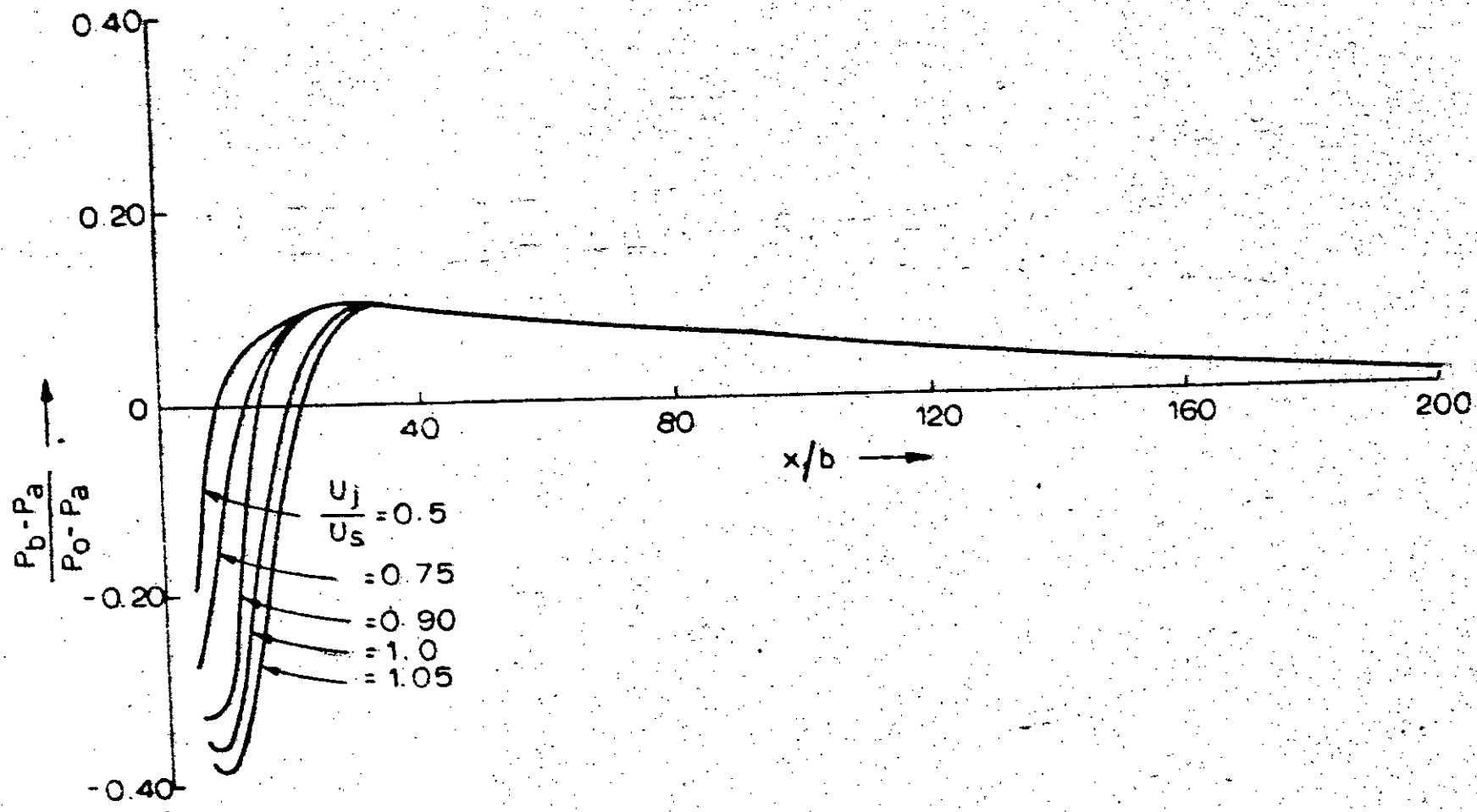

FIG. 5.2a: BASE PRESSURE DISTRIBUTION FOR 90° INJECTION

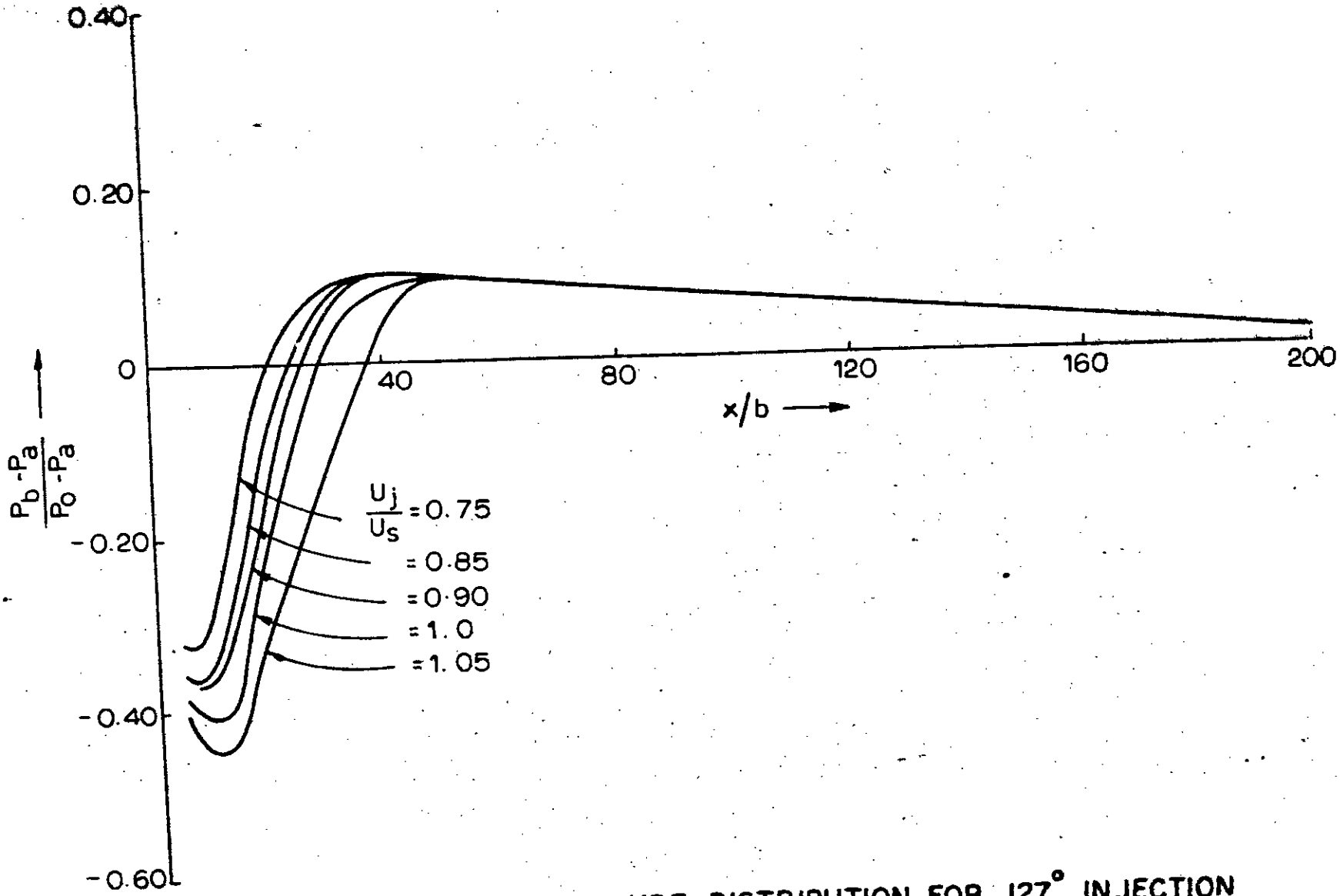

FIG. 5.2b: BASE PRESSURE DISTRIBUTION FOR 127° INJECTION

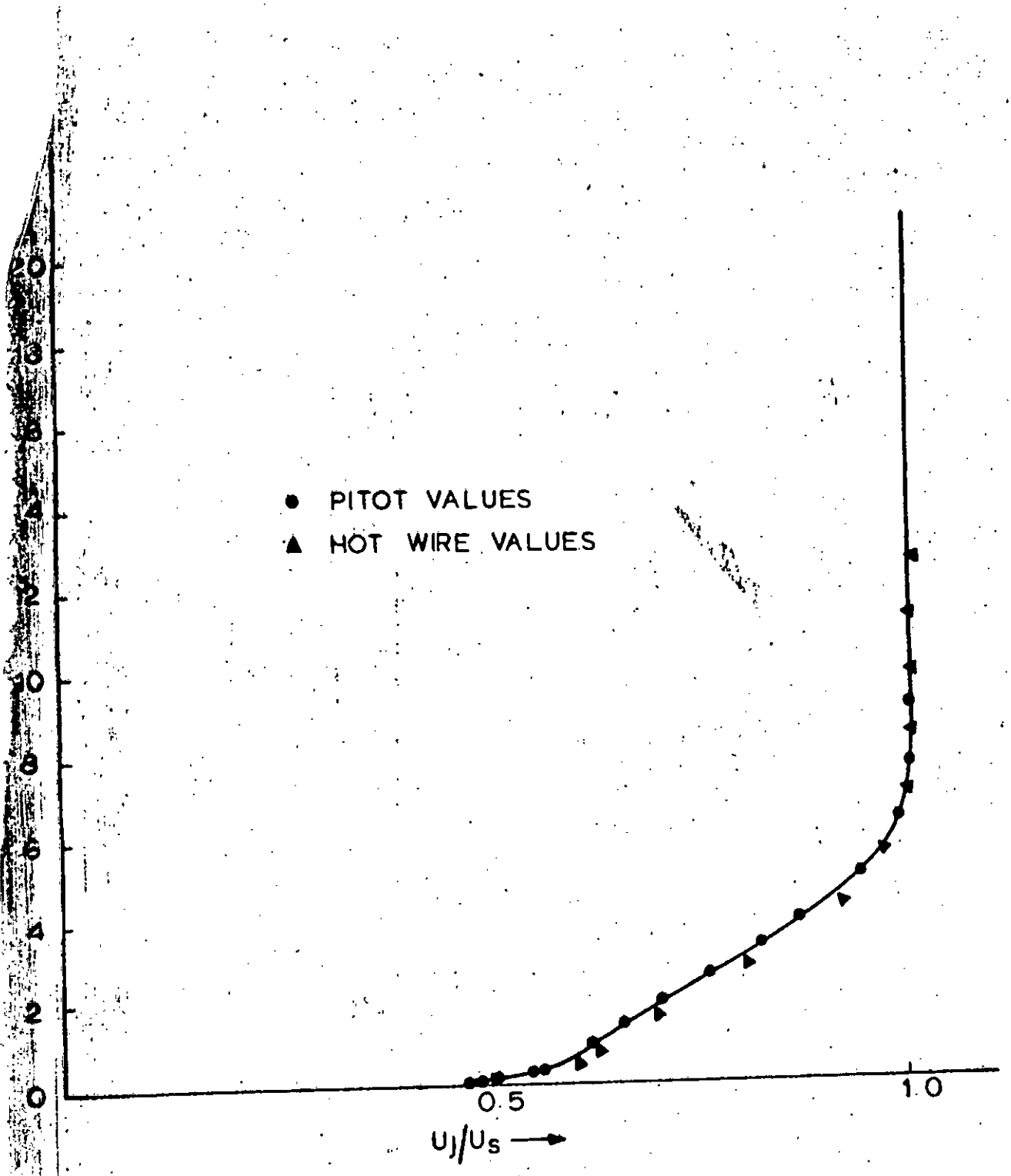

FIG. 5.3: MEAN VELOCITY PROFILE

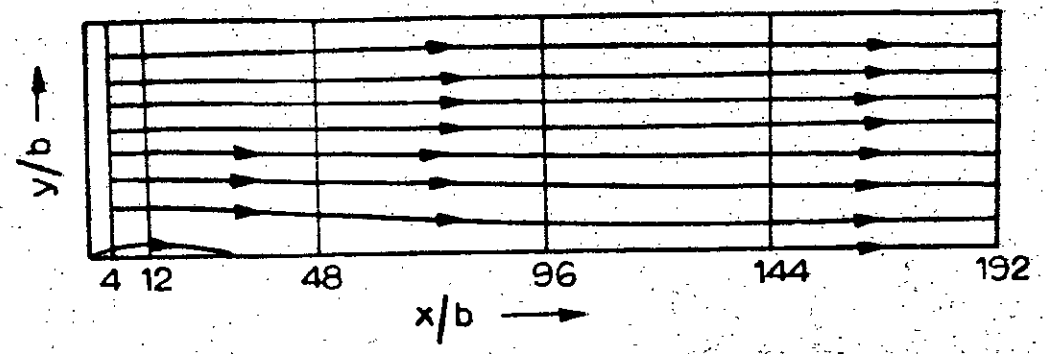

FIG. 5.4: TYPICAL STREAM LINE PATTERN FOR 127° INJECTION, U_j/U_s=1.0

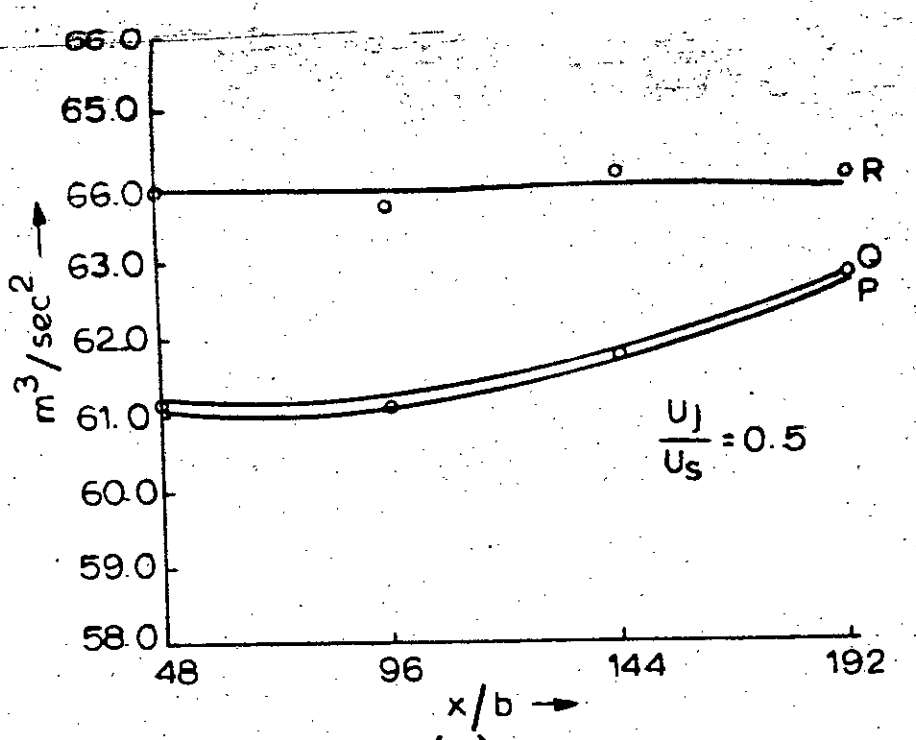

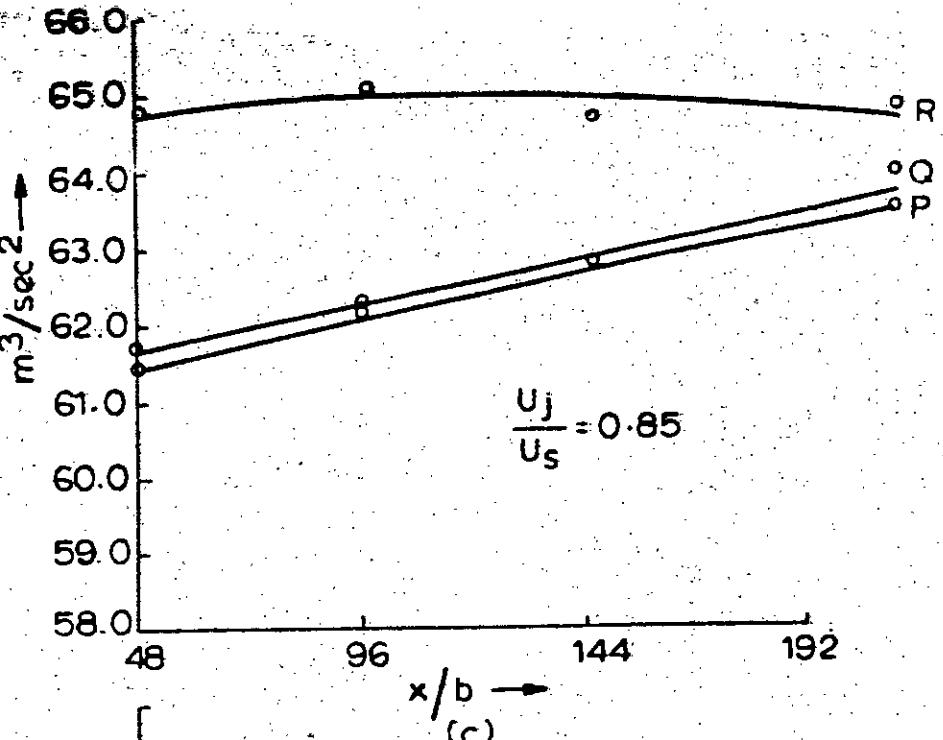

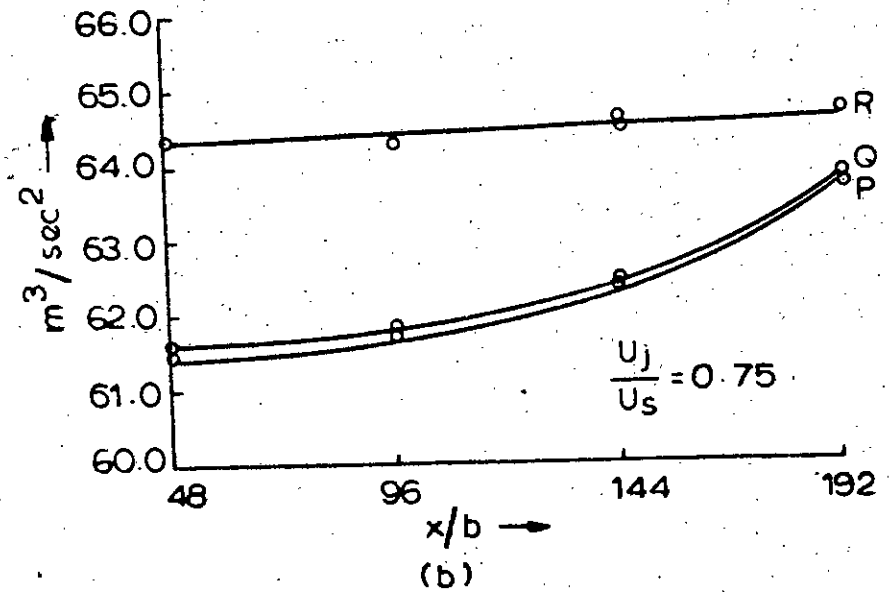

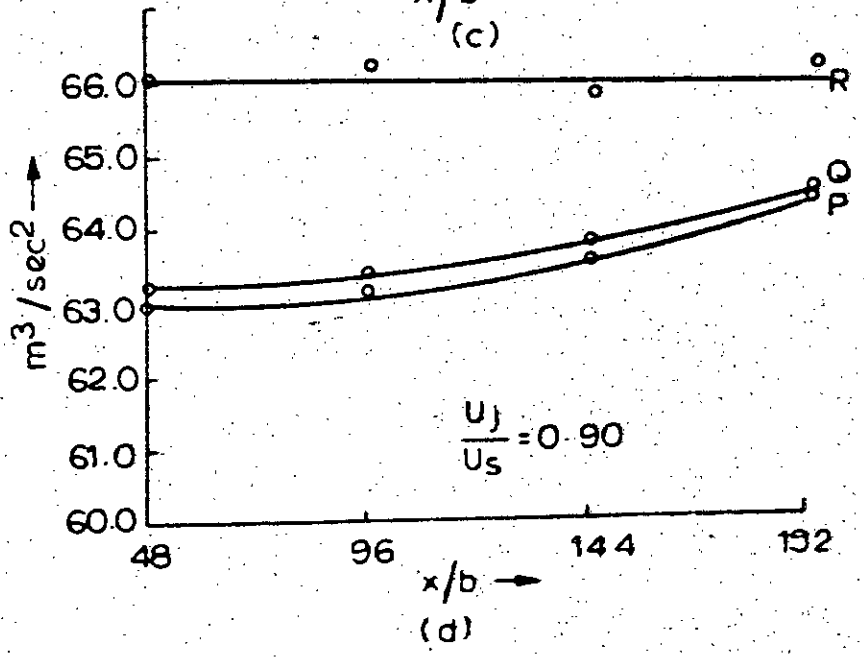

FIG. 5.5 : MOMENTUM ANALYSIS FOR 90° INJECTION

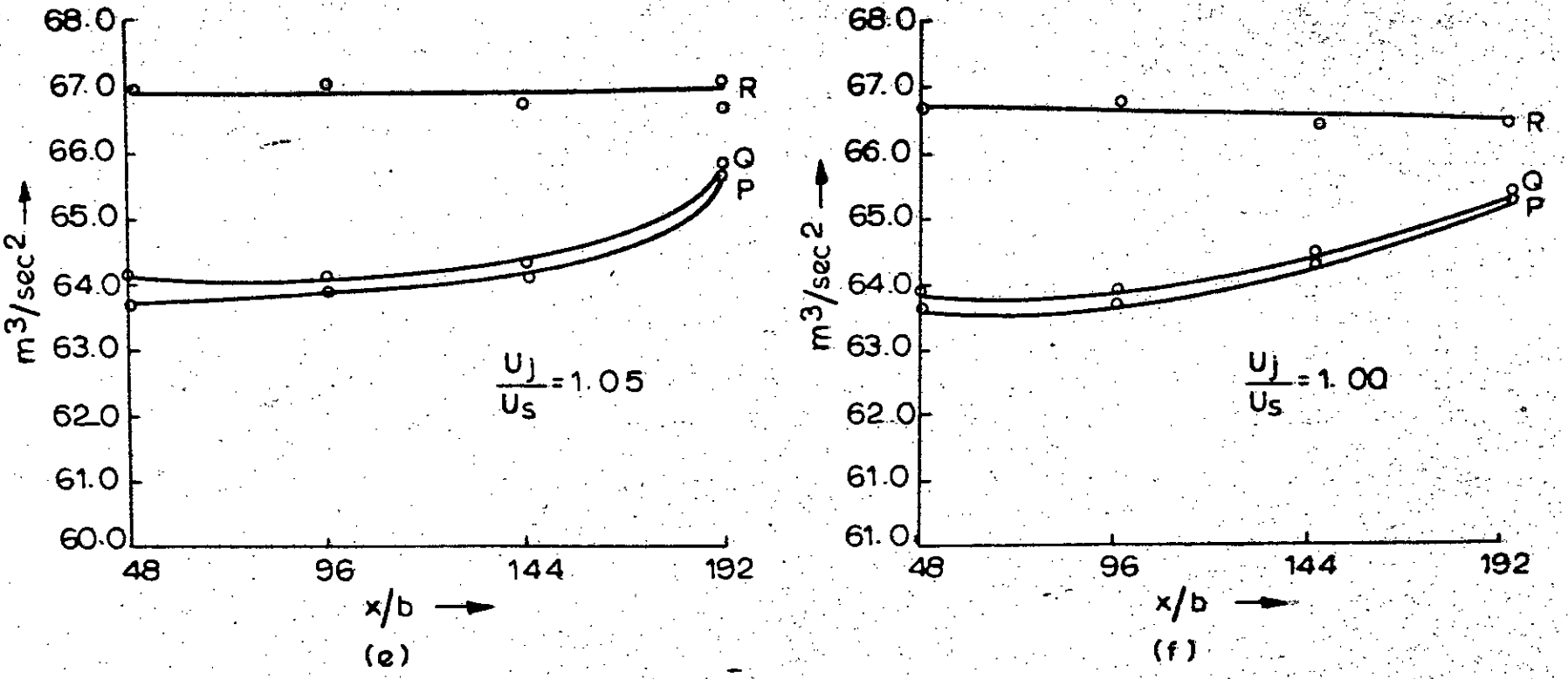

FIG. 5.5: MOMENTUM ANALYSIS FOR 90° INJECTION

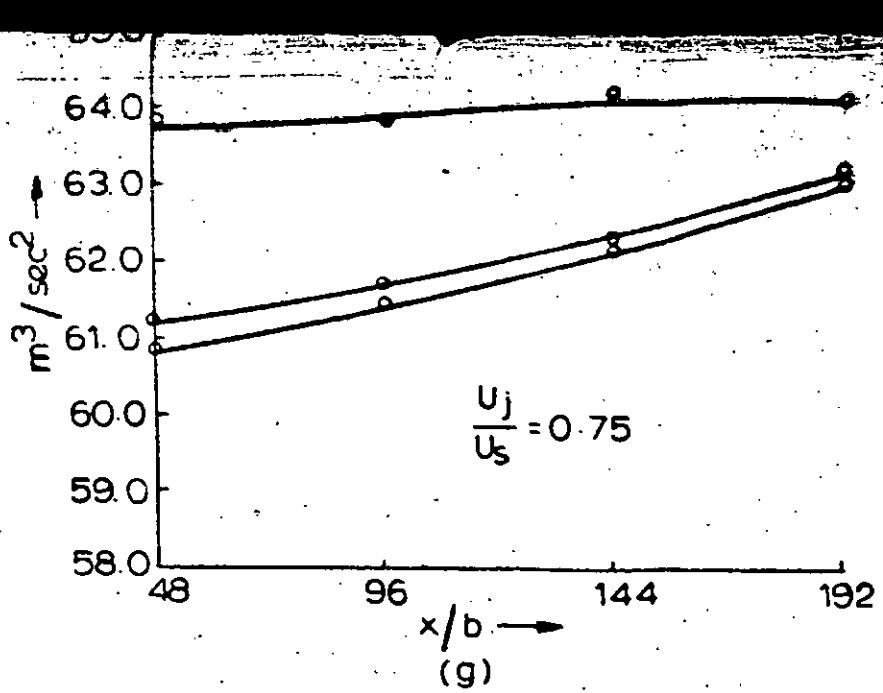

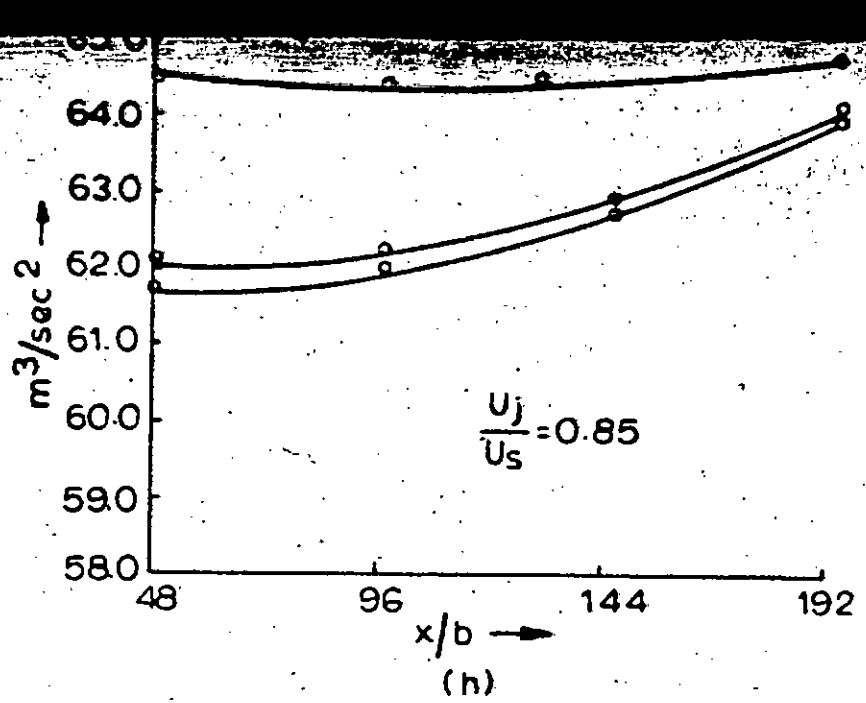

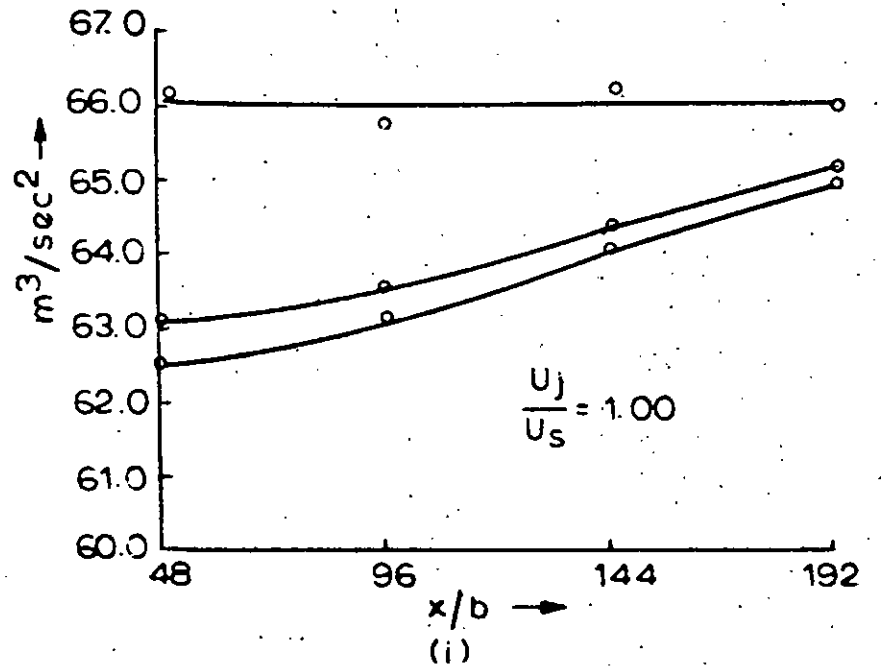

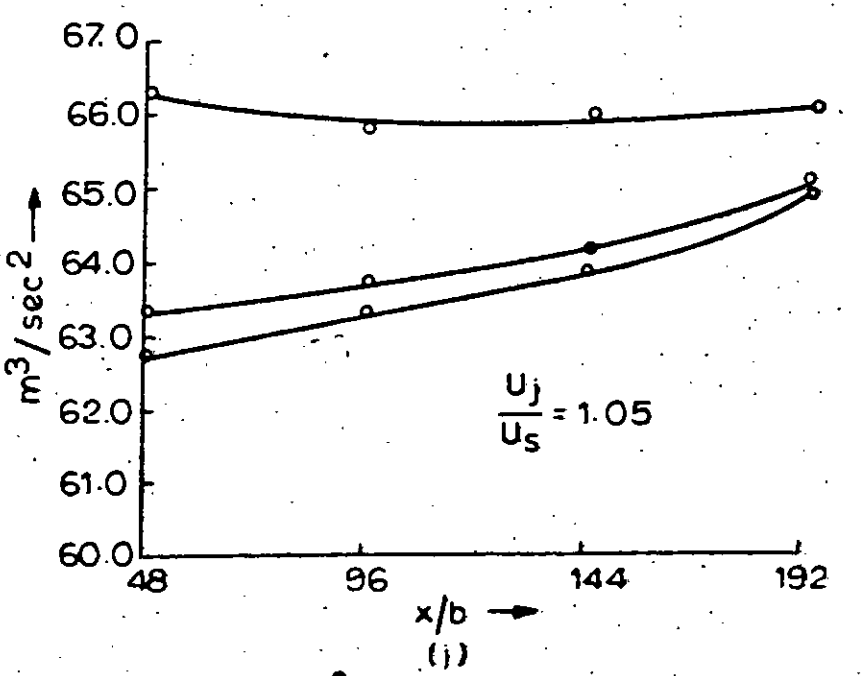

FIG. 5.5: MOMENTUM ANALYSIS FOR 127° INJECTION

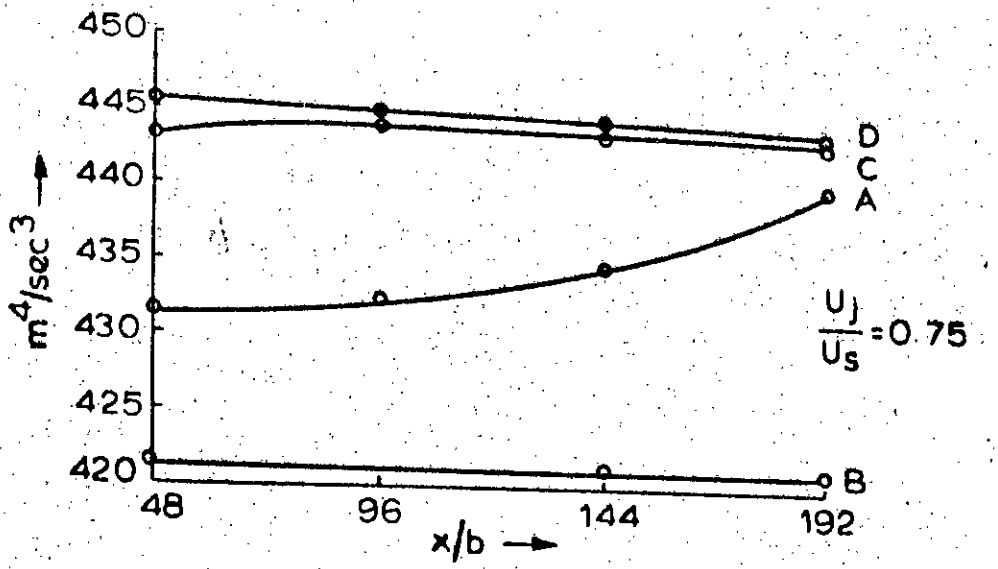

(a)

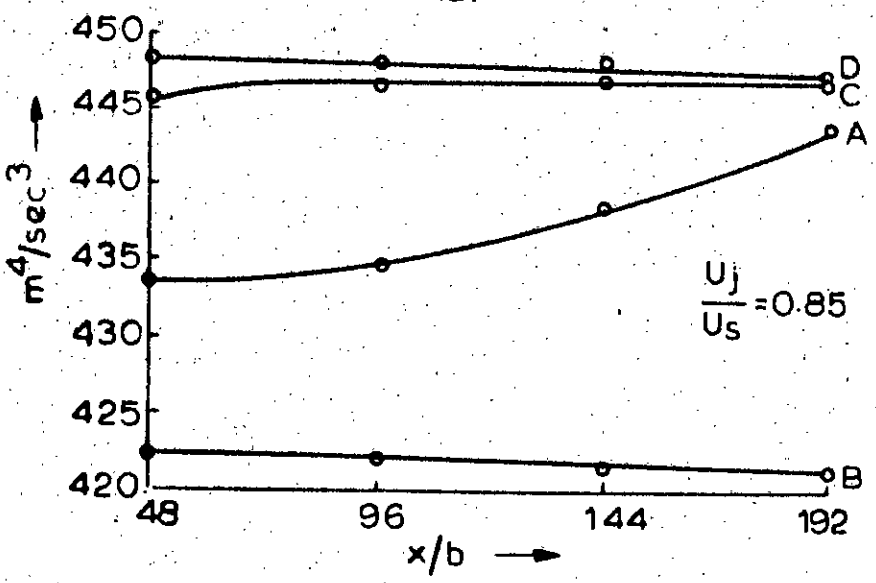

(b)

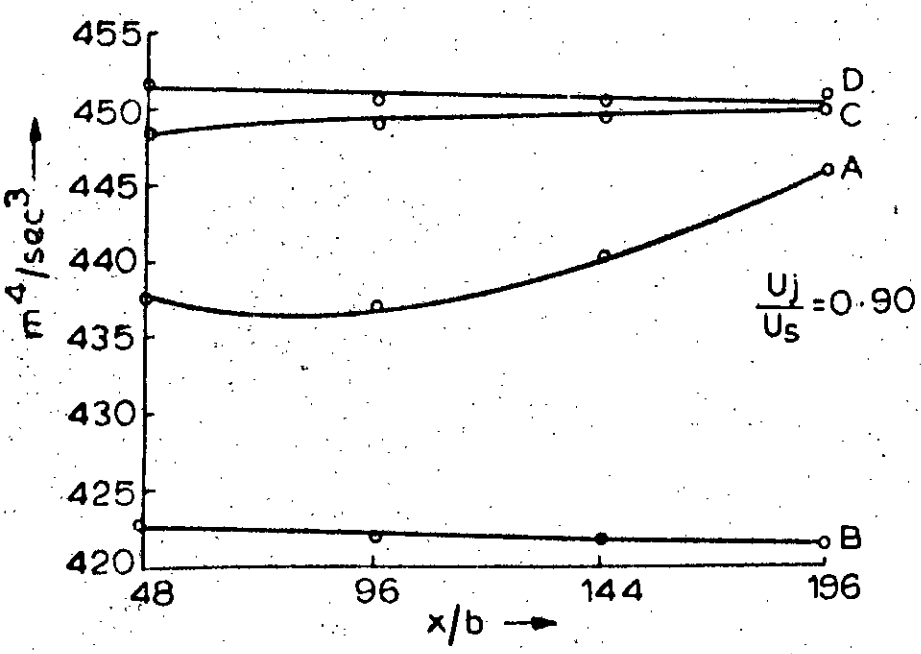

(c)

FIG. 5.61 MEAN ENERGY ANALYSIS 90° INJECTION

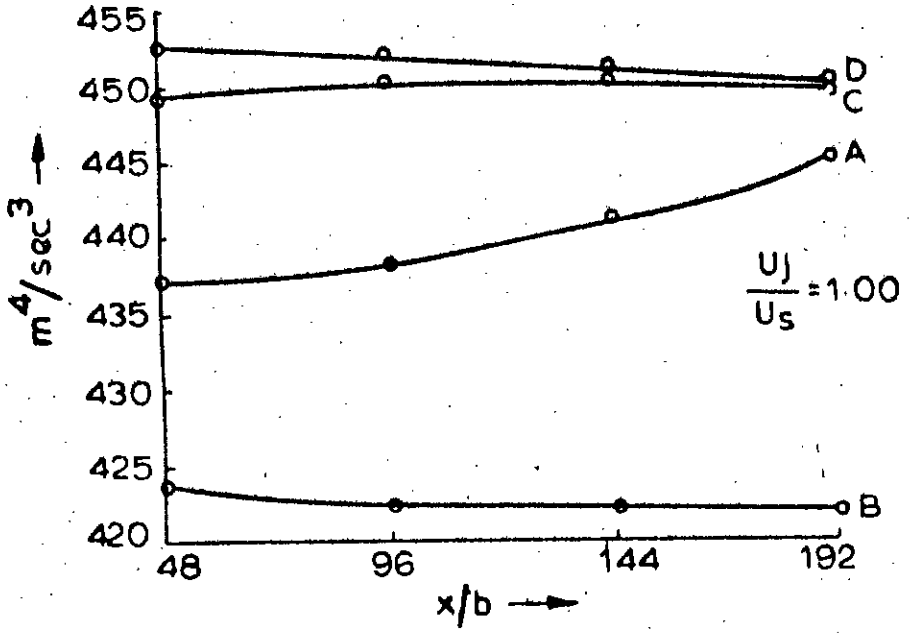

(d)

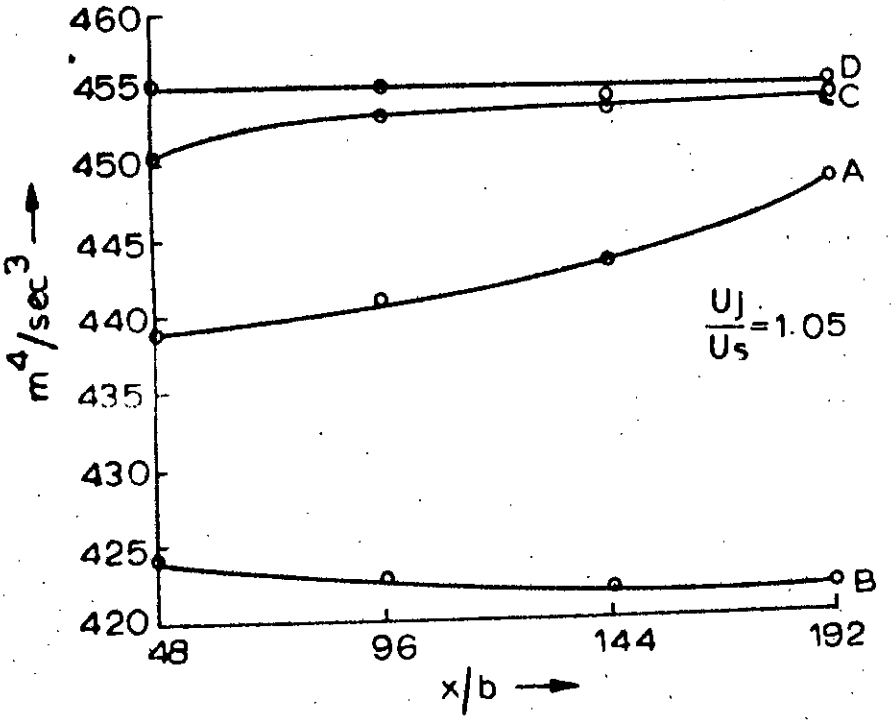

(e)

FIG. 5.6: MEAN ENERGY ANALYSIS 90° INJECTION

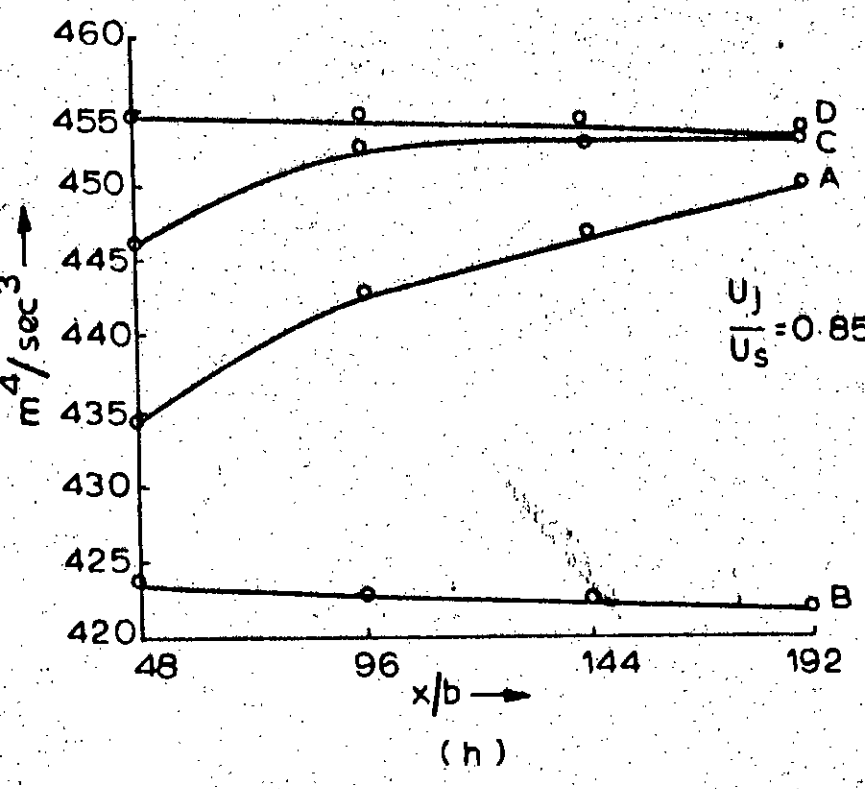

(h)

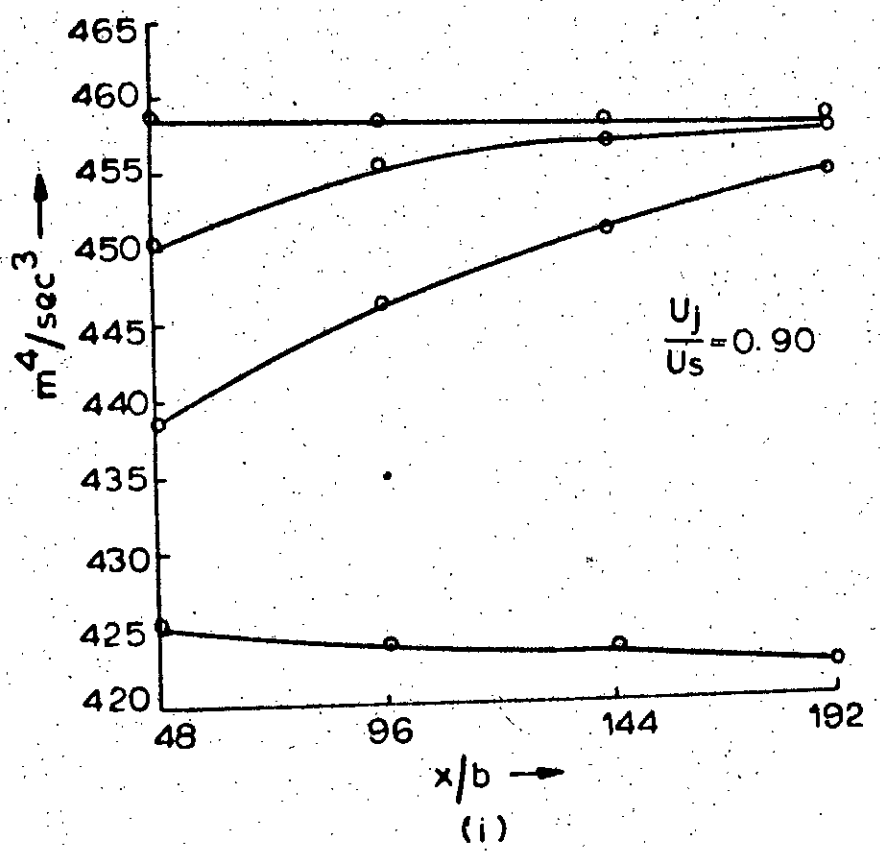

(i)

FIG. 5.6: MEAN ENERGY ANALYSIS 127° INJECTION

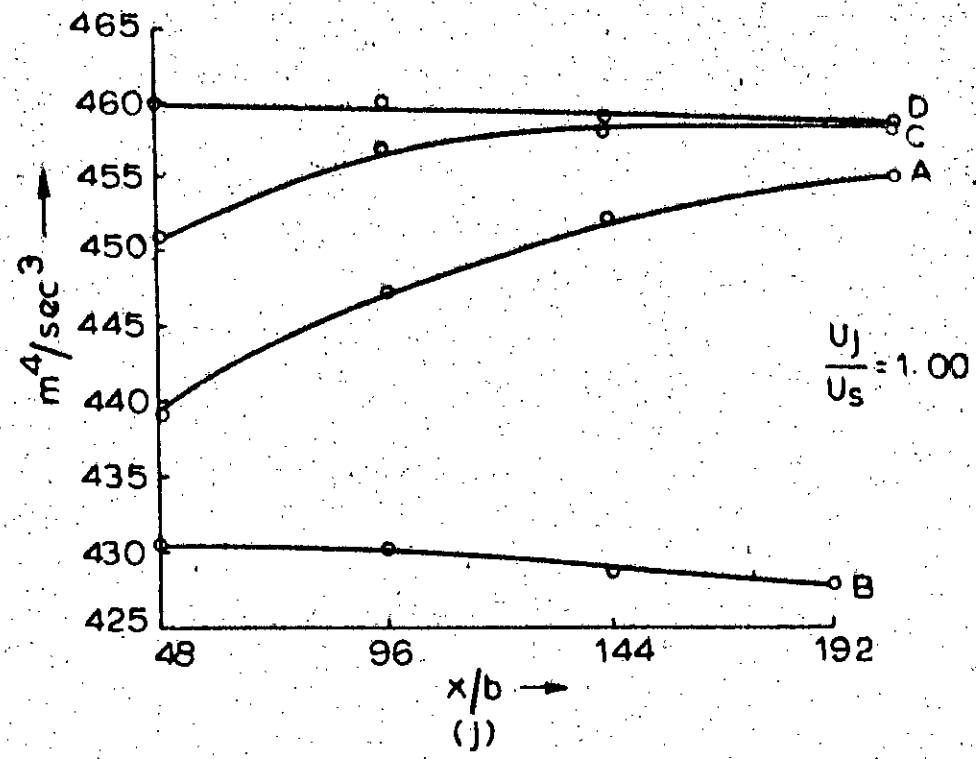

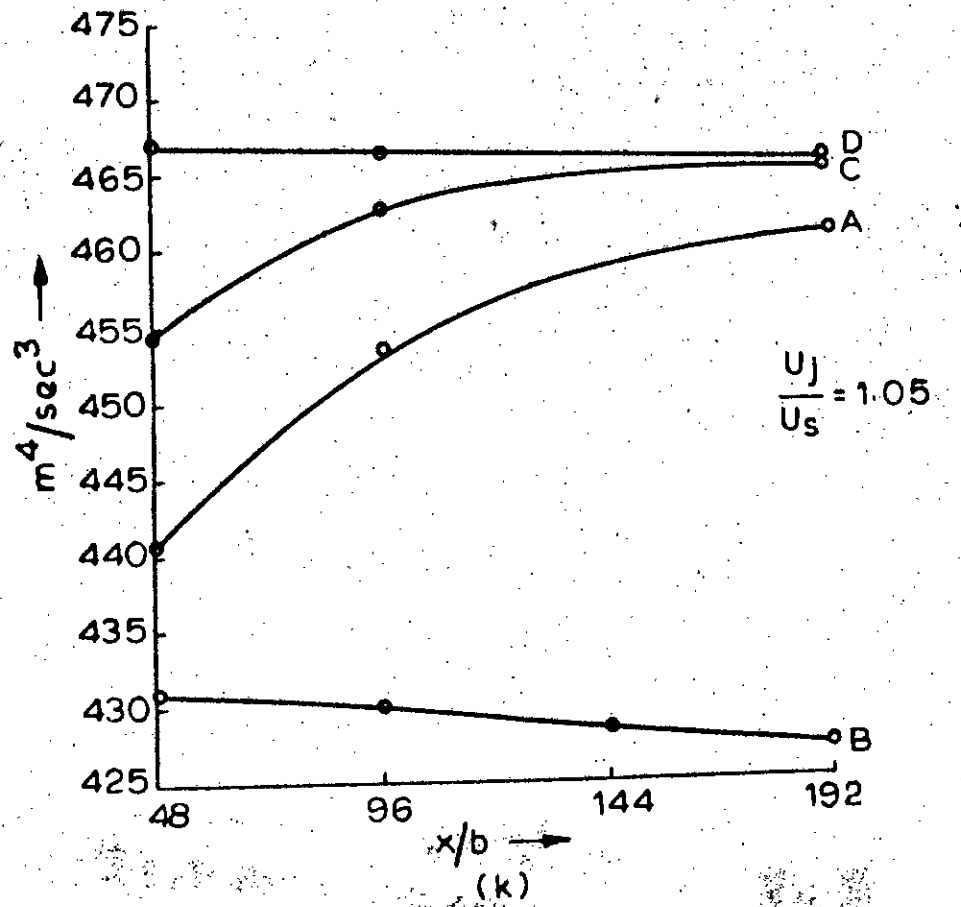

FIG.5.6: MEAN ENERGY ANALYSIS 127° INJECTION

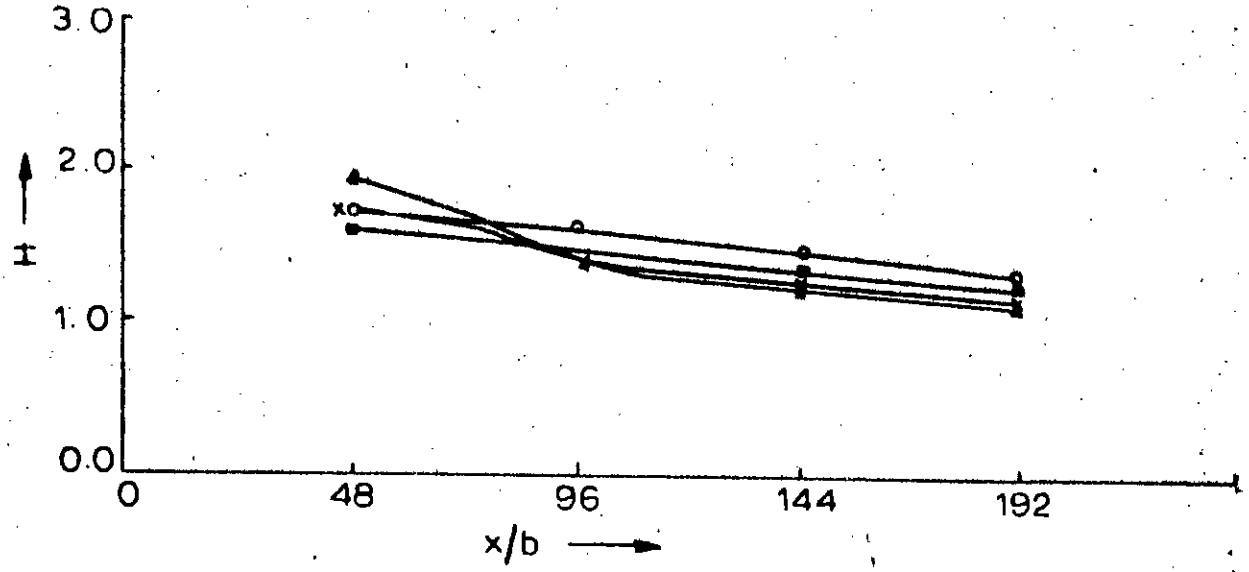

FIG. 5.7: H SHAPE FACTOR

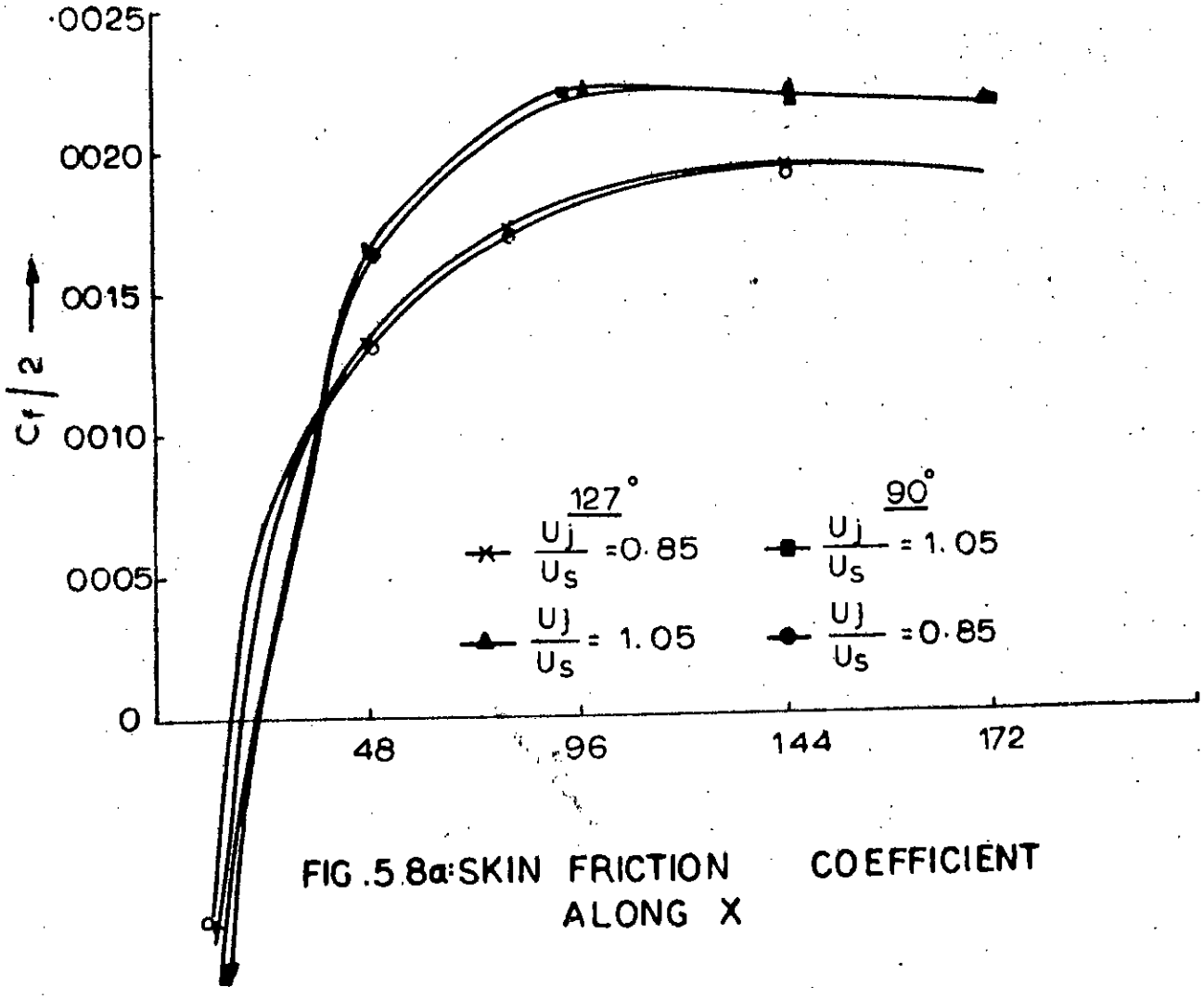

FIG .5.8a: SKIN FRICTION COEFFICIENT ALONG X

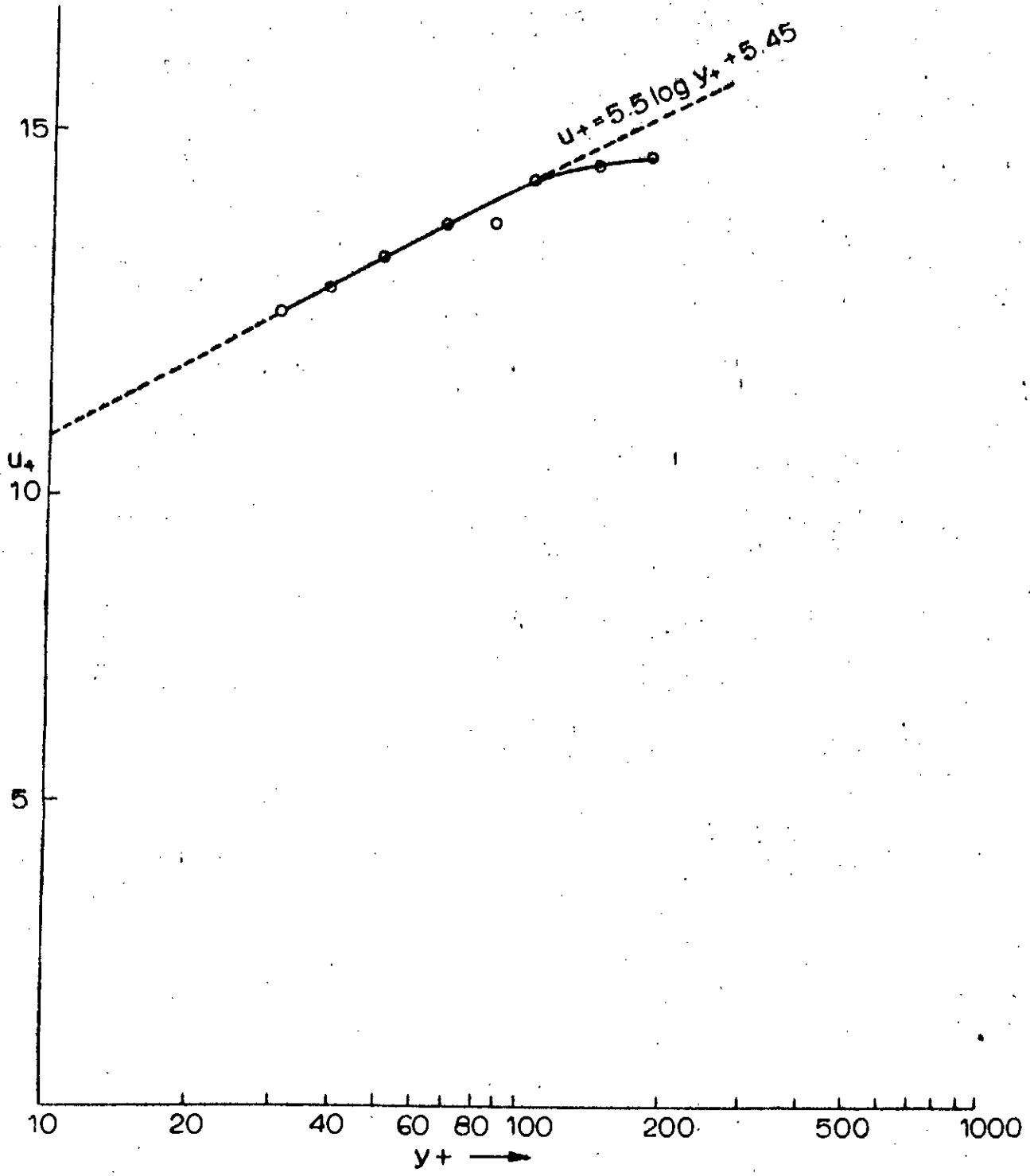

FIG. 5.8b: TYPICAL SEMILOGARTHMIC PLOT OF MEAN VELOCITY (U_J/U_S=0·9; 90° INJECTION)

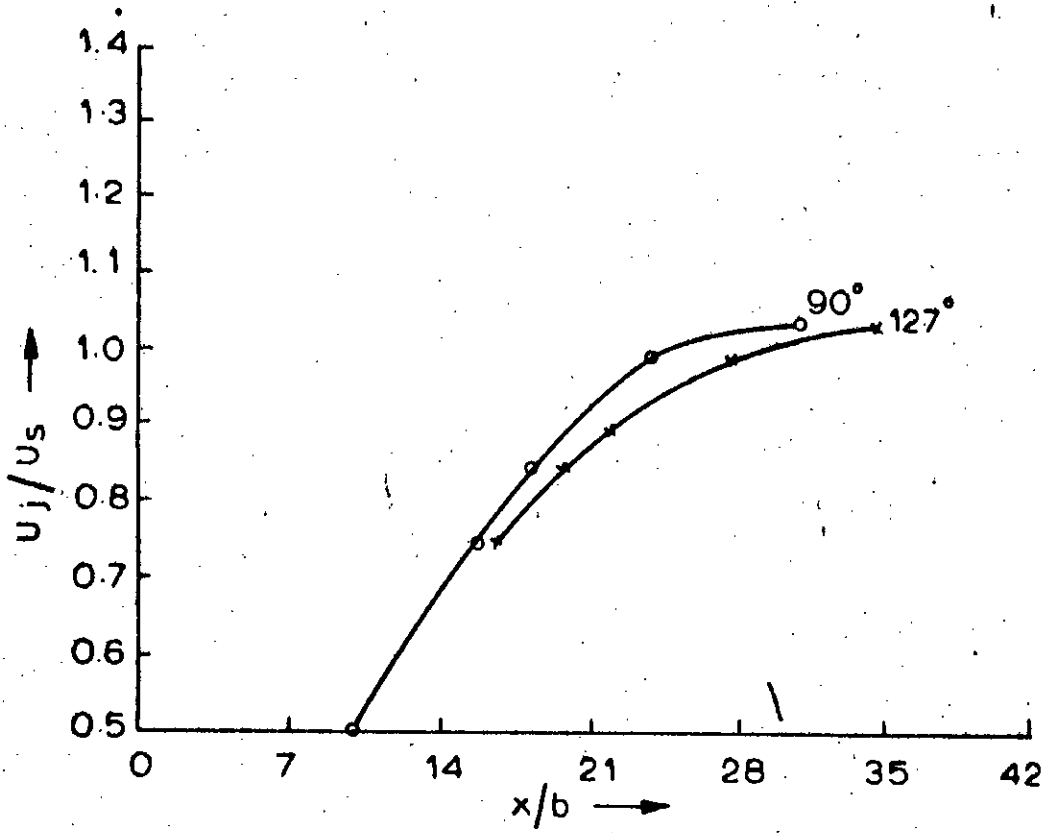

FIG. 5.9: REATTACHMENT DISTANCE

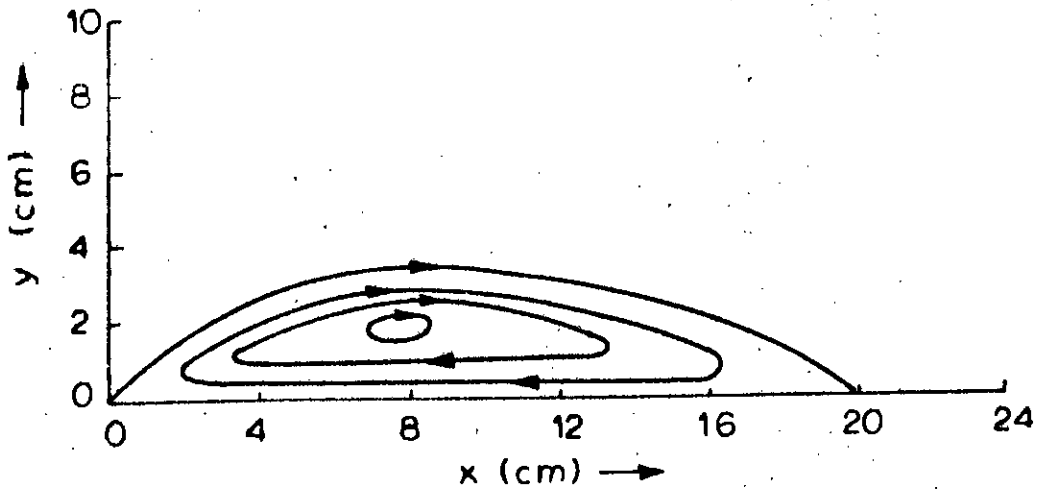

FIG. 5.10: APPROXIMATE STREAM LINE IN SEPARATION BUBBLE

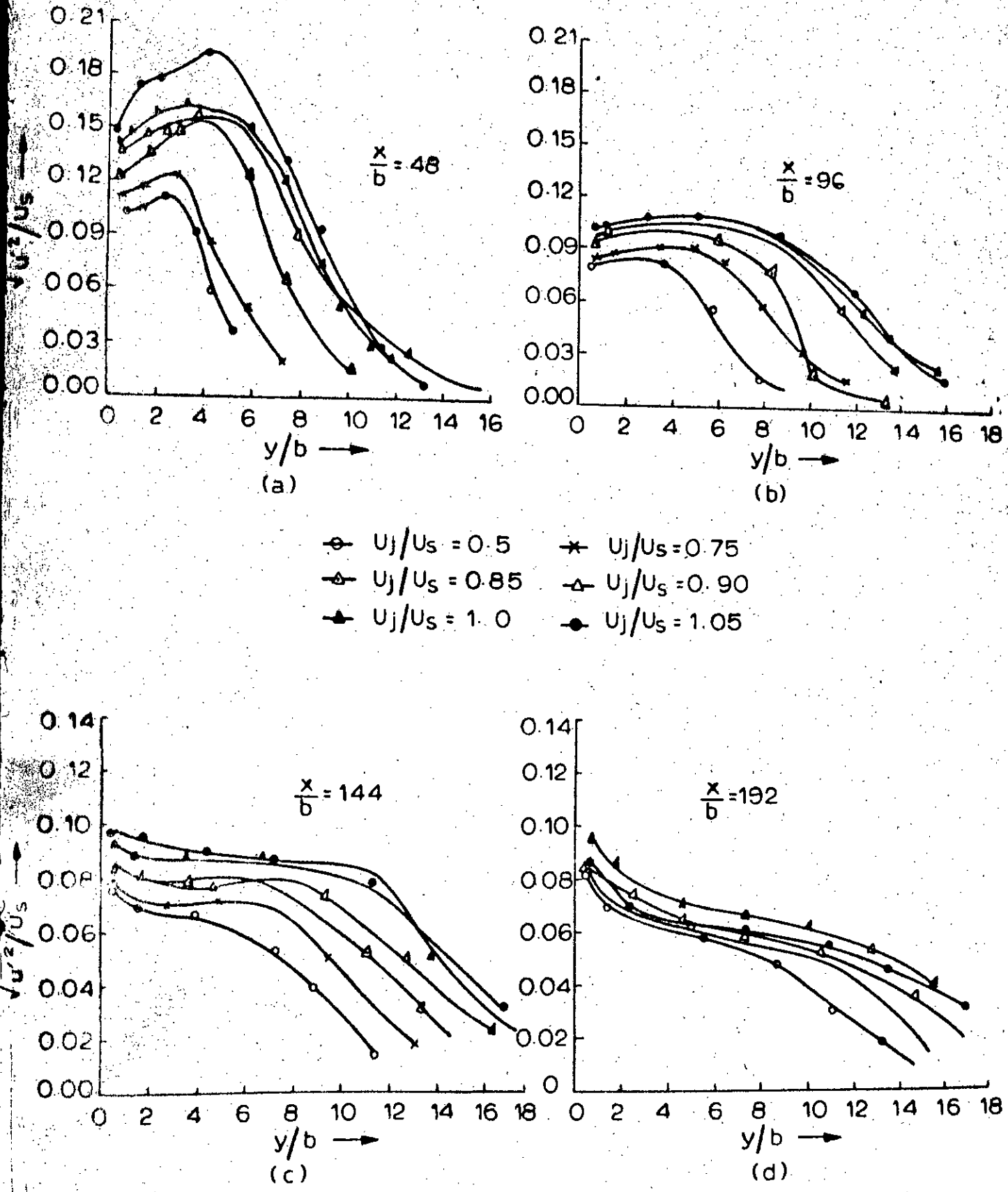

FIG. 5.11: $\sqrt{\overline{u'^2}}/U_S$ FOR 90° INJECTION

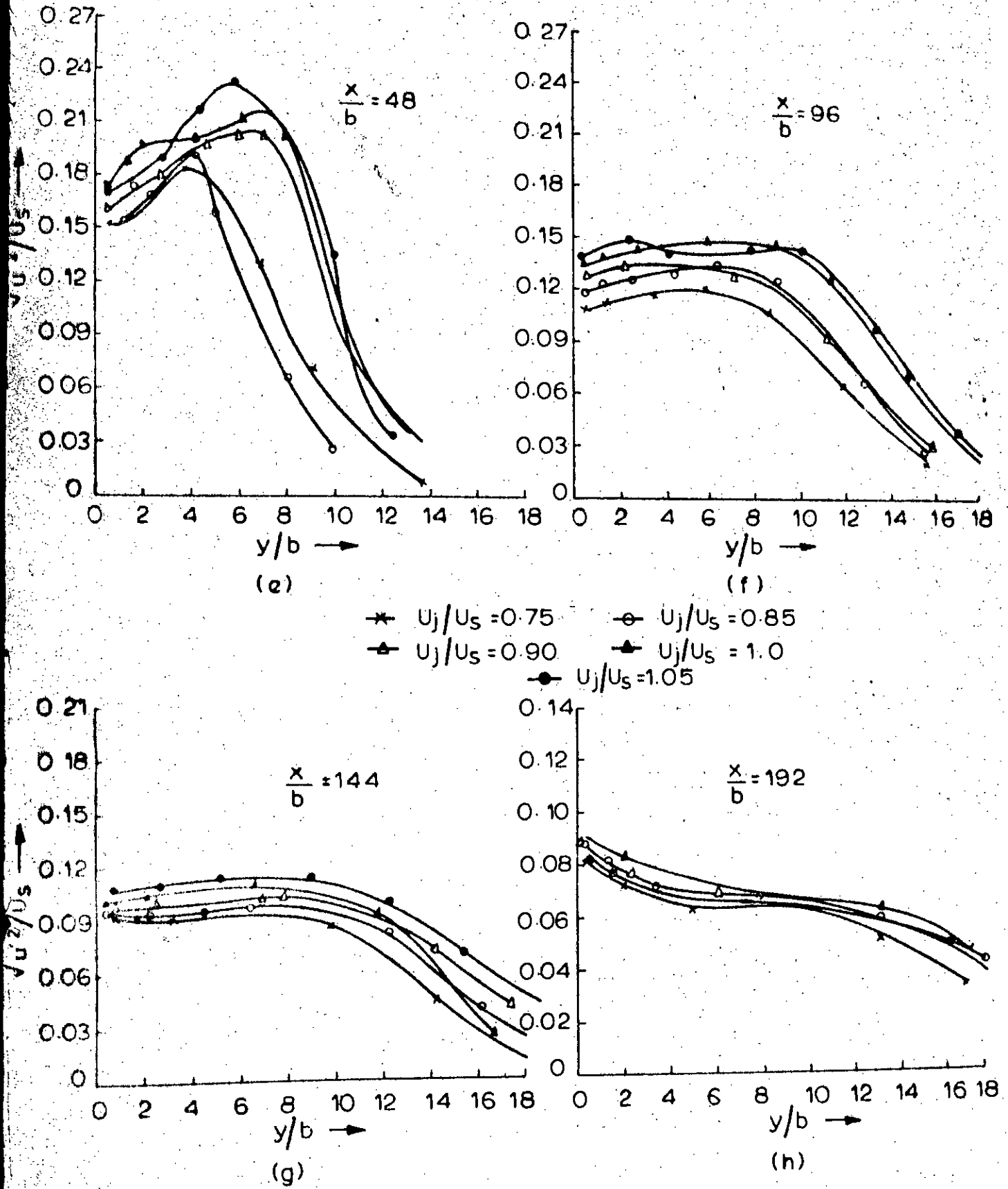

FIG. 5.11: $\sqrt{\overline{u'^2}}/U_s$ FOR 127° INJECTION

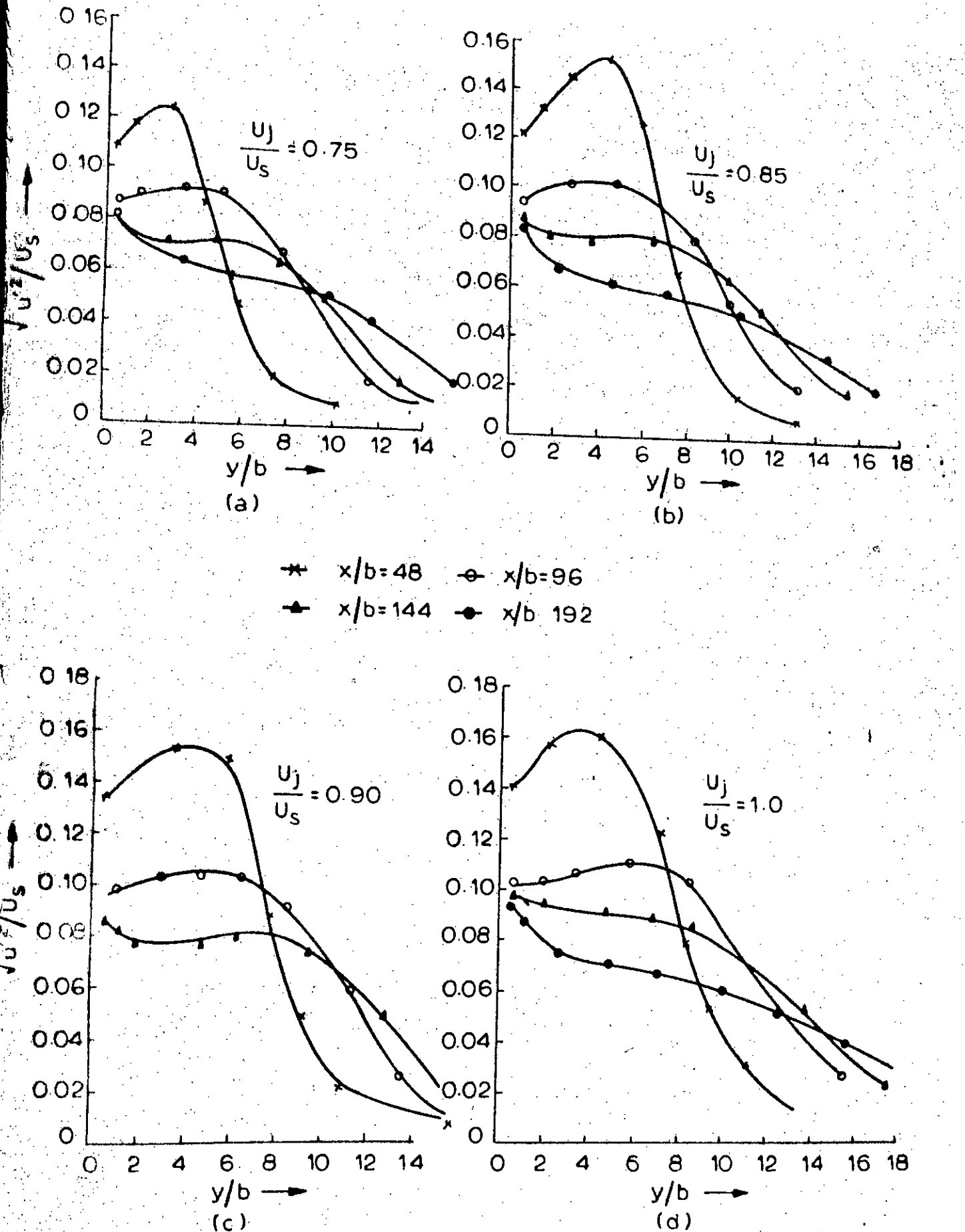

FIG. 5.12: $\sqrt{\overline{u'^2}}/U_s$ FOR 90° INJECTION

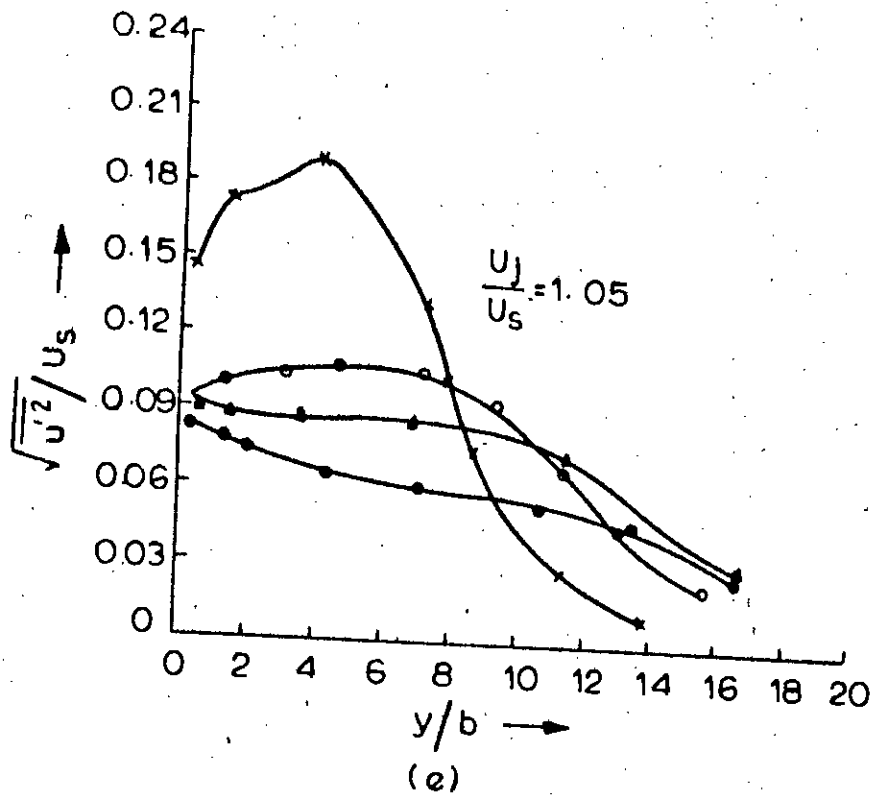

(e)

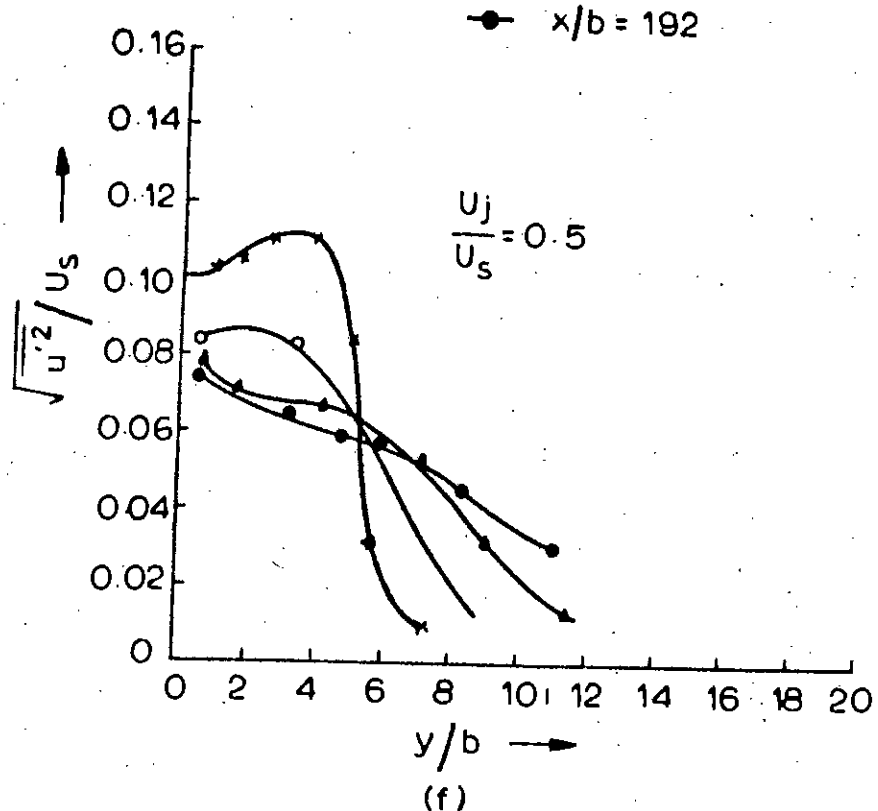

(f)

FIG.5.12: $\sqrt{\overline{u'^2}}/U_s$ FOR 90° INJECTION

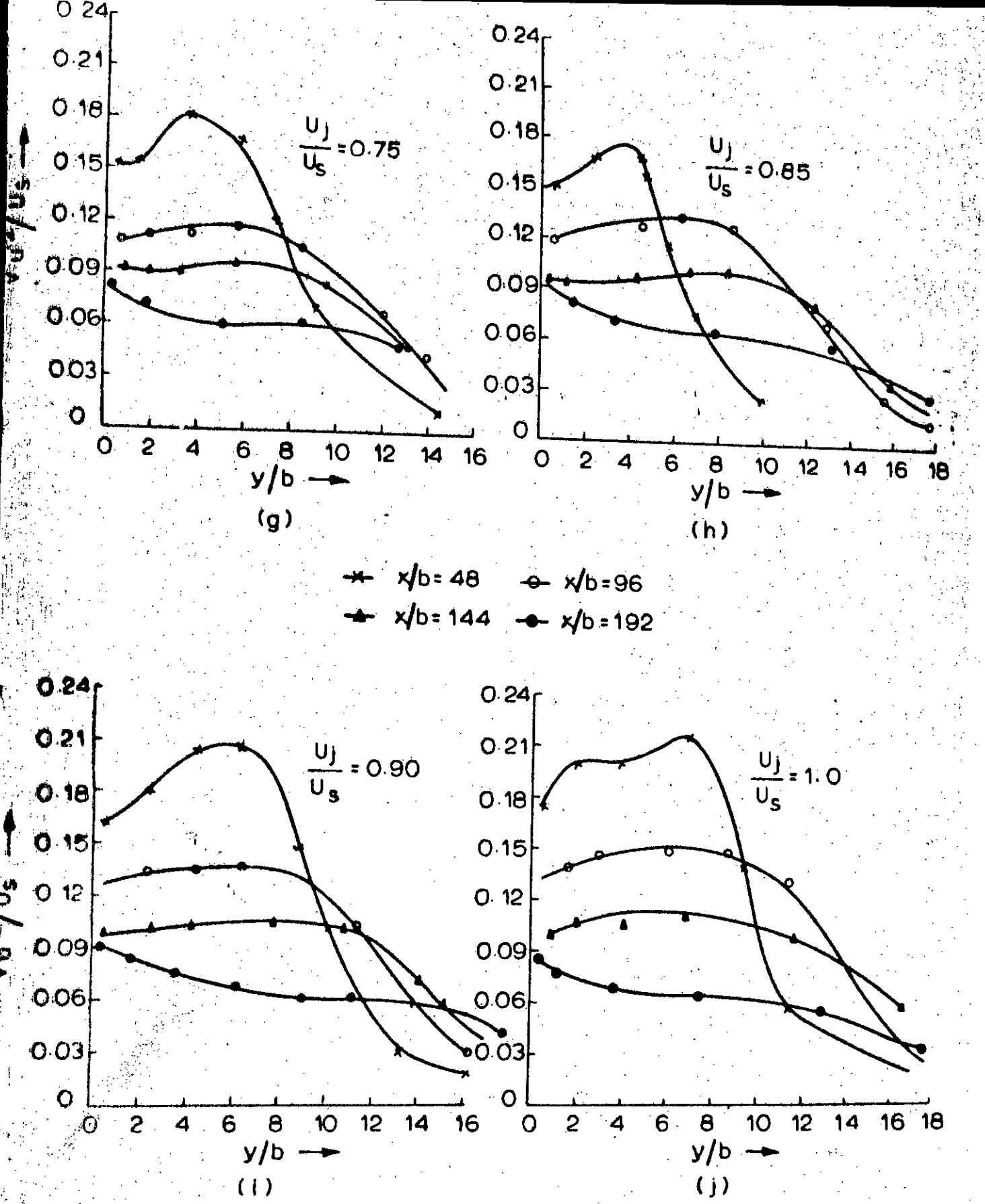

FIG. 5.12: $\sqrt{\overline{u'^2}}/U_s$ FOR 127° INJECTION

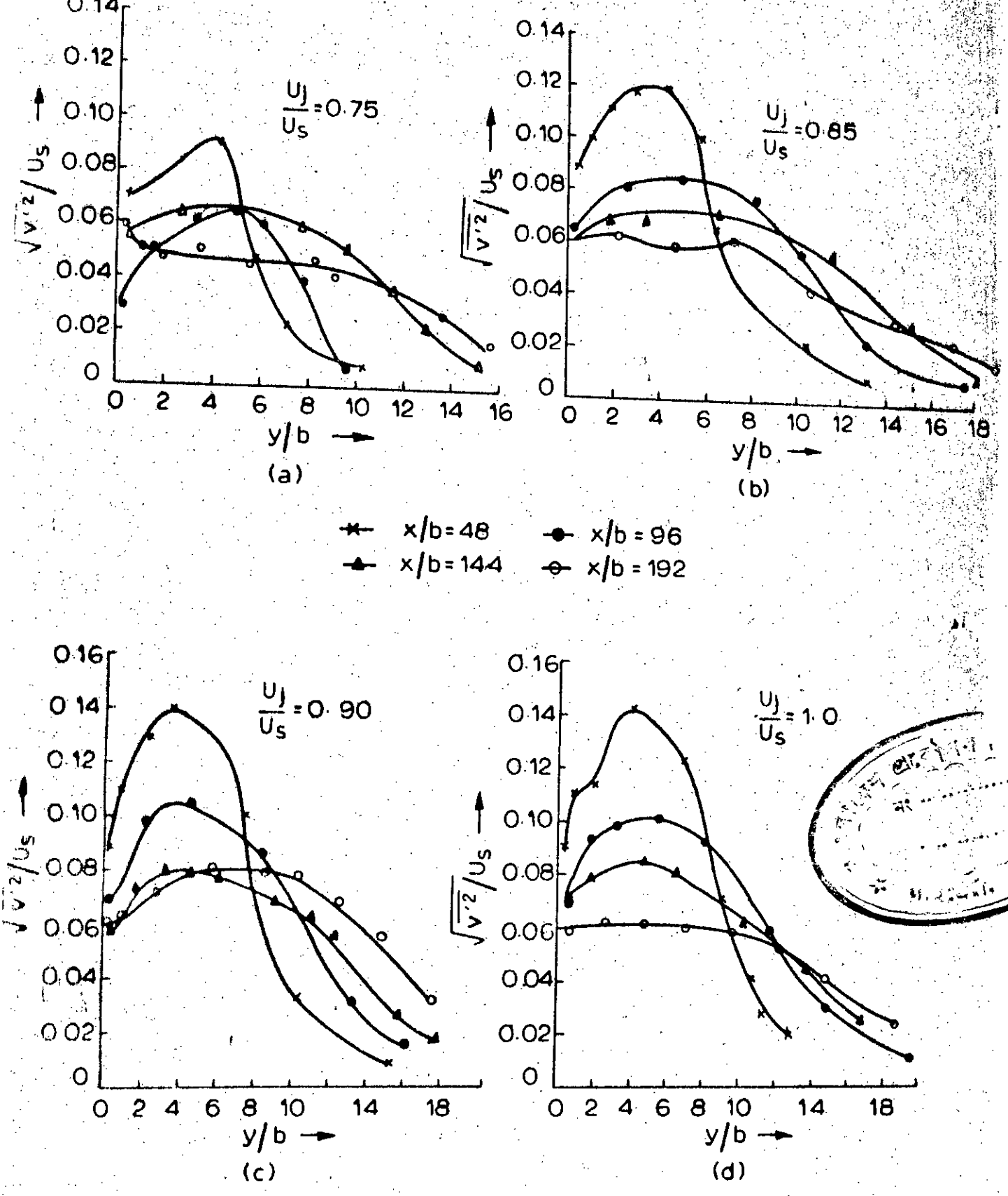

FIG. 5.13: $\sqrt{\overline{v'^2}}/U_s$ FOR 90° INJECTION

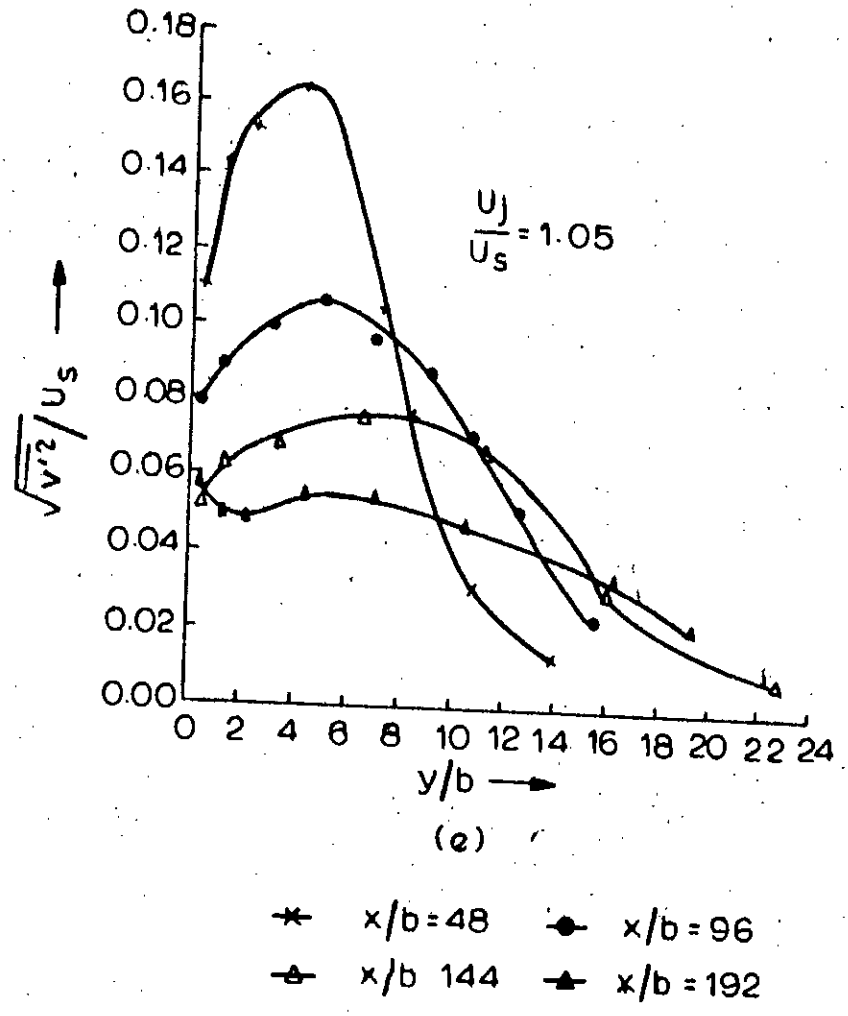

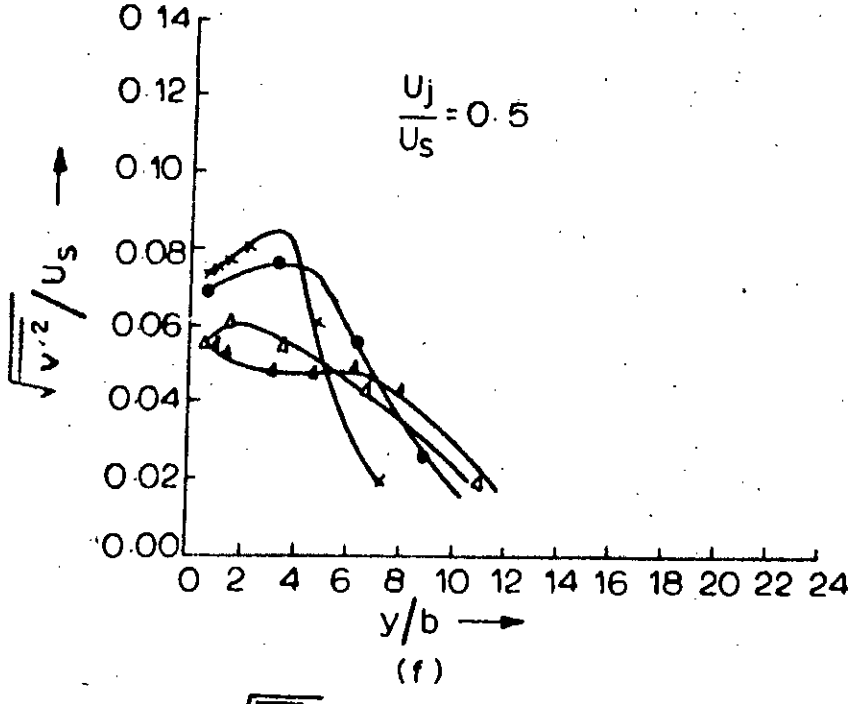

FIG. 5.13: $\sqrt{\overline{v'^2}}/U_S$ FOR 90° INJECTION

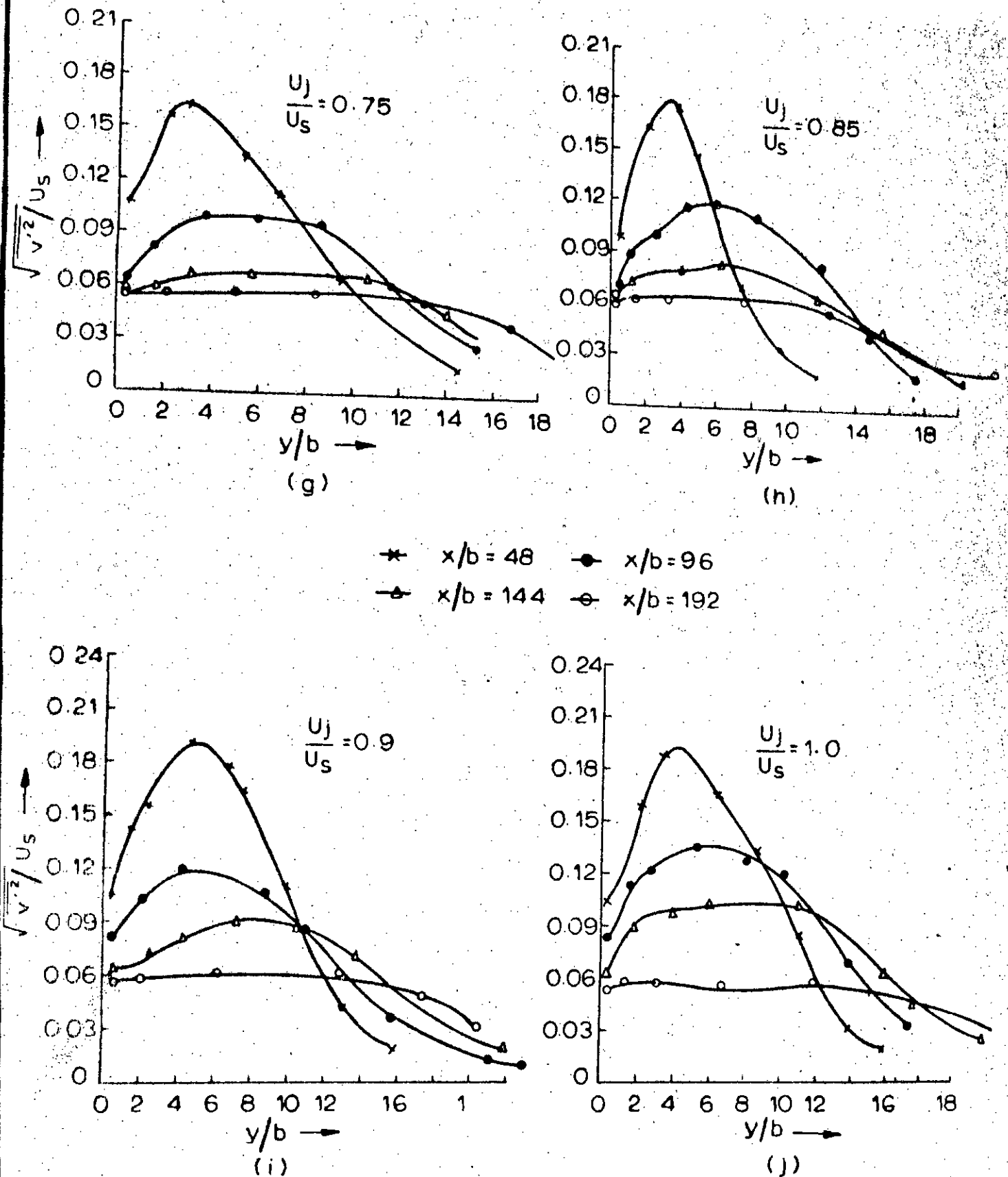

FIG. 5.13: $\sqrt{\overline{v'^2}}/U_s$ FOR 127° INJECTION

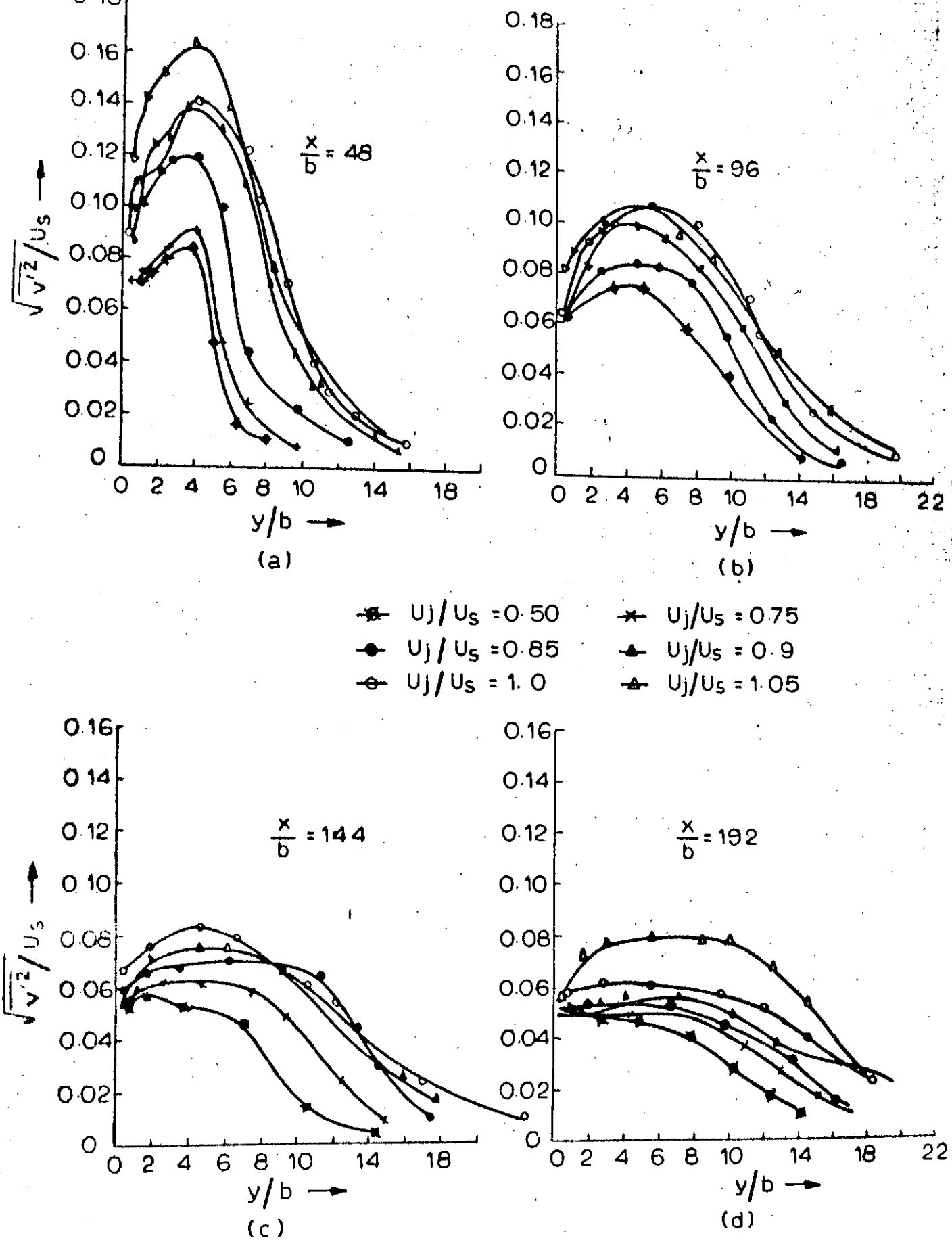

FIG. 5.14: $\sqrt{\overline{v'^2}}/U_s$ FOR 90° INJECTION

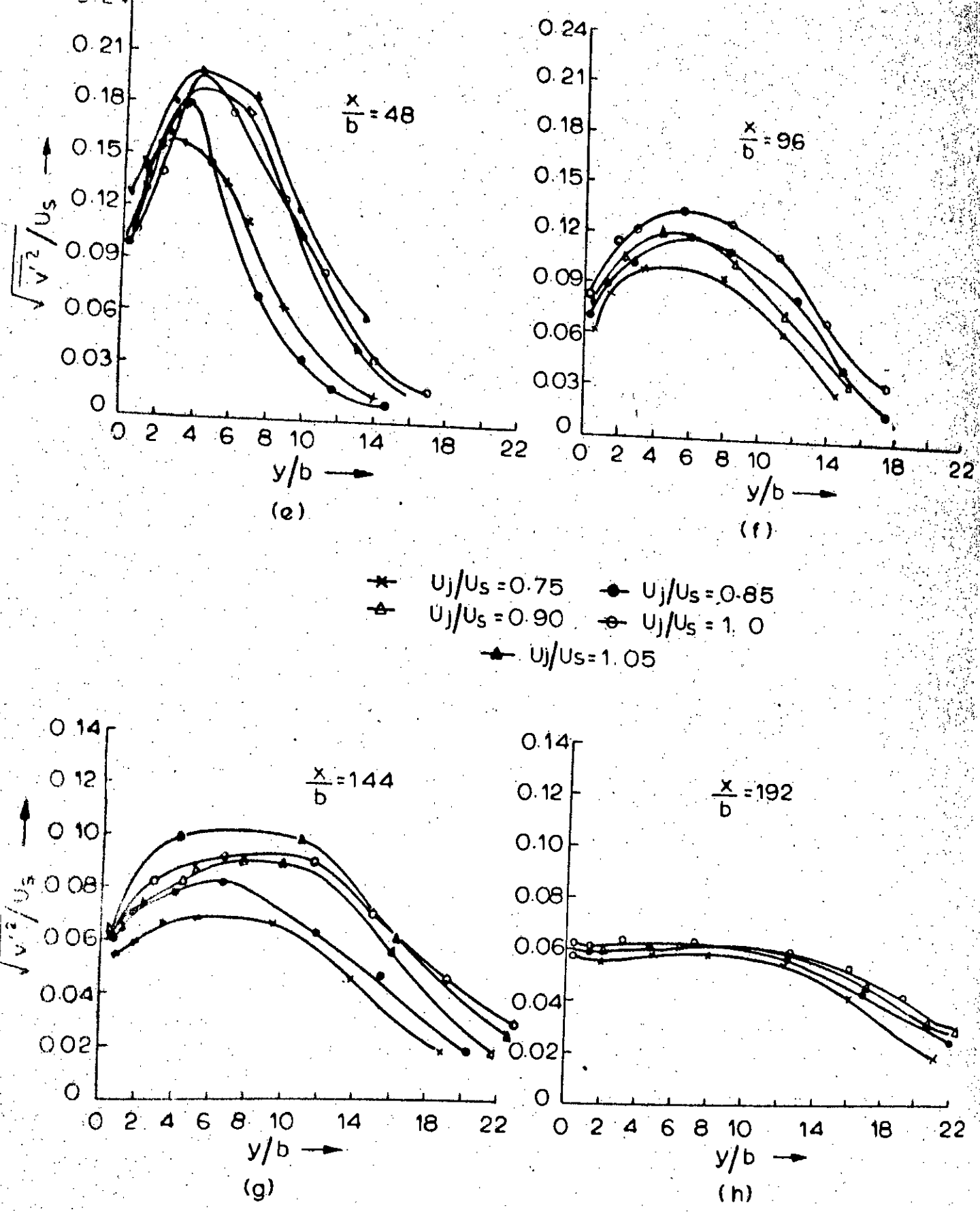

FIG. 5.14: $\sqrt{\overline{v'^2}}/U_S$ FOR 127° INJECTION

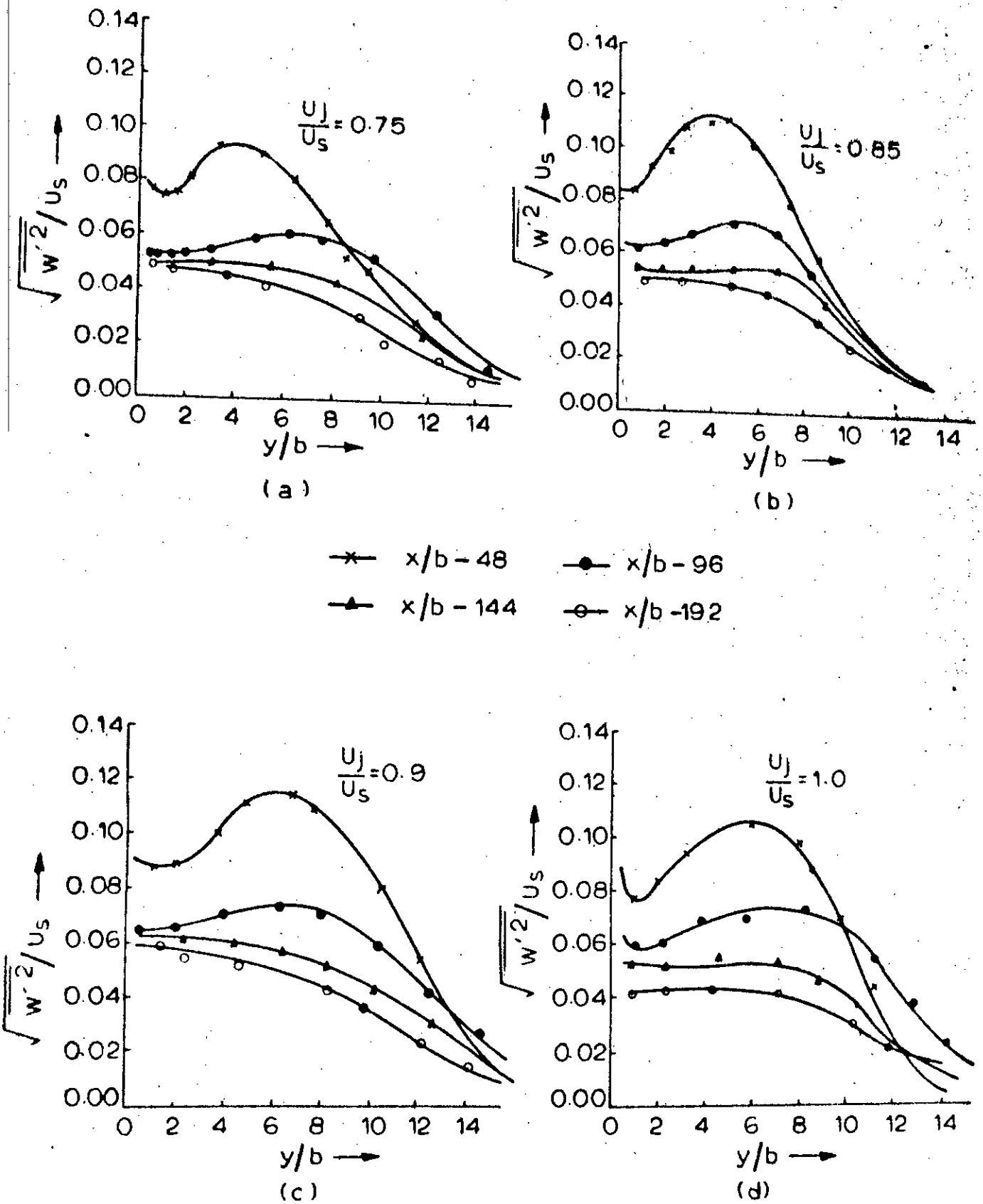

FIG. 5.15: $\sqrt{\overline{w'^2}}/U_s$ FOR 90° INJECTION

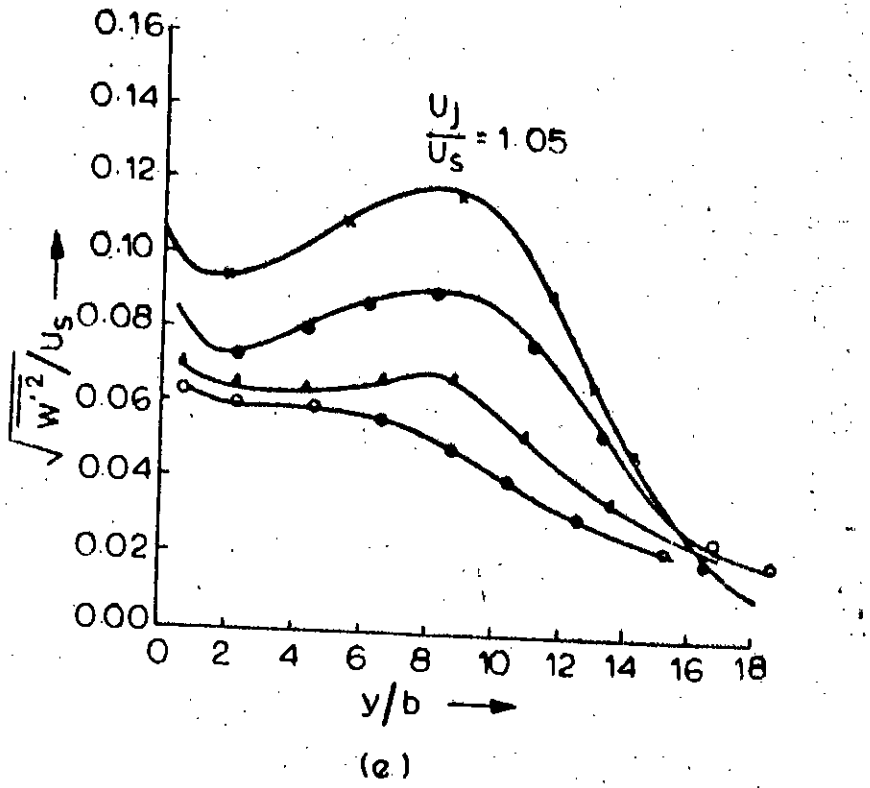

(e)

x/b - 48 x/b - 144
x/b - 96 x/b - 192

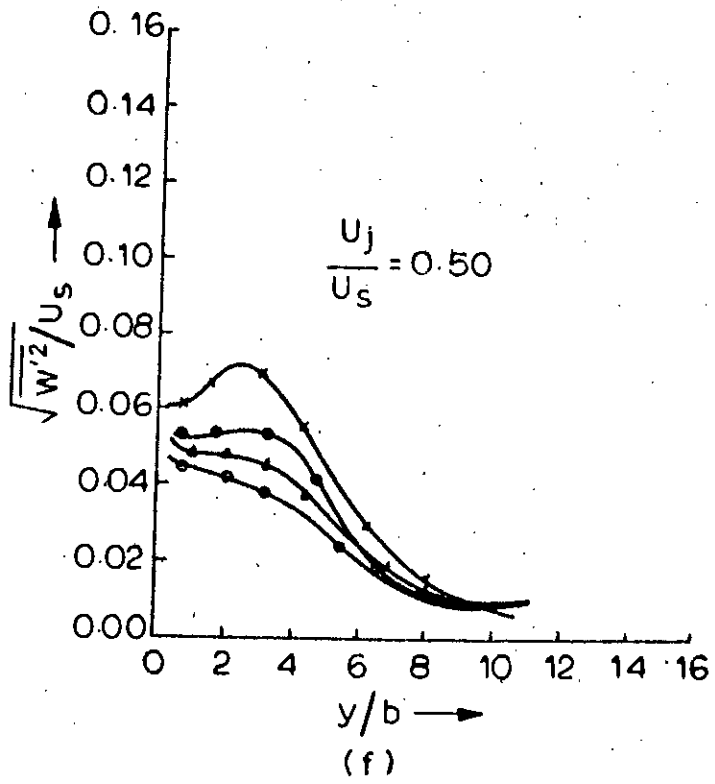

(f)

FIG. 5.15: $\sqrt{\overline{w'^2}}/U_S$ FOR 90° INJECTION

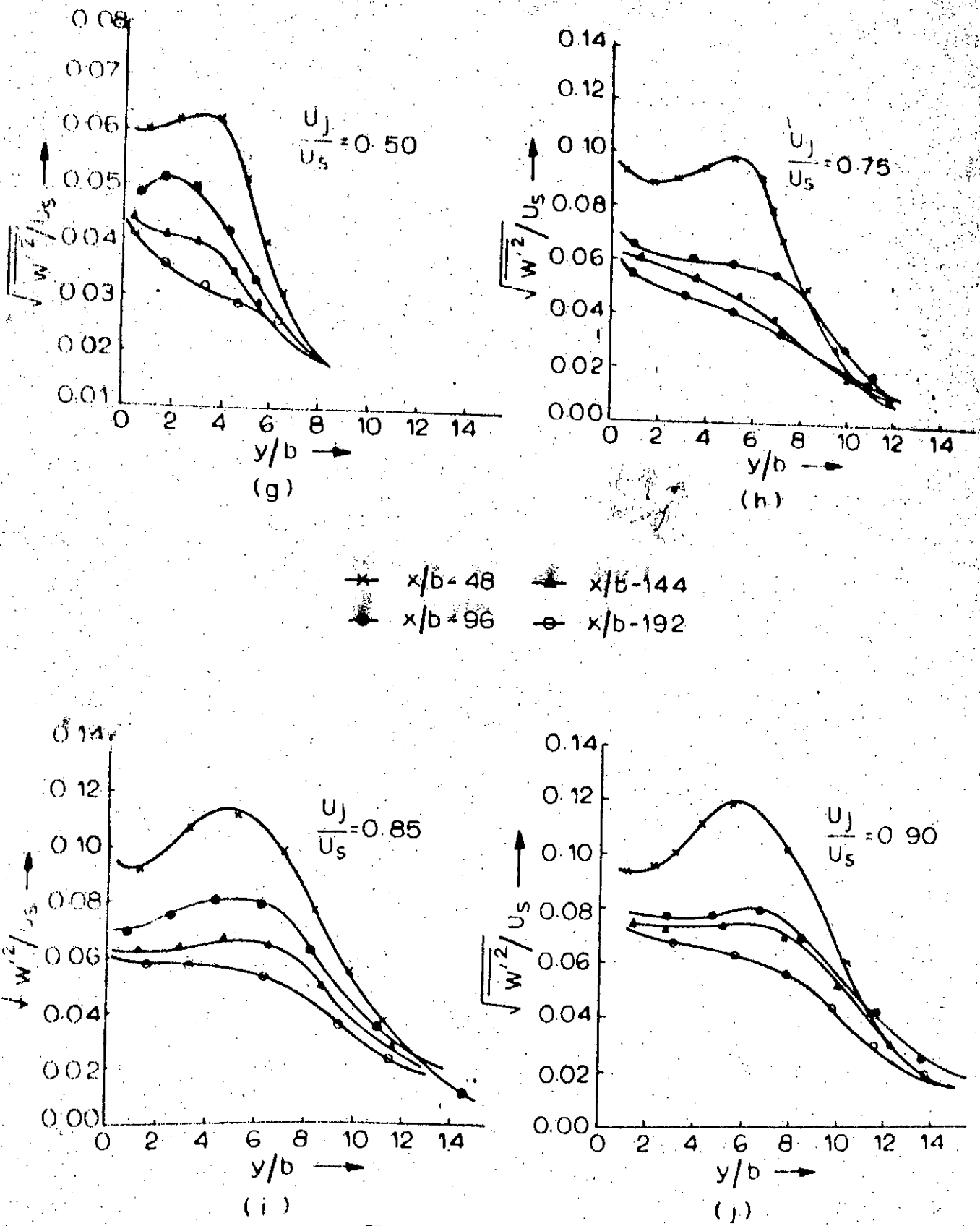

FIG. 5.15: $\sqrt{\overline{w'^2}}/U_s$ FOR 127° INJECTION

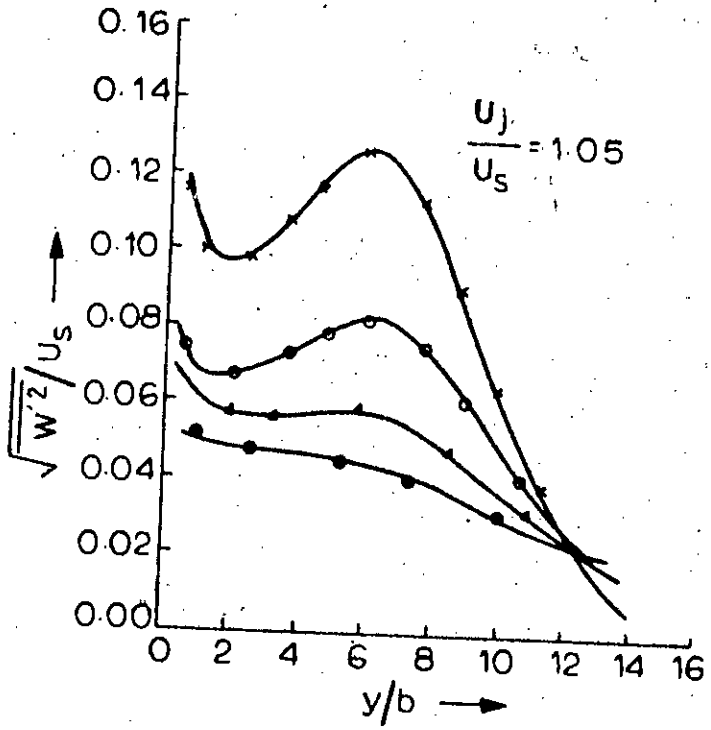

(k)

x/b-48
x/b-96
x/b-144
x/b-192

FIG. 5.15 : $\sqrt{\overline{W'^2}}/U_S$ FOR 127° INJECTION

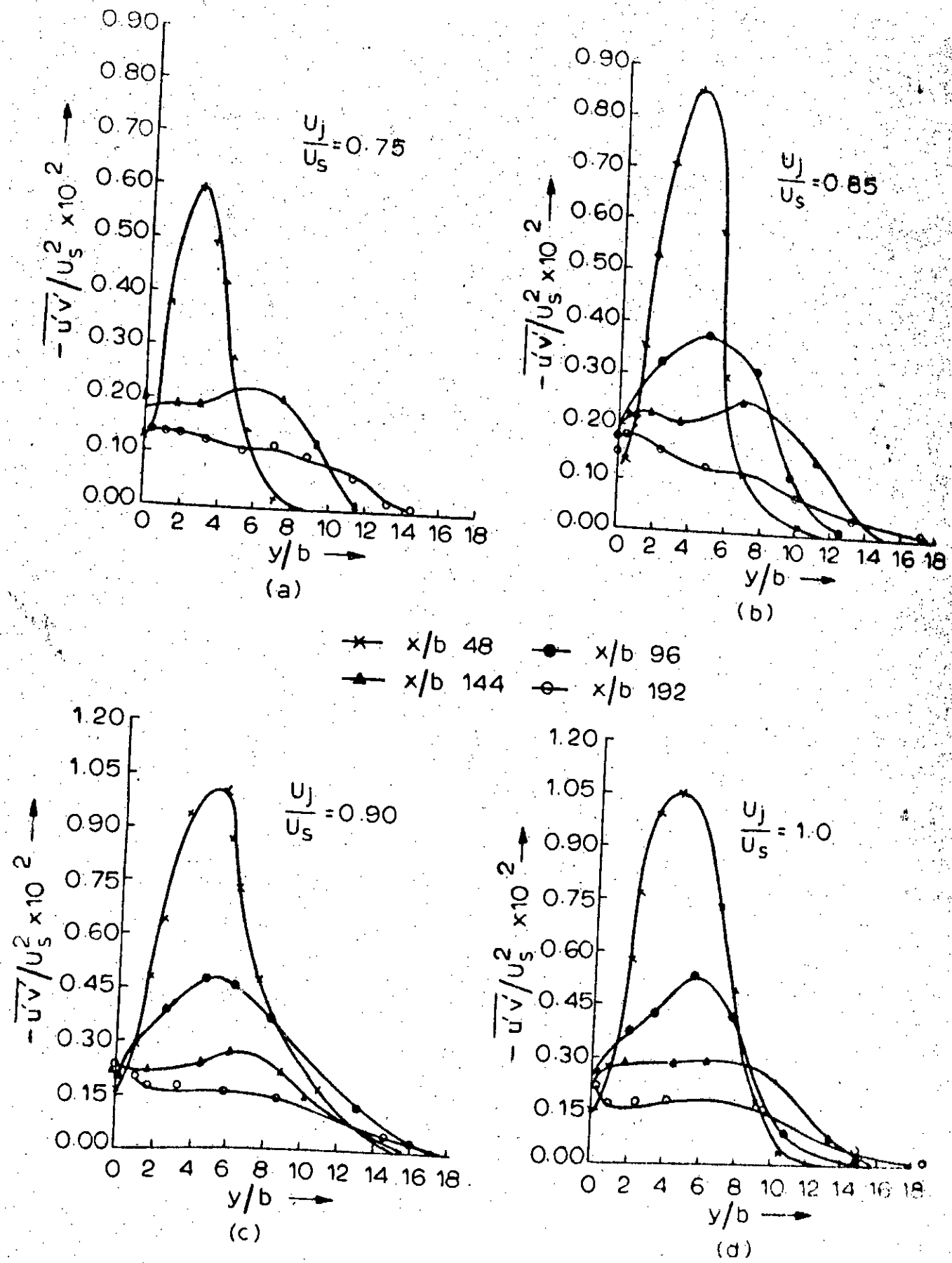

FIG. 5.17: $-\overline{u'v'}/U_s^2$ FOR 90° INJECTION

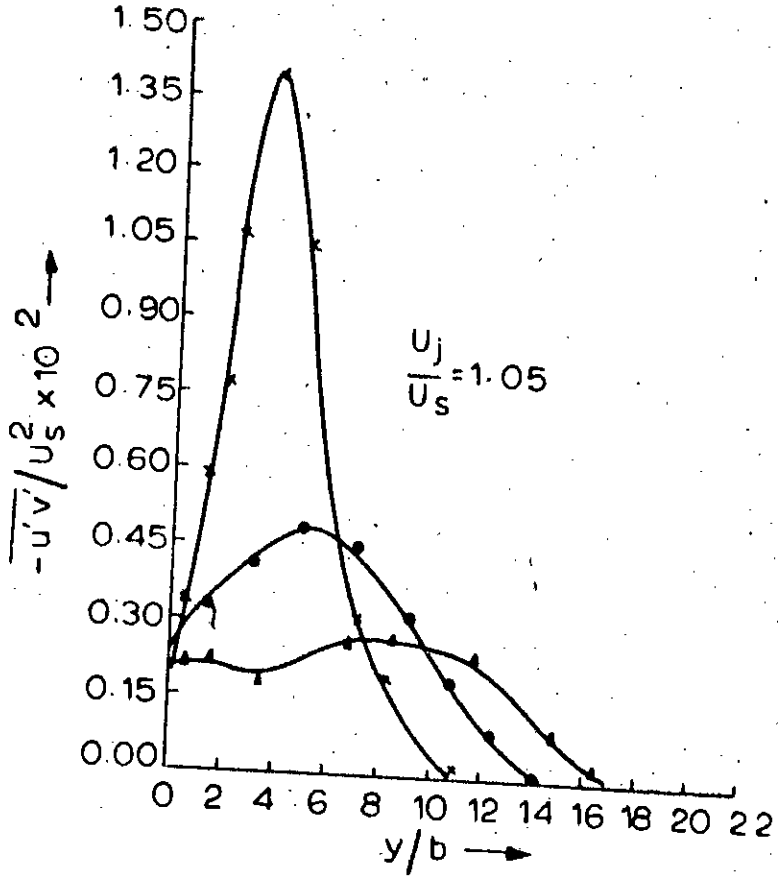

(e)

$-\overline{u'v'}/U_s^2$ FOR 127° INJECTION

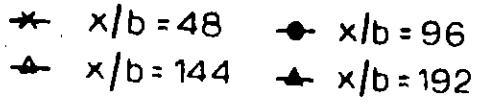

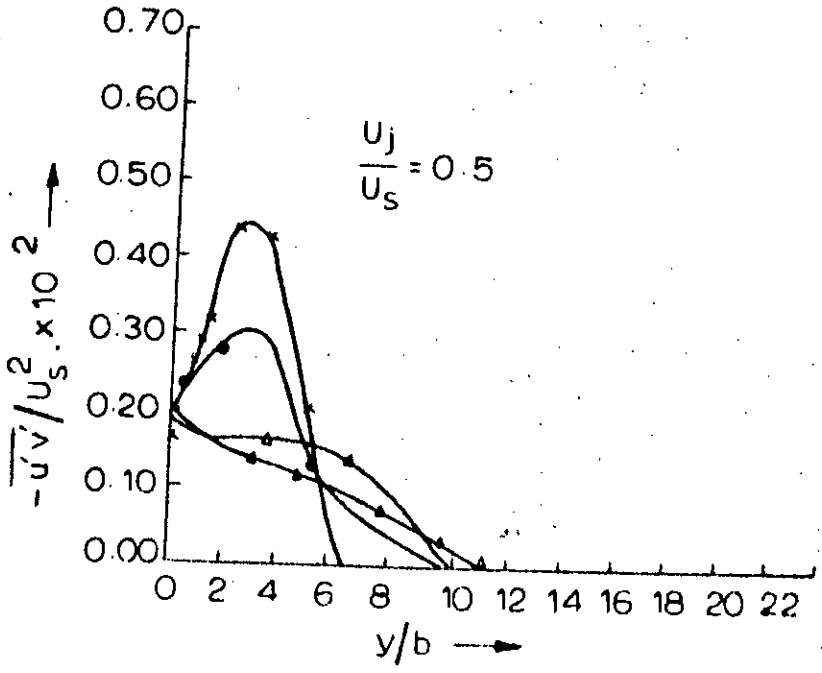

(f)

$\overline{u'v'}/U_s^2$ FOR 90° INJECTION

FIG: 5.17

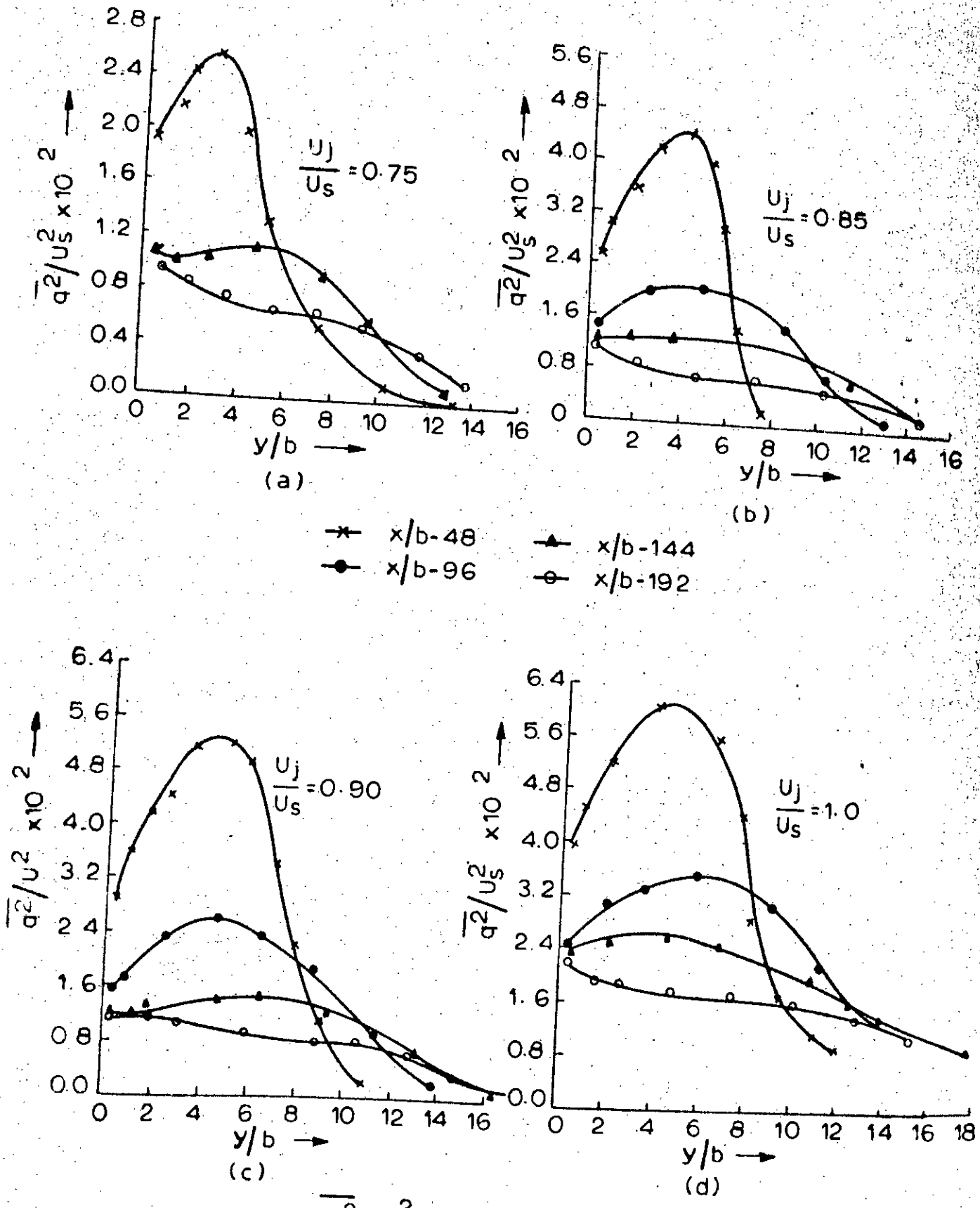

FIG. 5.18: $\overline{q^2}/U_S^2$ FOR 90° INJECTION

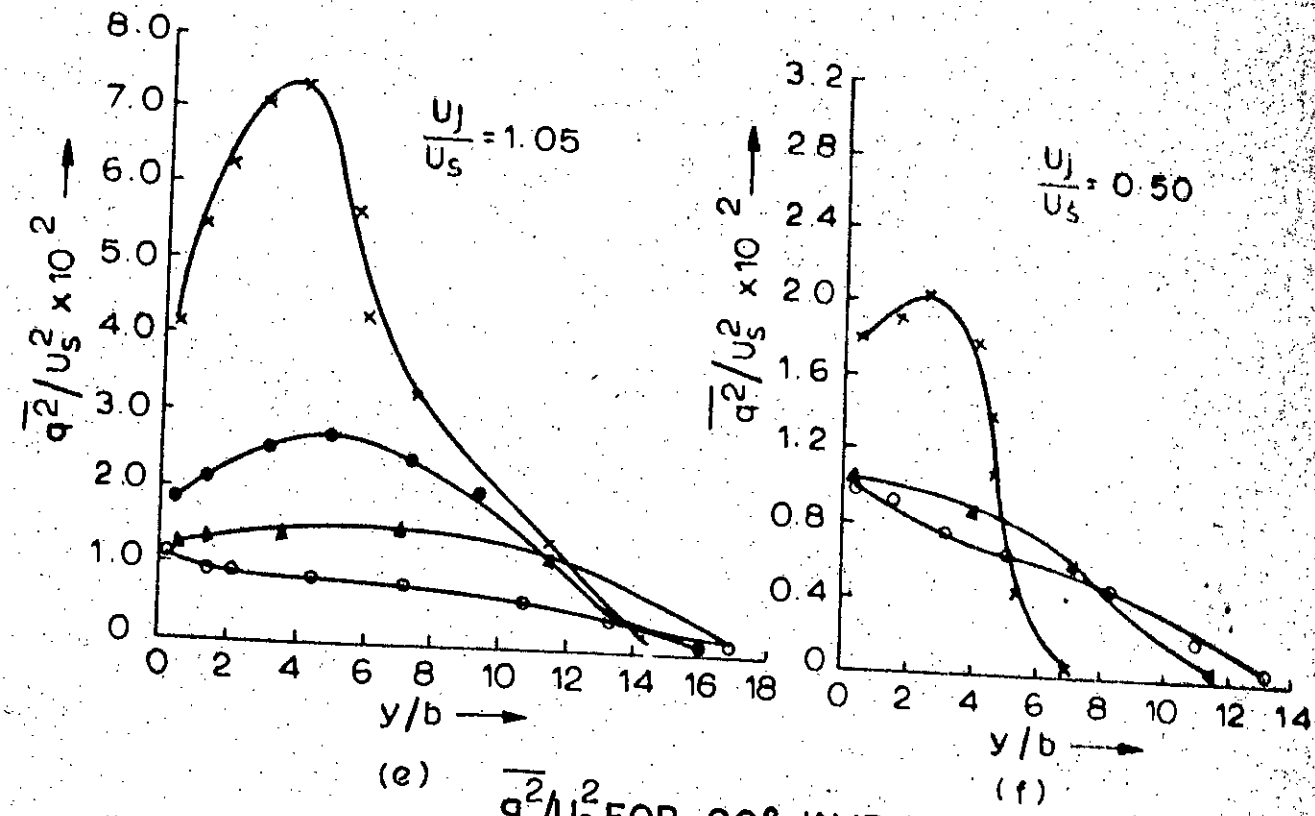

$\overline{q^2}/U_S^2$ FOR 90° INJECTION

x/b 48 x/b 96
x/b 144 x/b 192

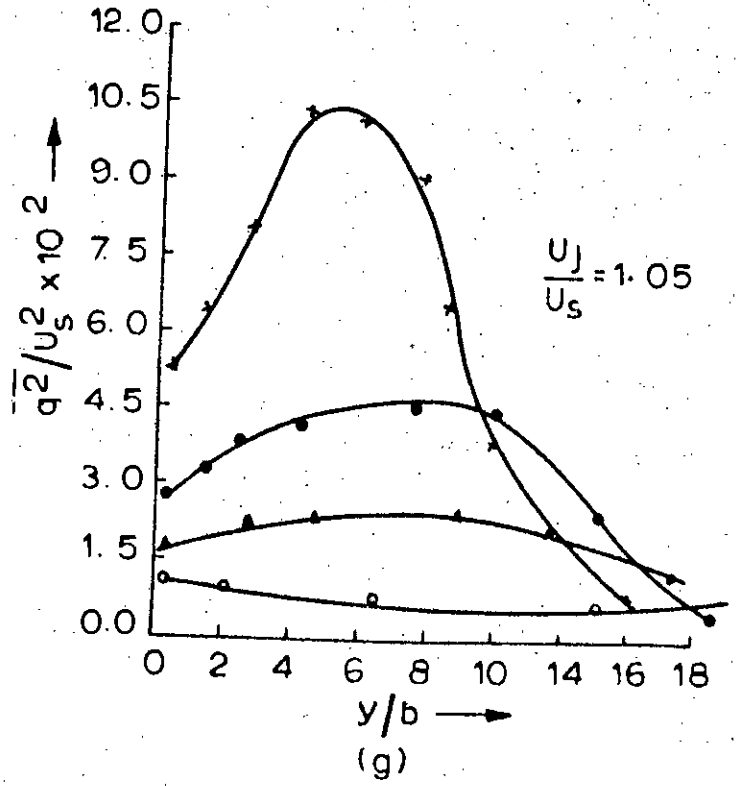

$\overline{q^2}/U_S^2$ FOR 127° INJECTION

FIG. 5.18

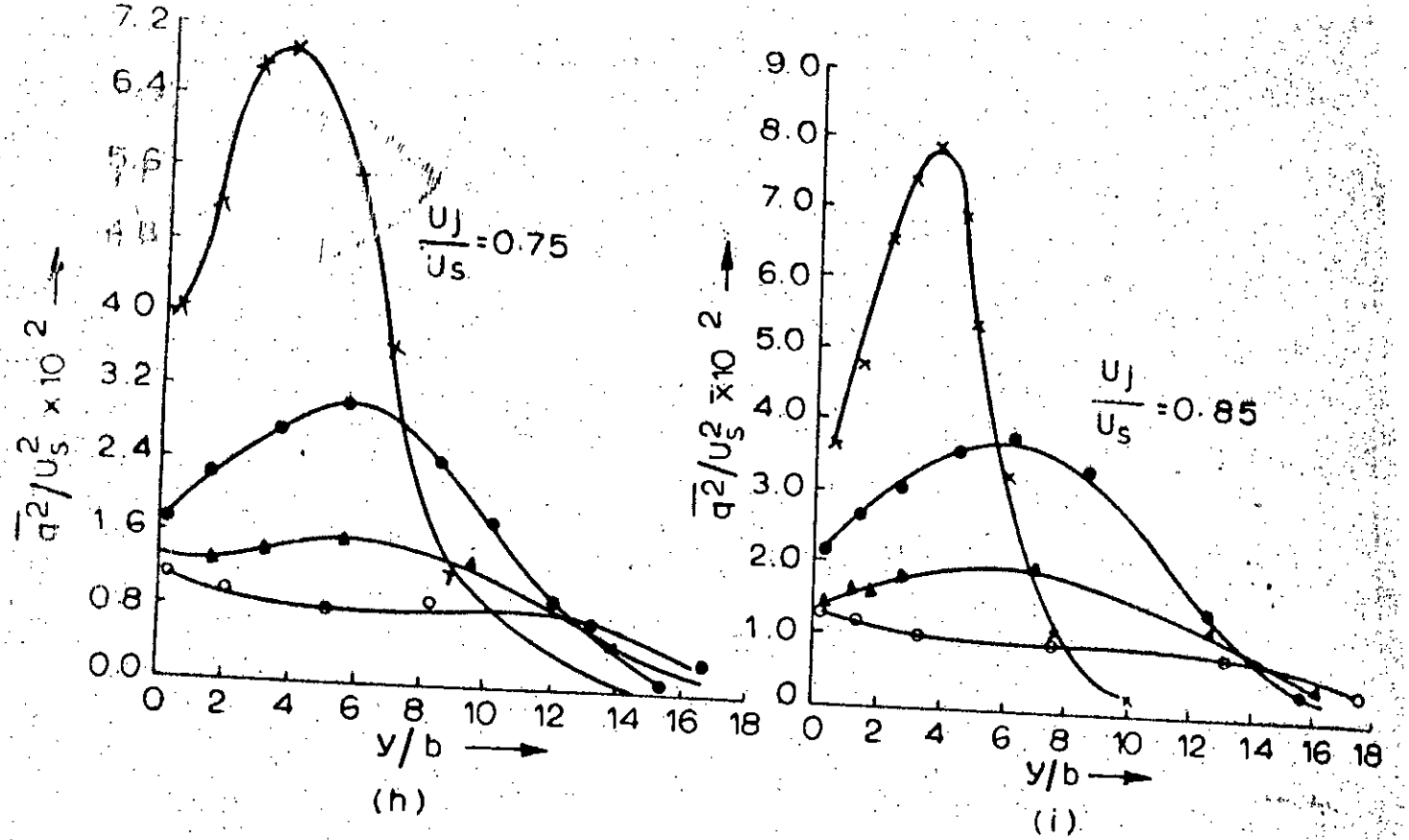

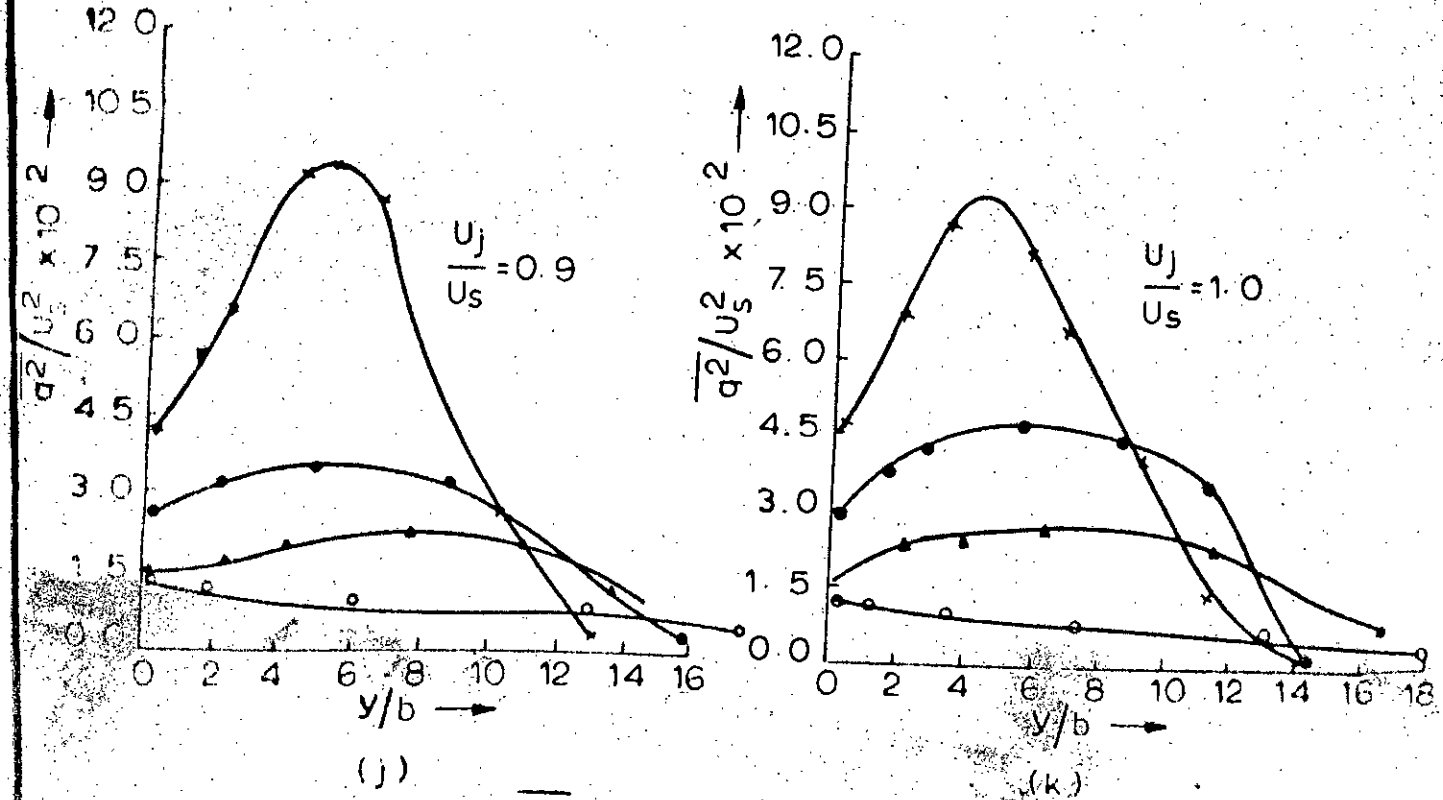

FIG. 5.18: $\overline{q^2}/U_s^2$ FOR 127° INJECTION

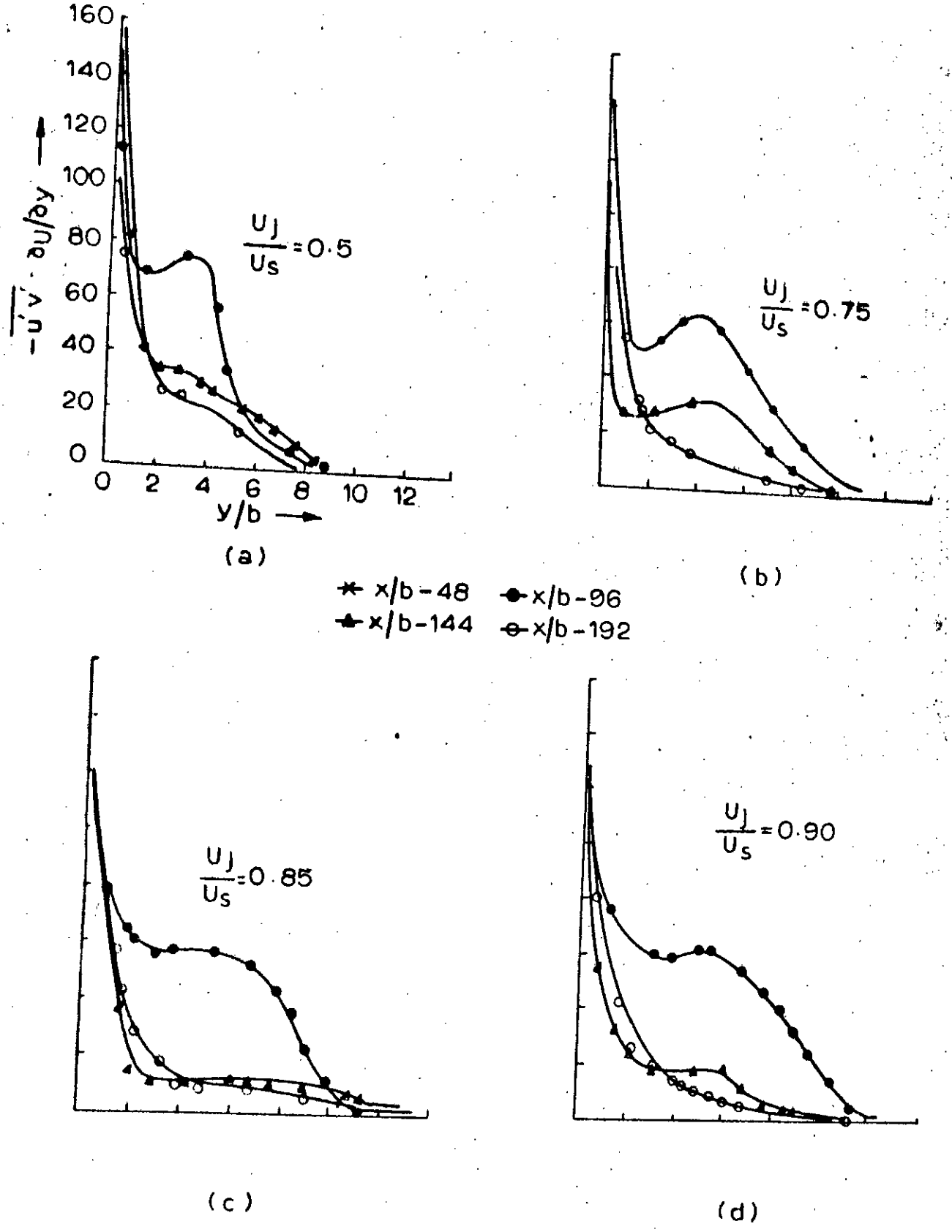

FIG. 5.19: TURBULENCE PRODUCTION FOR 90° INJECTION

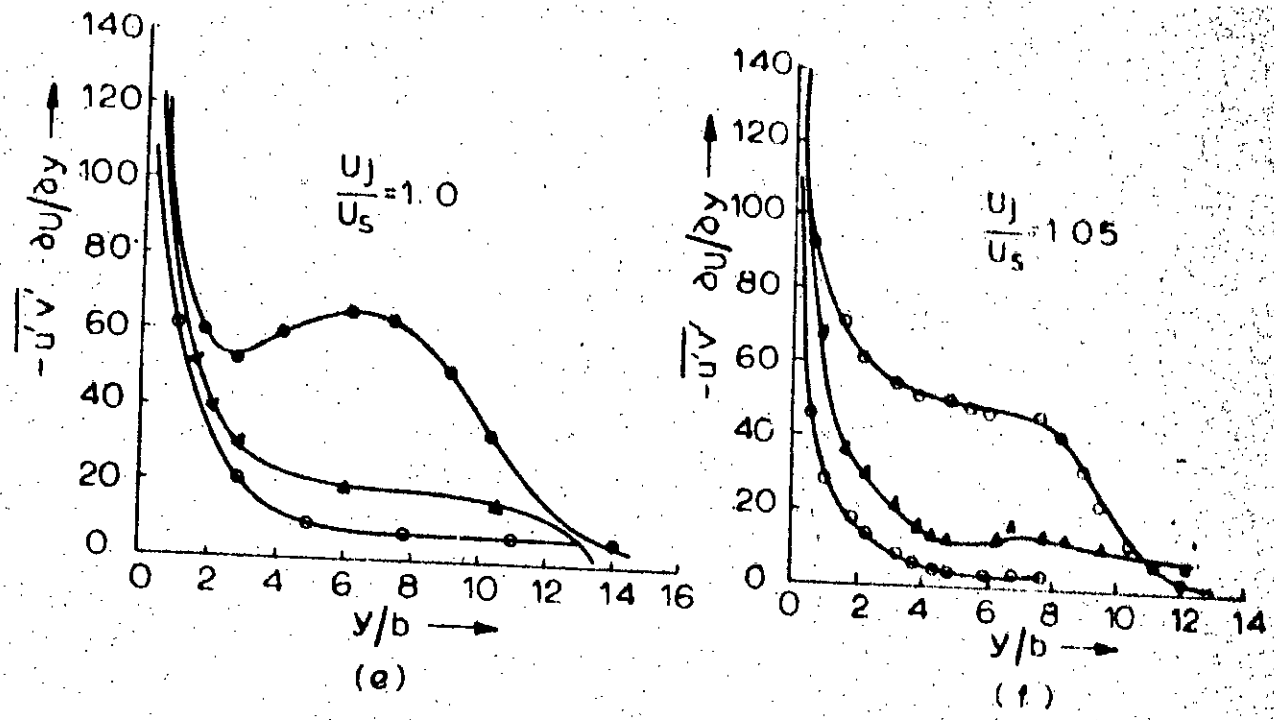

TURBULENCE PRODUCTION FOR 90° INJECTION

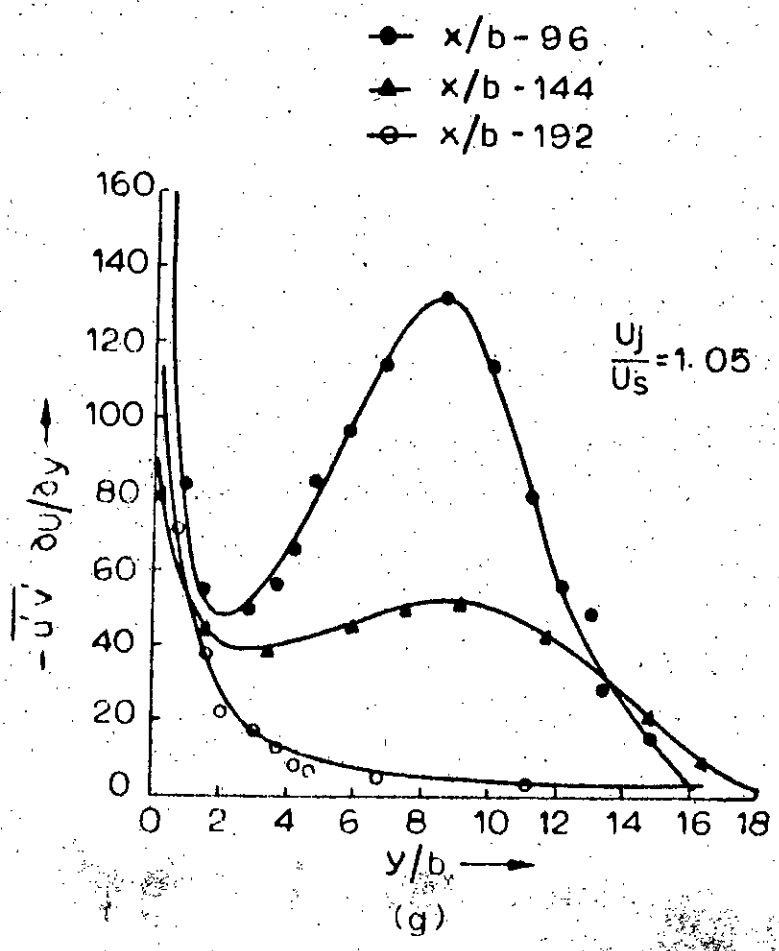

FIG. 5.19: TURBULENCE PRODUCTION FOR 127° INJECTION

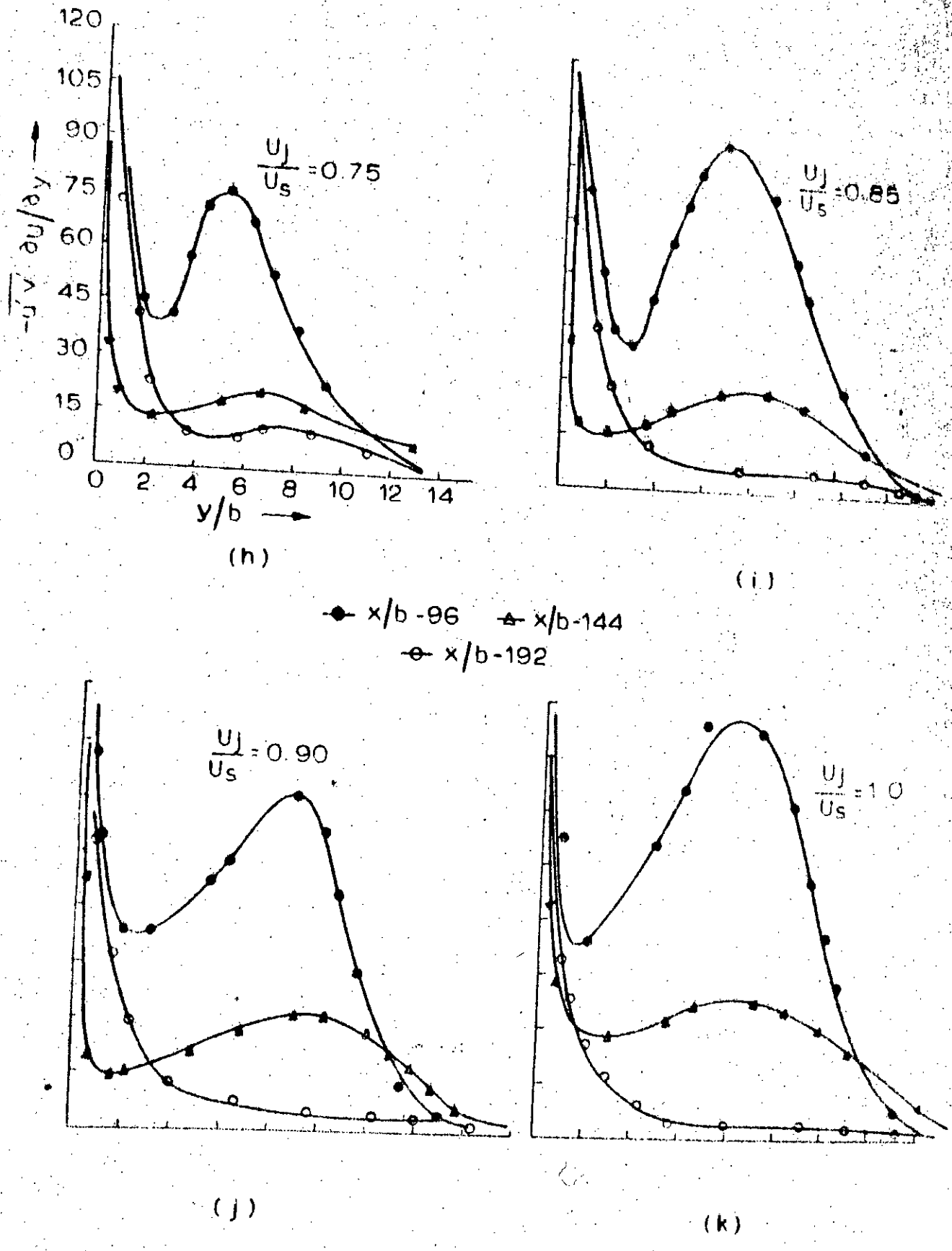

FIG. 5.19: TURBULENCE PRODUCTION FOR 127° INJECTION

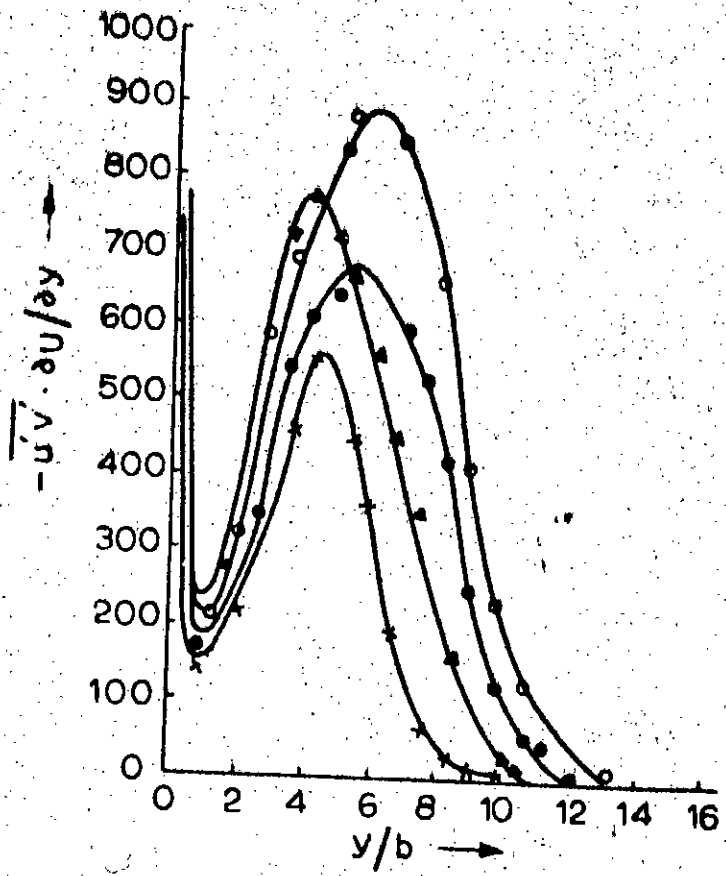

(ℓ)

TURBULENCE PRODUCTION FOR 127° INJECTION

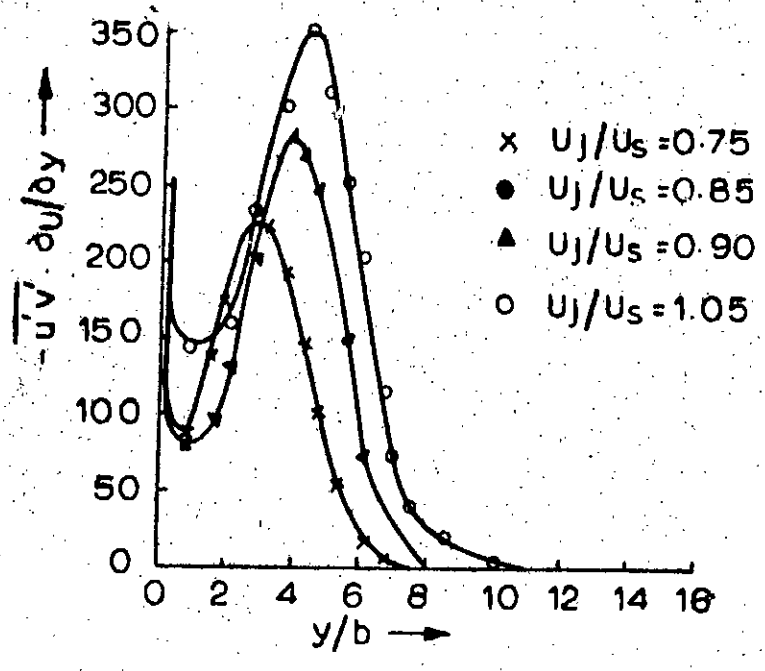

(m)

FIG. 5.19: TURBULENCE PRODUCTION FOR 90° INJECTION

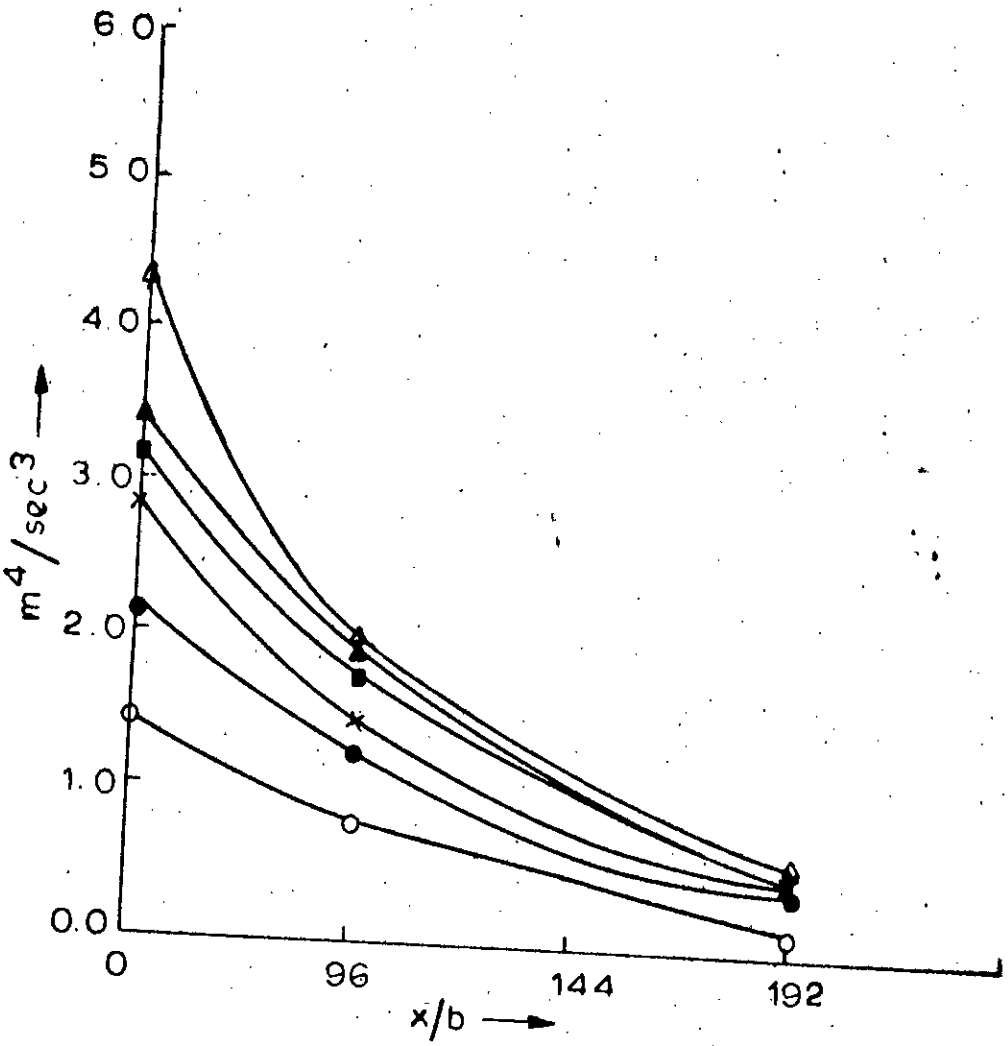

(a)

- o $U_j/U_s = 0.5$
- ● $U_j/U_s = 0.75$
- × $U_j/U_s = 0.85$
- ■ $U_j/U_s = 0.90$
- ▲ $U_j/U_s = 1.00$
- △ $U_j/U_s = 1.05$

FIG. 5.20 SHEAR WORK INTEGRAL FOR 90° INJECTION

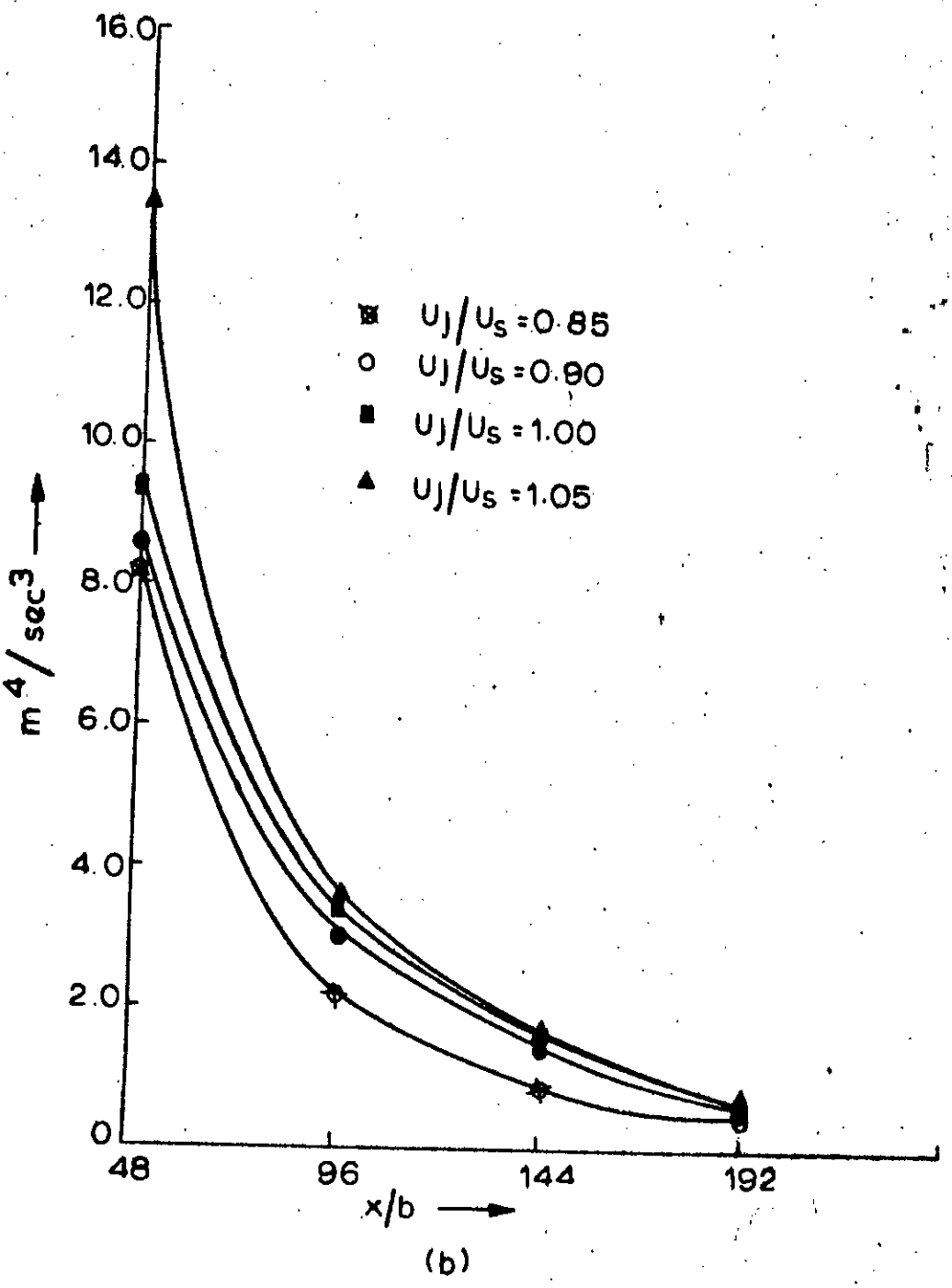

FIG. 5.20: SHEAR WORK INTEGRAL FOR 127° INJECTION

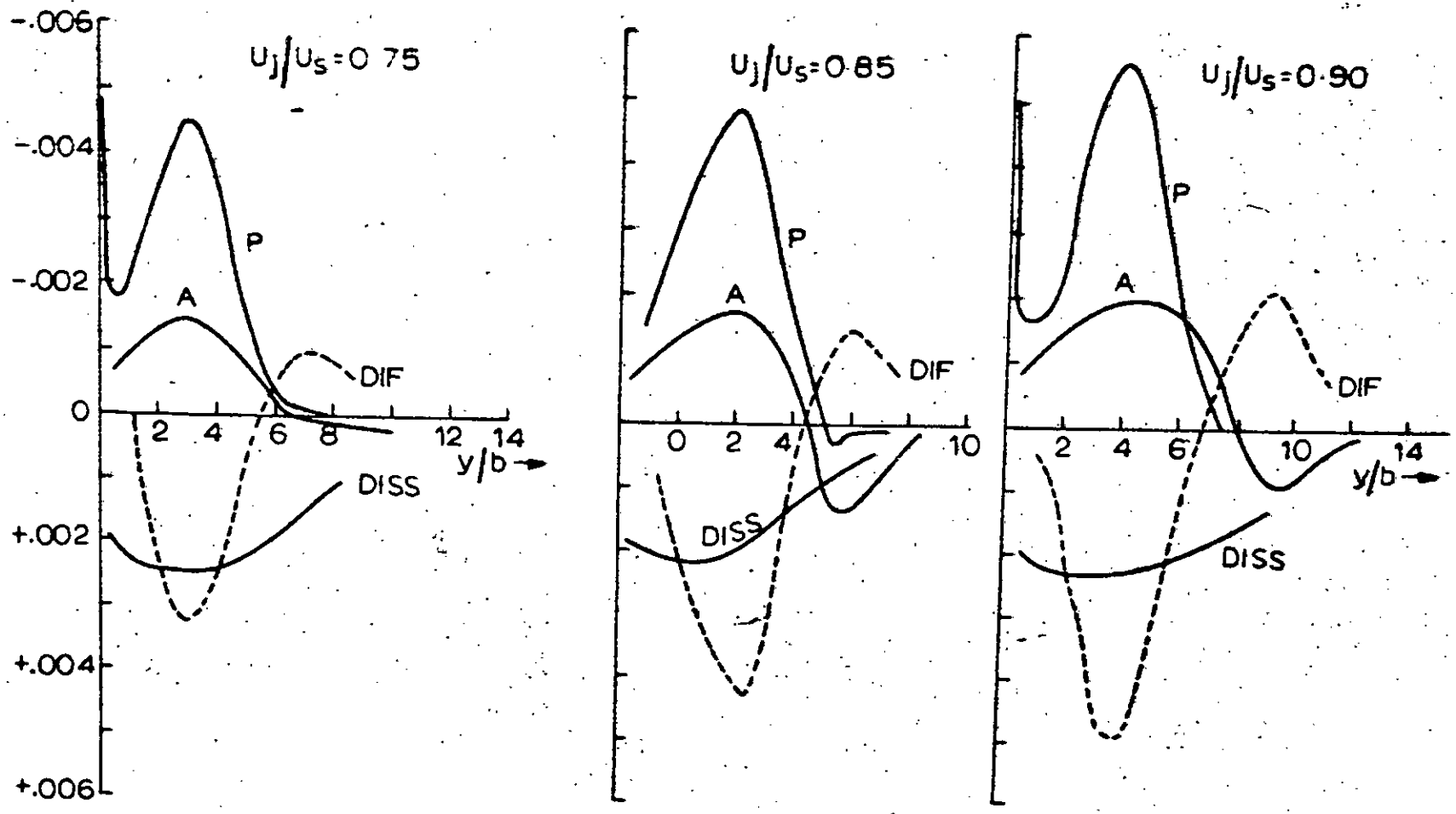

P-PRODUCTION A-ADVECTION DISS- DISSIPATION DIF- DIFFUSION

(a)

FIG.5.21: TURBULENT ENERGY BALANCE FOR 90° INJECTION AT X/b=48

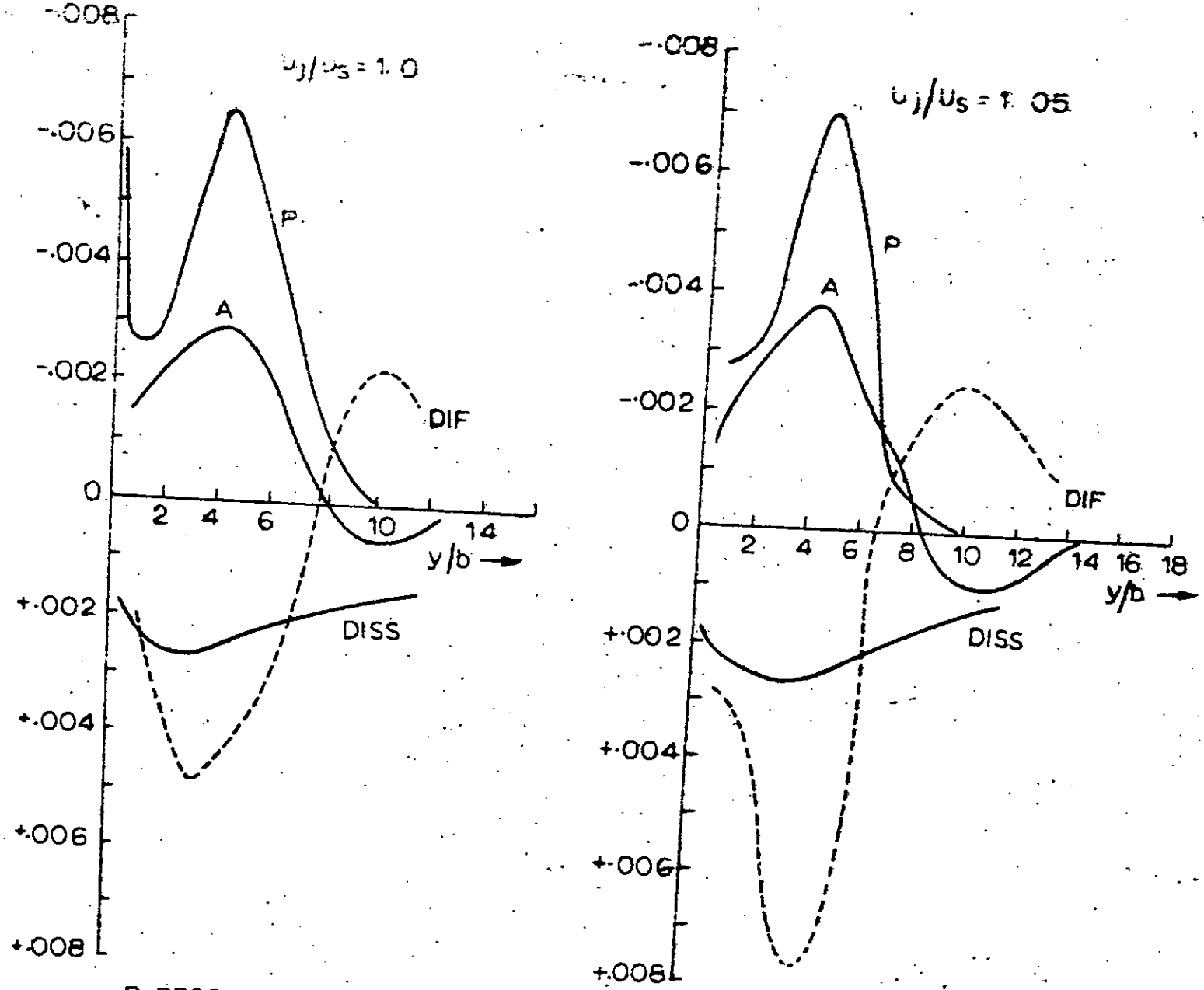

P-PRODUCTION A-ADVECTION DISS- DISSIPATION DIF-DIFFUSION

(b)

FIG. 5.21: TURBULENT ENERGY BALANCE FOR 90° INJECTION AT X/b=48

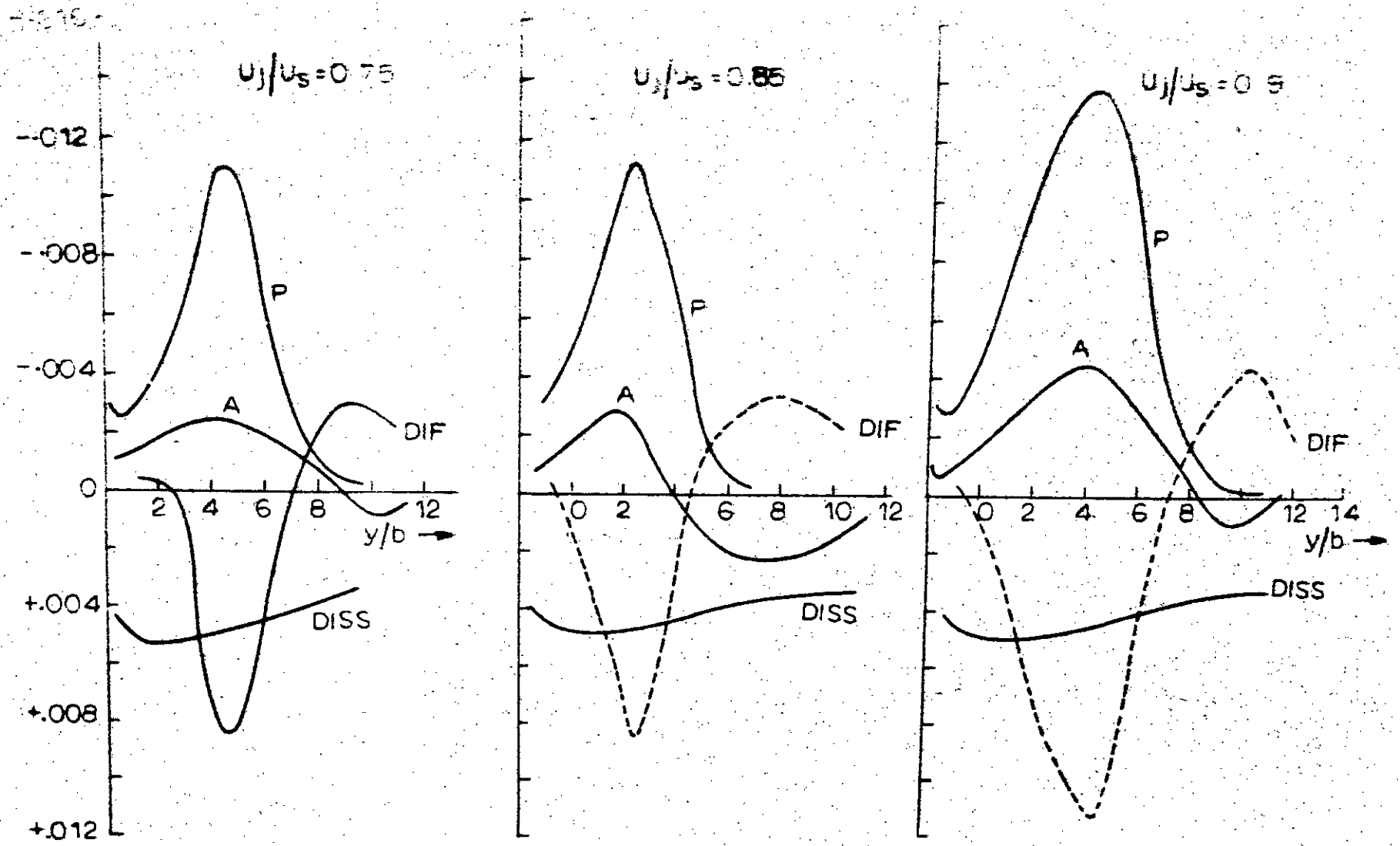

P- PRODUCTION A- ADVECTION DISS- DISSIPATION
DIF- DIFFUSION

(c)

FIG. 5.21: TURBULENT ENERGY BALANCE FOR 127° INJECTION AT x/b = 48

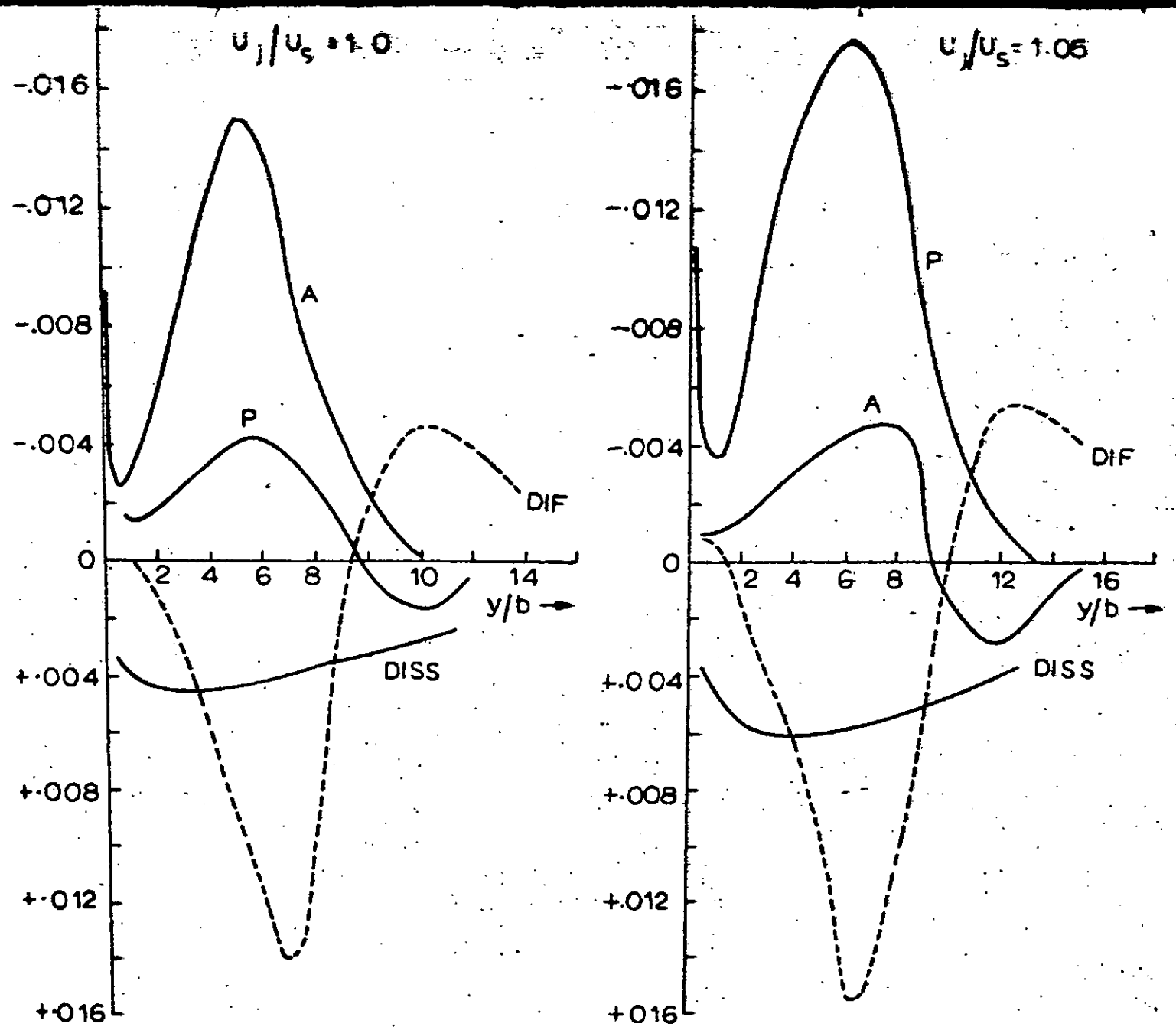

(d)

FIG.5.21: TURBULENT ENERGY BALANCE FOR 127° INJECTION AT X/b=48

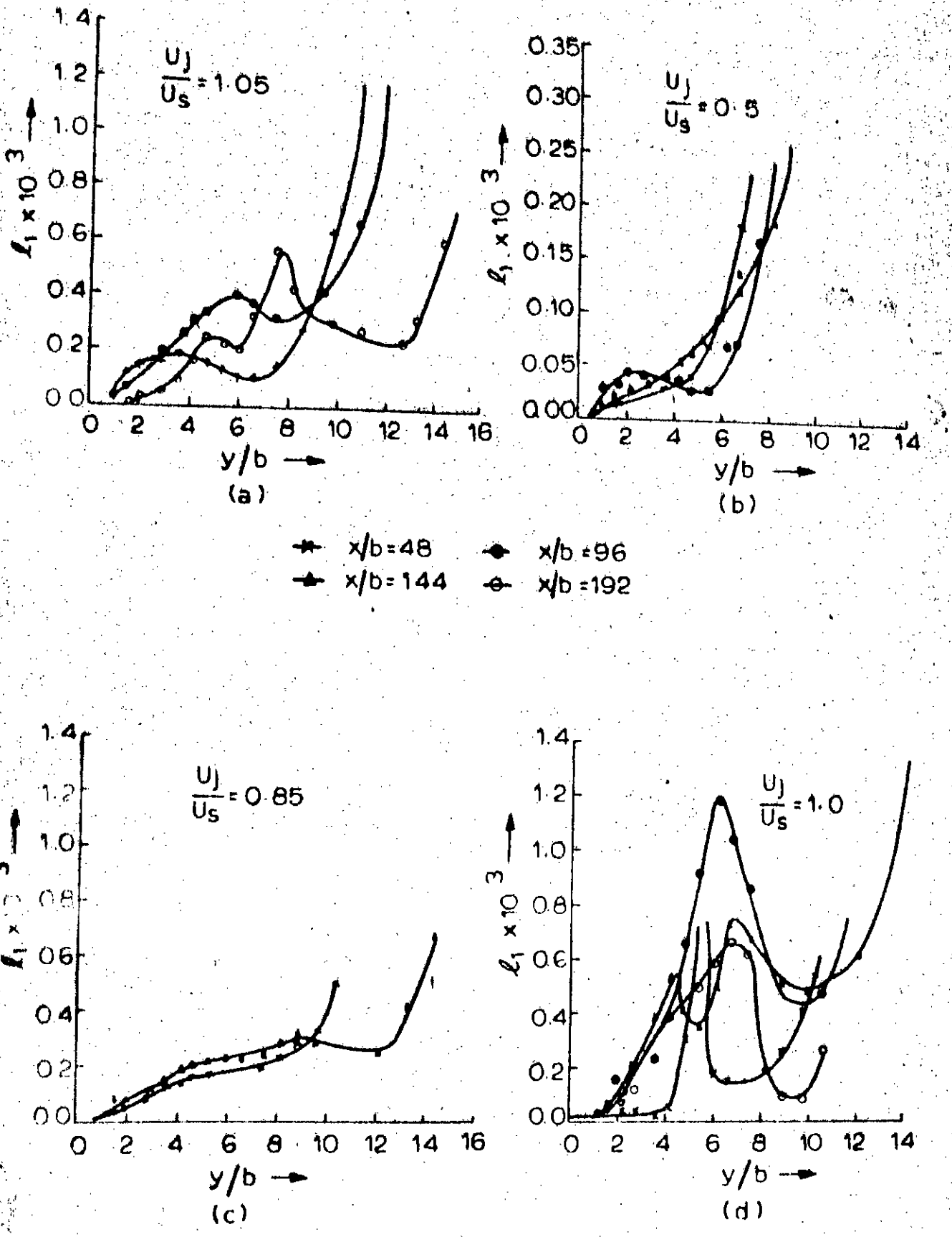

FIG. 5.22: PRANDTL MIXING LENGTH DISTRIBUTION

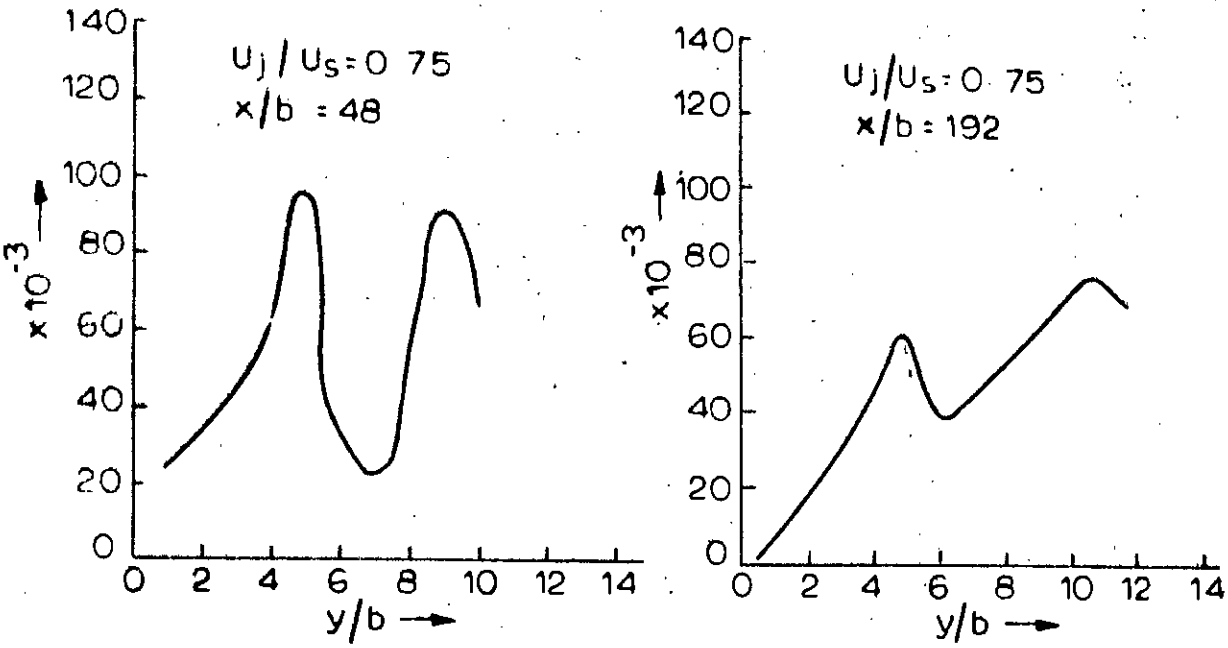

(a) 127° INJECTION

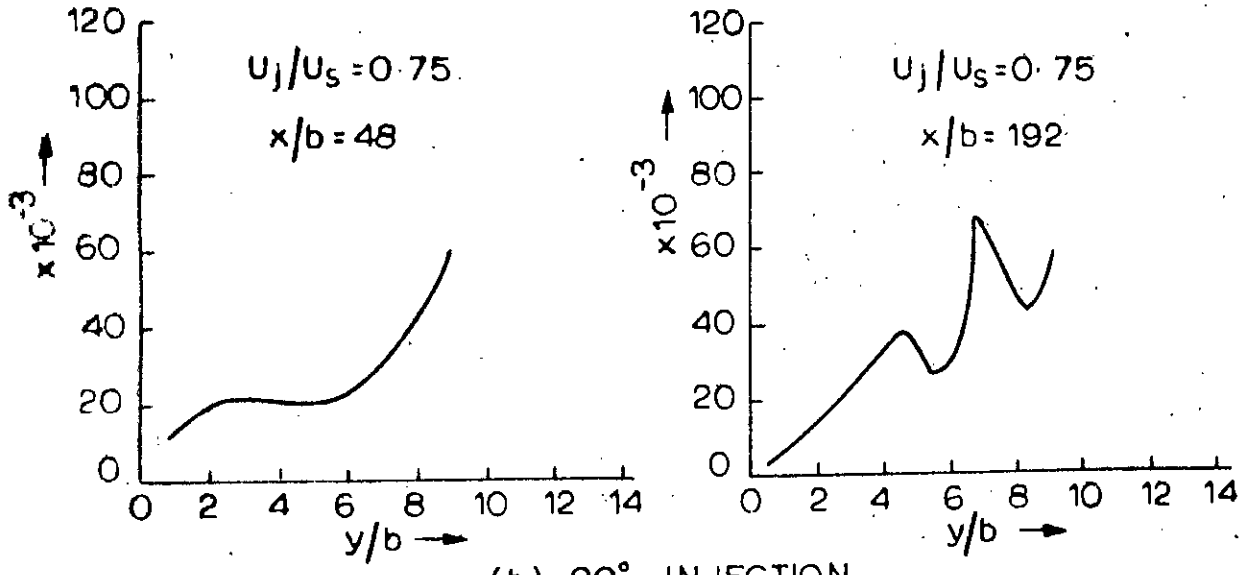

(b) 90° INJECTION

FIG. 5.23: PRANDTL- KOLOMOGOROV MIXING LENGTH DISTRIBUTION

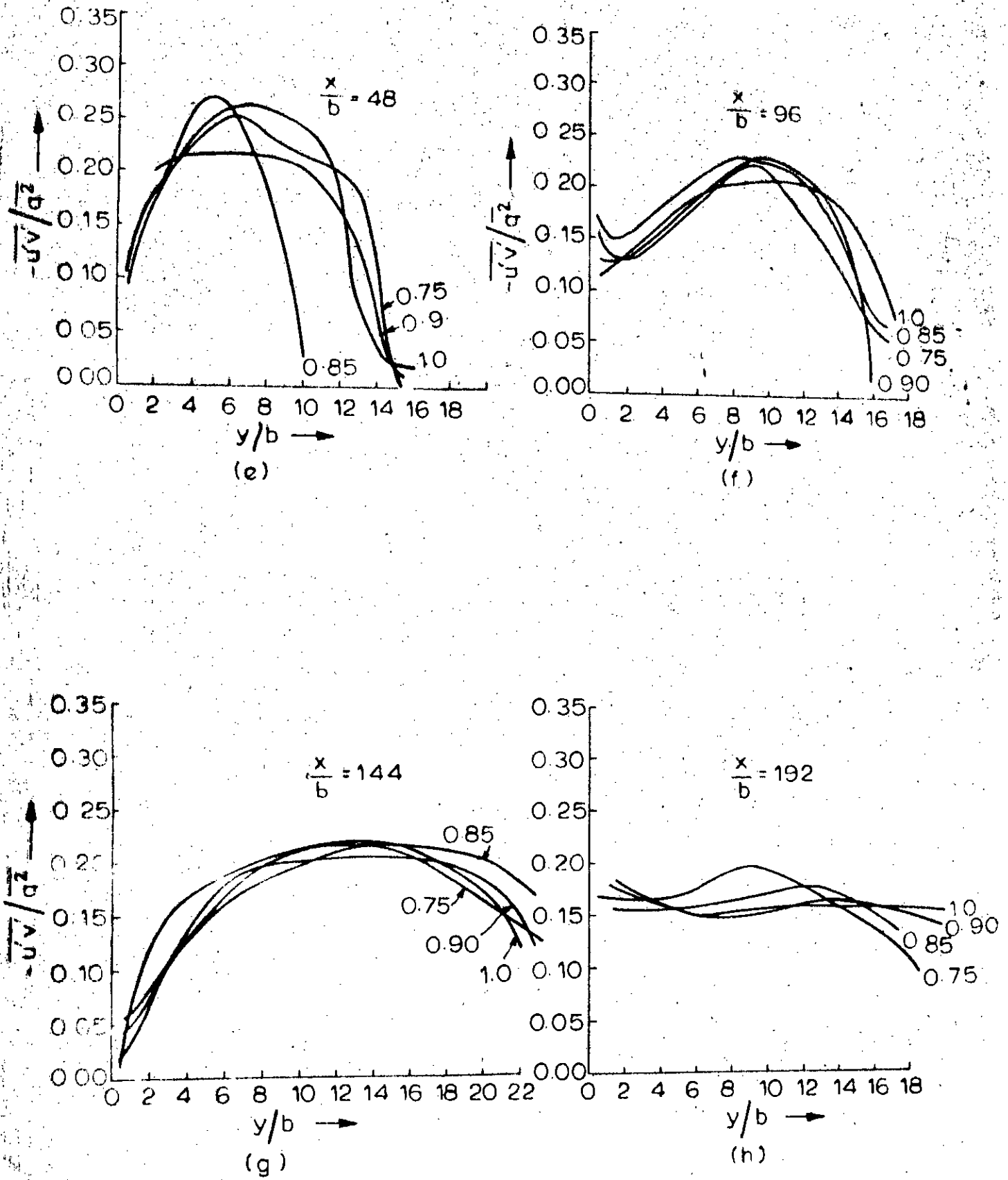

FIG. 5.24: BRAD SHAW PARAMETER FOR 127° INJECTION FOR DIFFERENT U_J/U_S

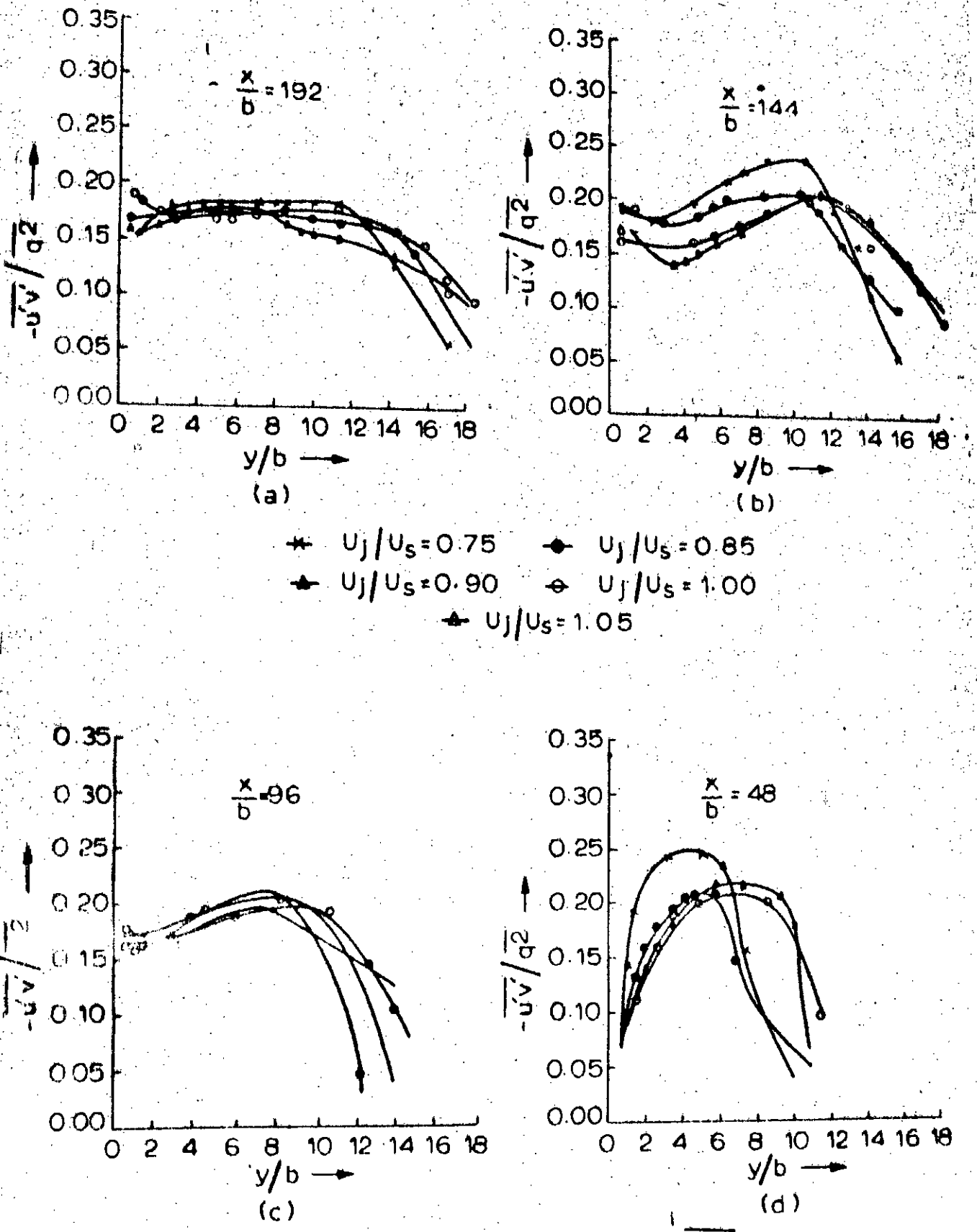

FIG.5.24: BRADSHAW PARAMETER $-\overline{u'v'}/q^2$ FOR 90° INJECTION

tuti of all these terms in the energy integral equation shows an error of 5 percent. The viscous terms were evaluated but was found to be of a negligible order. The dissipative term is higher for 127° injection for all cases of velocity ratios. The maximum energy dissipated is for the velocity ratio of 1.05, jet angle of 127° and is 3.5 percent of the sum of the energy of the original stream and the jet.

The skin friction coefficient evaluated agrees with the result obtained by Mackor and Whitelaw, as far as the trend is considered. Fig. (5.8). It reaches a negative value of 0.009 in the re-circulating zone and increases to 0.022 at the last section. All the curves are not shown to avoid cluttering. Also, the shape factor starts with a value above 1.75 at x/b of 48 and decreases to the value of 1.3 at the last station as shown in Fig.(5.7).

5.3a Analysis of Fluctuating Components

The graphs of $\overline{u'^2}$, $\overline{v'^2}$, $\overline{w'^2}$ shown in Fig.(5.11 - 5.13) indicate that $\overline{u'^2}$ is always the largest of the three with $\overline{v'^2}$ following it closely in magnitude. The $\overline{w'^2}$ and $\overline{u'^2}$ curves show peaks at nearly the same distance from the wall, where as $\overline{v'^2}$ maximum reached at a slightly larger distance from wall. Local turbulence intensity of more

than 35 percent was reached in some cases, at x/b of 48. Yet, the difference in turbulence values at x/b of 48 and x/b of 96 is tremendous as is evident from Fig. 5.11, 5.12 etc. In all cases of u_j/u_g, the turbulent quantities were higher for the 127° injection. This could be accounted by the slightly larger size of the re-circulating zone, the edge of which works as a production mill for turbulence. Fig. 5.16, 5.17 gives the turbulent shear stress $\overline{u'v'}$. The turbulent shear stress $\overline{u'v'}$ when extrapolated to the wall region is in good agreement with the value of wall shear stress evaluated earlier. Based on the $\overline{u'v'}$ and the derived $\frac{\partial \bar{u}}{\partial y}$, the production of turbulence term can be computed and is shown in Fig. (5.19).

5.3b Turbulent Energy Balance

Though all the terms of the secondary equation of flow cannot be measured an evaluation of the major terms is possible as shown in Fig.(5.21). The diffusion term which cannot be measured is computed as the balancing quantity. The advection and production terms are easily evaluated. The production is high near the wall, reaches a minimum and again increases to a maximum some distance away from the wall. The advection term is negative mostly, but towards the outer edge of the boundary layer changes

sign. This is also evident from the plots of $\overline{q^2}$ against y/b as seen in Fig.(5.18). The dissipation term does not show a minimum near the wall corresponding to the minimum in the production term. Dissipation is roughly uniform across the boundary layer. The diffusion term shown in Fig.(5.21) shows that peak of diffusion matches that of production. The production and diffusion are more or less matched, while advection and dissipation are roughly equal.

5.4 Analysis of Separation Bubble

The separation bubble is always larger for the 127° injection for all the velocity ratios as is evident from Fig.(5.9). The reattachment distance when plotted as a function of u_j/u_s with the injection angle as parameter appears to be of a form which may be expressed with a suitably adjusted mathematical expression. Yet a final firm opinion cannot be expressed because of the limited range of u_j/u_s.

5.5 Applicability of Turbulence Models

The objective was to see which of the turbulence model is applicable to the flow under consideration. All the turbulence models can be classified into one equation models, two equation models and three or more equation model,

based on the number of differential equations to be solved. The checking was done only for the algebraic part of the one-equation model.

A one equation model of turbulence has an algebraically specified length scale and a differential transport equation for one property of turbulence. The simplest and the oldest, yet one of the most popular model is the mixing length model proposed by Prandtl, though it does not come in the category of one equation model. The Boussinesq's equation of eddy viscosity form the basis for the model. Hence $\tau = \mu_{eff} \frac{\partial u}{\partial y}$ and $\mu_{eff} = \rho l_1^2 \left|\frac{\partial u}{\partial y}\right|$ where τ is the turbulent shear stress, l_1 is the mixing length and μ_{eff} is the eddy viscosity which is analogous to the molecular viscosity. Prandtl considered l_1 proportional to distance from wall. The plot of l_1, Fig. (5.22) shows l_1 is not a constant nor of a form which can be easily given an algebraic equation.

The next model considered is the one by Prandtl Kolmogorov which connects the effective viscosity with the turbulence energy, and is of the form, $\mu_{eff} = c_\mu \rho l_2 \sqrt{k}$ where c_μ is a constant usually taken as 0.2 and l_2 is a mixing length. The l_2 computed based on the measured data show that l_2 cannot be assigned a simple algebraic equation. The differential equation proposed is for the

transport of turbulent kinetic energy, which is broken up into terms of production, advection, diffusion and dissipation as was done in Chapter 3. There are a number of other one equation model based on the effective viscosity hypothesis, and the differential equation for transport of energy. The difference between the models lies in the algebraic expression for the length scale.

The disadvantages of the above models for the particular flow considered here can be written as follows. The plots of $\overline{u'v'}$ and measured mean velocity profile show that the shear stress do not vanish at the zero velocit gradient contrary to the implication in Boussiuesq hypothesis.

A one equation model which is quite different from the above models is the Bradshaw model. Bradshaw considers shear stress is related to the turbulent energy. Thus $\tau = a\ \rho\ \overline{q^2}/2$ as per his hypothesis where a is a constant. Also, in the transport equation for turbulent energy the dissipative term is approximated to $\rho\ q^3/\ell$ and diffusion term is $B\ \overline{q^2}/2\sqrt{\tau_{max}/\rho}$ where ℓ and B are functions of y/δ. The functional form of the dependence is given in (5). The diffusive flux of energy has been assumed to be proportional to the energy itself and also a diffusion velocity

given by $\frac{\tau_{max}}{\rho}$. The value of ' ' e pu show that for all cases 'a' tends to be a constant for x/b greater than x/b 96 Fig. (5.24). The main feature of this model is that shear stress is not related to the mean velocity gradient.

The two equation models of turbulence are too many to be discussed here. All of them are based on two differential equations, one for the length scale and one for the kn transport of energy. The shear stress is then calculated based on the Boussinesq eddy viscosity hypothesis. The length scale is obtained through a second differential equation for the transport of τ where τ is assumed to be of the form $q^m \ell^n$. A two equation model which is applicable for recirculating flow should be one of the choices. The model used by Runchal (28) for the flow in a duct with re-circulation is of this type. Yet, the constants involved here remains to be checked through experiments.

...

CHAPTER 6

CONCLUSION

6.1 Conclusion from Present Study

The study being more of an experimental type of an inclined jet and a stream, the conclusions are more qualitative than quantitative. It is particularly so, as the local level of turbulence reached is very high.

On the whole it can be seen that the jet which is opposing the main flow develops higher intensities of turbulence. Though the jets studied are inclined to the stream, the flow field develop in a fashion similar to that of a thick lipped zero degree wall jet of corresponding velocities of u_j / u_s, although the magnitude of the terms are more for the inclined jet.

The lateral pressure gradient which resulted along with the reattachment bubble makes the solution, semi-empirical or analytical, impossible using boundary layer simplifications. The re-circulating zone which gives rise to a zone of intense turbulence production along its edge because of the high values of shear involved. Thus the velocity maximum and the high velocity gradient which existed at the re-attaching zone gets reduced considerably by x/b of 48. At and after x/b of 48, the velocity profile is

more or less uniform. The mean velocity distribution close to the wall is logarithmic right from x/b of 40. This could be attributed to the large turbulence present in the boundary layer itself.

Regarding the aspect of energy dissipation it is found that the 127° injection is more efficient than the 90° as expected. The energy dissipated is between 2 to 3.5 percent of the original stream. It is to be noted that this 2.5 percent is over and above the dissipation of the energy added to the stream in the form of a jet. Yet the study being in a limited range of u_j/u_s range of 0.5 to 1.05, a definite conclusion that whatever energy added is dissipated cannot be made for ranges of u_j/u_s above 1.05. Although, the combined flow system may not be encouraging as a primary energy dissipation device, it may be used for the stabilisation of jump location.

The turbulent terms of interest show that $\overline{u'^2}$ is always the highest of the three fluctuating quantities and $\overline{w'^2}$ is the least. A point of interest which had been noticed earlier is that the point of zero shear stress does not coincide with the point of zero velocity gradient. For a weak wall jet it has been observed that the point of zero shear stress lies nearer to the velocity maximum than the wall unlike that of

a wall jet. The turbulent energy balance shows that the production and diffusion terms are more or less matched and the advection and dissipation terms are much smaller than the first two. A generalisation, as yet, cannot be done as the conclusion is arrived on the basis of the measured dissipation term. The accuracy of the dissipation term obtained through time differentiation of u' has been doubted recently (16,19).

The turbulence models of turbulence of Prandtl and Prandtl-Kolomogorov which are dependent on some form of an algebraic equation for mixing length cannot be applied as is evident from Fig. 5.22 and 5.23. The Fig. (5.24) show the Bradshaw parameter 'a' for different x-stations. The Bradshaw model cannot be applied before x/b of 48. The model applicable should take into account, the lateral pressure gradient and the difference in location of the zero shear stress point and zero velocity gradient location. Through extensive measurements it has been possible to delineate the different turbulence characteristics, but so far we have not been able to develop a generalised turbulence model for this type of flows.

6.2 Scope of Extension of Present Study

The first area of extension can be development of a generalized analytical expression. May be it is necessary to extend the present study for a larger range of velocity ratio of u_j/u_s for this purpose. Also, an upper limit which must exist for the energy dissipation can be located. That is, after some range of velocity ratio of u_j/u_s the dissipation achieved may be negative when compared to the energy of the main stream.

Also, triple and quadruple correlation measurements and spectra measurement can be done for the present case so as to give a more complete picture of turbulence structure. With the existing data over the limited range an attempt can be made to formulate a working model of turbulence. Yet, for testing such a model a larger volume of experimental data over a larger range is required.

...

APPENDIX

Equations of continuity for turbulent flow are:-

$$\frac{\partial \bar{u}}{\partial x} + \frac{\partial \bar{v}}{\partial y} + \frac{\partial \bar{w}}{\partial z} = 0 \qquad (1)$$

$$\frac{\partial u'}{\partial x} + \frac{\partial v'}{\partial y} + \frac{\partial w'}{\partial z} = 0 \qquad (2)$$

Equation of motion in the x-direction is

$$\frac{D}{Dt}(\bar{u}+u') = -\frac{1}{\rho}\frac{\partial}{\partial x}(\bar{p}+p') + \frac{\mu}{\rho}\nabla^2(\bar{u}+u')$$

which after taking time averages simplifies to:-

$$\bar{u}\frac{\partial \bar{u}}{\partial x} + \bar{v}\frac{\partial \bar{u}}{\partial y} + \bar{w}\frac{\partial \bar{u}}{\partial z} + \overline{u'\frac{\partial u'}{\partial x}} + \overline{v'\frac{\partial u'}{\partial y}} + \overline{w'\frac{\partial u'}{\partial z}}$$

$$= -\frac{1}{\rho}\frac{\partial \bar{p}}{\partial x} + \frac{\mu}{\rho}\left(\frac{\partial^2 \bar{u}}{\partial x^2} + \frac{\partial^2 \bar{u}}{\partial y^2} + \frac{\partial^2 \bar{u}}{\partial z^2}\right) \qquad (3)$$

The L.H.S. of equation (3) can be re-arranged in the following form of which the last two groups of terms reduce to zero

$$\frac{\partial}{\partial x}(\overline{u^2}) + \frac{\partial}{\partial y}(\overline{uv}) + \frac{\partial}{\partial z}(\overline{uw}) + \frac{\partial}{\partial x}\overline{u'^2} + \frac{\partial}{\partial y}(\overline{u'v'}) + \frac{\partial}{\partial z}(\overline{u'w'})$$

$$-\bar{u}\left(\frac{\partial \bar{u}}{\partial x} + \frac{\partial \bar{v}}{\partial y} + \frac{\partial \bar{w}}{\partial z}\right) - \left(\overline{u'\frac{\partial u'}{\partial x}} + \overline{u'\frac{\partial v'}{\partial y}} + \overline{u'\frac{\partial w}{\partial z}}\right)$$

Hence eqn. (3) can be rewritten as

$$\frac{\partial}{\partial x}\bar{u}^2 + \frac{\partial}{\partial y}\bar{u}\bar{v} + \frac{\partial}{\partial z}\bar{u}\bar{w} + \frac{\partial}{\partial x}\overline{u'^2} + \frac{\partial}{\partial y}\overline{u'v'} + \frac{\partial}{\partial z}\overline{u'w'}$$

$$= -\frac{1}{\rho}\frac{\partial \bar{p}}{\partial x} + \frac{\mu}{\rho}\left(\frac{\partial^2 \bar{u}}{\partial x^2} + \frac{\partial^2 \bar{u}}{\partial y^2} + \frac{\partial^2 \bar{u}}{\partial z^2}\right)$$

Similarly y and z components of equation of motion can be written.

All these equation can be summarised into tensor notations

$$\frac{\partial}{\partial x_j}(\bar{u}_i \bar{u}_j) + \frac{\partial}{\partial x_j}(\overline{u_i' u_j'}) = -\frac{1}{\rho}\frac{\partial \bar{p}}{\partial x_i} + \frac{\mu}{\rho}\frac{\partial \bar{u}_i}{\partial x_j \partial x_j} \qquad (4)$$

Energy Equation:

The energy equation can be derived from the momentum equations by multiplying the momentum equation with the corresponding velocity and adding all the three equations of eqn. (4). The equation thus derived can be grouped into work energy equation for mean flow and for turbulence. The work energy equation for mean flow is

$$\bar{u}_j \frac{\partial}{\partial x_j}\left(\frac{V_t^2}{2}\right) + \bar{u}_i \frac{\partial}{\partial x_j}(\overline{u_i' u_j'}) = -\frac{\bar{u}_i}{\rho}\frac{\partial \bar{p}}{\partial x_i} + \frac{\mu}{\rho}\bar{u}_i \frac{\partial^2 \bar{u}_i}{\partial x_j \partial x_j} \qquad (5)$$

and for turbulent fluctuations

$$\bar{u}_j \frac{\partial}{\partial x_j}\left(\overline{\frac{V'^2}{2}}\right) + \overline{u_j' \frac{\partial}{\partial x_j}\frac{V'^2}{2}} + \overline{u_i' u_j'}\frac{\partial \bar{u}_i}{\partial x_j}$$

$$= -\overline{\frac{u_i'}{\rho}\frac{\partial p'}{\partial x_i}} + \frac{\mu}{\rho}\overline{u_i' \frac{\partial^2 u_i'}{\partial x_j \partial x_j}} \qquad (6)$$

where

$$V_t^2 = \bar{u}^2 + \bar{v}^2 + \bar{w}^2$$

$$q'^2 = u'^2 + v'^2 + w'^2$$

Integrating over the control volume, momentum eqn (4) becomes

$$\int_V \frac{\partial}{\partial x_j}(\bar{u}_i \bar{u}_j)dV + \int_V \frac{\partial}{\partial x_j}(\overline{u'_i u'_j})dV$$

$$= -\frac{1}{\rho}\int_V \frac{\partial \bar{p}}{\partial x_i} dV + \frac{\mu}{\rho}\int_V \frac{\partial^2 \bar{u}_i}{\partial x_j \partial x_j} dV \qquad (7)$$

Reducing to surface integrals by Gauss's theorem

$$\int_S \bar{u}_i \bar{u}_j \frac{\partial x_i}{\partial n} dS + \int_S \overline{u'_i u'_j} \frac{\partial x_i}{\partial n} dS$$

$$= -\frac{1}{\rho}\int_S \bar{p} \frac{\partial x_i}{\partial n} dS + \int \frac{\mu}{\rho} \frac{\partial \bar{u}_i}{\partial x_j} \frac{\partial x_i}{\partial n} dS \qquad (8)$$

When applied to a control volume in the form of a parallelepiped, (the test section of the wind tunnel), the terms of equations (8) gets simplified as follows:

$$\int_S \bar{u}_i \bar{u}_j \frac{\partial x_i}{\partial n} dS = \int_0^d \bar{u}^2 \, dy$$

$$\int_S \overline{u'_i u'_j} \frac{\partial x_i}{\partial n} dS = \int_0^d \overline{u'^2} \, dy$$

$$\int_S \frac{\bar{p}}{\rho} \frac{\partial x_1}{\partial n}\, ds = \int_0^d \frac{\bar{p}}{\rho}\, dy$$

$$\int_S \frac{\mu}{\rho} \frac{\partial \bar{u}_1}{\partial x_j} \frac{\partial x_1}{\partial n}\, ds = \int_0^x \frac{\mu}{\rho} \frac{\partial \bar{u}}{\partial y}\, dx$$

$$\text{and} \int_0^d \frac{\mu}{\rho} \frac{\partial u}{\partial x}\, dy$$

Similarly y-direction equation can be observed. Work energy equation for the control volume is

$$\int_V \bar{u_j} \frac{\partial}{\partial x_j} \left(\frac{V_k^2}{2}\right) dV + \int_V \bar{u_i} \frac{\partial}{\partial x_j} (\overline{u_i' u_j'}) dV$$

$$= -\int \frac{\bar{u_i}}{\rho} \frac{\partial \bar{p}}{\partial x_i} dV + \frac{\mu}{\rho} \int \bar{u}_i \frac{\partial^2 \bar{u_i}}{\partial x_j \partial x_j} \qquad (9)$$

Taking term by term

$$\int_V \bar{u_j} \frac{\partial}{\partial x_j} \left(\frac{V_k^2}{2}\right) dV = \int_V \frac{\partial}{\partial x_j} \left(u_j \frac{V_k^2}{2}\right) dV - \int_V \frac{V_k^2}{2} \frac{\partial u_j}{\partial x_j}\, dV$$

$$= \int_S \bar{u_j} \frac{\overline{V_k^2}}{2} \frac{\partial x_j}{\partial n}\, ds.$$

$$\int_V \bar{u_i} \frac{\partial}{\partial x_j} (\overline{u_i' u_j'}) dV = \int_V \frac{\partial}{\partial x_j} (\bar{u_i}\, \overline{u_i' u_j'}) dV - \int_V \overline{u_i' u_j'} \frac{\partial}{\partial x_j} (\bar{u_i}) dV$$

$$= -\int_S \bar{u}_i \, \overline{u_i' u_j'} \frac{\partial x_i}{\partial n} \, dS - \int_V \overline{u_i' u_j'} \frac{\partial \bar{u}_i}{\partial x_j} \, dV.$$

$$\frac{1}{\rho} \int \bar{u}_i \frac{\partial \bar{p}}{\partial x_i} \, dV = \frac{1}{\rho} \left(\int_V \frac{\partial}{\partial x_i} (\bar{p} \, \bar{u}_i) dV - \int_V \bar{p} \frac{\partial \bar{u}_i}{\partial x_i} \, dV \right)$$

$$= \frac{1}{\rho} \int_S \bar{p} \, \bar{u}_i \frac{\partial x_i}{\partial n} \, dS.$$

$$\int_V \frac{\mu}{\rho} \bar{u}_i \frac{\partial^2 \bar{u}_i}{\partial x_j \partial x_j} \, dV = \int_V \frac{\mu}{\rho} \frac{\partial}{\partial x_j} \left[\left(\frac{\partial \bar{u}_i}{\partial x_j} + \frac{\partial \bar{u}_j}{\partial x_i} \right) \bar{u}_i \right] dV - \int_V \frac{\mu}{\rho} \left(\frac{\partial \bar{u}_i}{\partial x_j} \right)^2 dV$$

$$- \int_V \frac{\mu}{\rho} \left(\frac{\partial \bar{u}_i}{\partial x_j} \frac{\partial \bar{u}_j}{\partial x_i} + \frac{\bar{u}_i \partial^2 \bar{u}_j}{\partial x_i \partial x_j} \right) dV$$

$$= \int_S \frac{\mu}{\rho} \left(\frac{\partial \bar{u}_i}{\partial x_j} + \frac{\partial \bar{u}_j}{\partial x_i} \right) \bar{u}_i \frac{\partial}{\partial n} dS - \int_V \frac{\mu}{\rho} \left(\frac{\partial \bar{u}_i}{\partial x_j} + \frac{\partial \bar{u}_j}{\partial x_i} \right) \frac{\partial \bar{u}_i}{\partial x_j} \, dV$$

Substituting all the terms in the work energy equation for mean flow (9)

$$\int_S \bar{u}_j \frac{\rho V_\infty^2}{2} \frac{\partial x_j}{\partial n} \, dS + \int_S \rho \, \bar{u}_i \, \overline{u_i' u_j'} \frac{\partial x_j}{\partial n} \, dS - \int_V \rho \, \overline{u_i' u_j'} \frac{\partial \bar{u}_i}{\partial x_j} \, dV$$

$$= - \int_S \bar{p} \, \bar{u}_i \frac{\partial x_i}{\partial n} \, dS + \int_S \mu \left(\frac{\partial \bar{u}_i}{\partial x_j} + \frac{\partial \bar{u}_j}{\partial x_i} \right) \bar{u}_i \frac{\partial x_j}{\partial n} \, dS$$

$$- \int_V \mu \left(\frac{\partial \bar{u}_i}{\partial x} + \frac{\partial \bar{u}_j}{\partial x_i} \right) \frac{\partial \bar{u}_i}{\partial x_j} \, dV \qquad (10)$$

Applying this eqn. (10) to the control volume, the terms simplify as given below

$$\int_S \bar{u}_j \frac{\rho V_k^2}{2} \frac{\partial x_i}{\partial n} ds = \int_0^d u \frac{\rho V_k^2}{2} dy$$

$$\int_S \rho \bar{u}_i \overline{u_i' u_j'} \frac{\partial x_i}{\partial n} ds = \int \rho \bar{u} \overline{u'^2} dy + \int_0^d \rho \bar{v} \overline{u'v'} dy$$

$$\int_V \rho \overline{u_i' u_j'} \frac{\partial \bar{u}_i}{\partial x_j} dV = \int_0^d \int_0^x \left(\frac{\partial \bar{u}}{\partial x} \overline{u'^2} + \frac{\partial \bar{u}}{\partial y} \overline{u'v'} + \overline{u'v'} \frac{\partial \bar{v}}{\partial x} + \overline{v'^2} \frac{\partial \bar{v}}{\partial y} \right) dx dy$$

$$= \rho \int_0^d \int_0^x \left[\left(\frac{\partial \bar{u}}{\partial y} + \frac{\partial \bar{v}}{\partial x} \right) \overline{u'v'} + (\overline{u'^2} - \overline{v'^2}) \frac{\partial \bar{u}}{\partial x} \right] dx dy$$

$$\int_S \bar{p} \bar{u}_i \frac{\partial x_i}{\partial n} ds = \int_0^d \bar{u} \bar{p} dy$$

$$\int_S \mu \left(\frac{\partial \bar{u}_i}{\partial x_j} + \frac{\partial \bar{u}_j}{\partial x_i} \right) \bar{u}_i \frac{\partial x_j}{\partial n} ds$$

$$= \int_0^d \left[\mu \left(2\bar{u} \frac{\partial \bar{u}}{\partial x} + \left(\frac{\partial \bar{v}}{\partial x} + \frac{\partial \bar{u}}{\partial y} \right) \bar{v} \right) \right] dy$$

$$\int_V \mu \left(\frac{\partial \bar{u}_i}{\partial x_j} + \frac{\partial \bar{u}_j}{\partial x_i} \right) \frac{\partial \bar{u}_i}{\partial x_j} dV$$

$$= \int_0^d \int_0^x \mu \left(\frac{\partial \bar{u}_i}{\partial x_j} + \frac{\partial \bar{u}_j}{\partial x_i} \right) \frac{\partial \bar{u}_i}{\partial x_j} dx dy$$

$$= \mu \int_0^x \int_0^d \frac{\partial \bar{u}}{\partial x} \left(\frac{\partial \bar{u}}{\partial x} + \frac{\partial \bar{u}}{\partial x} \right) + \left(\frac{\partial \bar{u}}{\partial y} + \frac{\partial \bar{v}}{\partial x} \right) \frac{\partial \bar{u}}{\partial y} +$$

$$\left(\frac{\partial \bar{v}}{\partial x} + \frac{\partial \bar{u}}{\partial y} \right) + \left(2 \frac{\partial \bar{v}}{\partial y} + \frac{\partial \bar{v}}{\partial y} \right) dx dy$$

$$= \mu \int_0^d \int_0^x \left[2 \left(\frac{\partial \bar{u}}{\partial x} \right)^2 + 2 \left(\frac{\partial \bar{v}}{\partial y} \right)^2 + \left(\frac{\partial \bar{u}}{\partial y} + \frac{\partial \bar{v}}{\partial x} \right)^2 \right] dx dy$$

$$= \mu \int_0^d \int_0^x \left[4 \left(\frac{\partial \bar{u}}{\partial x} \right)^2 + \left(\frac{\partial \bar{u}}{\partial y} + \frac{\partial \bar{v}}{\partial x} \right)^2 \right] dx dy$$

The Energy Equation for Secondary Flow:

$$\bar{u}_j \frac{\partial}{\partial x_j} \left(\frac{\rho \overline{V'^2}}{2} \right) + \overline{u_j' \frac{\partial}{\partial x_j} \left(\rho \frac{V'^2}{2} \right)} + \rho \overline{u_i' u_j'} \frac{\partial \bar{u}_i}{\partial x_j}$$

$$= - \overline{u_i' \frac{\partial p'}{\partial x_i}} + \mu \overline{u_i' \frac{\partial^2 u_i'}{\partial x_j \partial x_j}}$$

Integrating it over control volume

$$\int_V \bar{u}_j \frac{\partial}{\partial x_j} \left(\frac{\rho \overline{V'^2}}{2} \right) dV + \int_V \overline{u_j' \frac{\partial}{\partial x_j} \left(\frac{\rho V'^2}{2} \right)} dV + \int_V \rho \overline{u_i' u_j'} \frac{\partial \bar{u}_i}{\partial x_j} dV$$

$$= \int_V \overline{u_i' \frac{\partial p'}{\partial x_i}} dV + \int_V \mu \overline{\frac{u_i' \partial^2 u_i'}{\partial x_j \partial x_j}} dV \qquad (11)$$

$$\int_V \bar{u}_j \frac{\partial}{\partial x_j} \left(\frac{\rho \overline{V'^2}}{2} \right) dV = \int_V \frac{\partial}{\partial x_j} \left(\bar{u}_j \frac{\rho \overline{V'^2}}{2} \right) dV - \int_V \frac{\rho \overline{V'^2}}{2} \frac{\partial \bar{u}_i}{\partial x_i} dV.$$

$$= \int_S \bar{u}_j \frac{\rho \overline{V'^2}}{2} \frac{\partial x_j}{\partial n} dS$$

$$\int_V \overline{u_j' \frac{\partial}{\partial x_j}\left(\frac{\rho v'^2}{2}\right)} dV = \int_S \overline{u_j' \frac{\rho v'^2}{2} \frac{dx_1}{dn}} ds$$

$$\int_V \rho \overline{u_i' u_j'} \frac{\partial \bar{u}_i}{\partial x_j} dV = \int_V \rho \overline{u_i' u_j'} \frac{\partial \bar{u}}{\partial x_j} dV$$

$$\int_V \overline{u_i' \frac{\partial p'}{\partial x_i}} dV = \int_S \overline{u_i' p_i'} \frac{dx_i}{dn} ds$$

$$\int \mu \overline{\frac{u_i' \partial^2 u_i'}{\partial x_j \partial x_j}} = \int_S \mu \overline{\left(\frac{\partial u_i'}{\partial x_j} + \frac{\partial u_j'}{\partial x_i}\right) u_i'} \frac{dx_1}{dn} ds$$

$$- \int \mu \overline{\left(\frac{\partial u_i'}{\partial x_j} + \frac{\partial u_j'}{\partial x_i}\right) \frac{\partial u_i'}{\partial x_j}} dV.$$

Substituting all the equations, the work energy equation becomes

$$\int_S \overline{\frac{\rho v'^2}{2}} \bar{u}_j \frac{dx_1}{dn} ds + \int_S \overline{\frac{\rho v'^2}{2} u_j'} \frac{dx_1}{dn} ds + \int_V \rho \overline{u_i' u_j'} \frac{\partial \bar{u}_i}{\partial x_j} dV$$

$$= - \int_S \overline{p' u_i'} \frac{dx_i}{dn} ds + \int_S \mu \overline{\left(\frac{\partial u_i'}{\partial x_j} + \frac{\partial u_j'}{\partial x_i}\right) u_i} \frac{dx_1}{dn} ds$$

$$- \int_V \mu \overline{\left(\frac{\partial u_i'}{\partial x_j} + \frac{\partial u_j'}{\partial x_i}\right) \frac{\partial u_i'}{\partial x_j}} dV$$

$$\int_S \rho \overline{\frac{v'^2}{2}} \bar{u}_j \frac{dx_1}{dn} ds = \int_0^d \rho \overline{\frac{v'^2}{2}} \bar{u} dy$$

$$\int_S \rho \overline{\frac{v'^2}{2} u_j'} \frac{dx_1}{dn} ds = \int_0^d \rho \overline{\frac{v'^2}{2} u'} dy$$

$$\int_V \rho \overline{u_i' u_j'} \frac{\partial \bar{u}_i}{\partial x_j} dV = \int_0^d \int_0^x \rho [\overline{u'v'}\left(\frac{\partial \bar{u}}{\partial y} + \frac{\partial \bar{v}}{\partial x}\right) + (\overline{u'^2} - \overline{v'^2}) \frac{\partial \bar{u}}{\partial x}] dx dy$$

$$\int_S \overline{p' u'} \frac{\partial x_1}{\partial n} dS = - \int_0^d \overline{p' u'} dy$$

$$\int_S \mu \overline{\left(\frac{\partial u_i'}{\partial x_j} + \frac{\partial u_j'}{\partial x_i}\right) u_i'} \frac{\partial x_j}{\partial n} dS$$

$$= \mu \int_0^d [\overline{\left(\frac{\partial u'}{\partial x} + \frac{\partial u'}{\partial x}\right) u'} + \overline{\left(\frac{\partial v'}{\partial x} + \frac{\partial u'}{\partial y}\right) v'}] dy$$

$$= \mu \int_0^d [\frac{\partial \overline{u'^2}}{\partial x} + \frac{\partial}{\partial y} \overline{u'v'} + \overline{u' \frac{\partial u'}{\partial x}} + \overline{v' \frac{\partial v'}{\partial x}}] dy$$

$$= \mu \int_0^d [\frac{\partial}{\partial x} \overline{u'^2} + \frac{\partial}{\partial x} \left(\frac{\overline{u'^2 + v'^2}}{2} \right) + \frac{\partial}{\partial y} (\overline{u'v'})] dy$$

$$= \mu \int_0^d [\frac{\partial}{\partial x} \overline{u'^2} + \frac{\partial}{\partial x} \left(\frac{\overline{v'^2}}{2} \right) + \frac{\partial}{\partial y} (\overline{u'v'})] dy$$

All these terms are positive of the outer normal to the area coincides with the positive co-ordinate direction.

...

BIBLIOGRAPHY

1. Bakke, P. 1957 : An experimental investigation of a wall jet. Journal of Fluid Mechanics, Vol. 2, p.467.

2. Bloor, M.S. 1964 : The transition to turbulence in the wake of a circular cylinder. Journal of Fluid Mechanics, Vol. 19, p. 290.

3. Bourque, C. and Newman, B.G. 1960 : Reattachment of a two dimensional incompressible jet to an adjacent flat plate. The Aeronautical quarterly, Vol. XI, p. 201.

4. Bradbury, L.J.S., 1965 : The Structure of a self preserving plane jet. Journal of Fluid Mechanics, Vol. 23, p. 31.

5. Bradshaw, P, Ferris, D.H. and Atwell, N.P. 1967 : Calculation of boundary layer using the turbulent energy method. Journal of Fluid Mechanics, Vol. 28, p. 593.

6. Chaturvedi, M.C. 1963 : Flow characteristics of axi-symmetric expansions. Journal of Hydraulics Division, Proc. ASCE, Vol. 89, p. 61.

7. Dodd, AS reported in 3

8. Krich, J. 1953 : Penetration and deflection of jets obliquo to a general stream. Journal of Aeronautical Science, p. 99.

9. Eskinazi, S. and Kruka, V. 1964 : The wall jet in a moving stream. Journal of Fluid Mechanics, Vol. 20, p. 555.

10. Forthmann, 1936 : Turbulent jet expansion, NACA TM No. 789.

11. Gartshore, I.S. and Newman, B.G. 1969 : The turbulent wall jet in an arbitrary pressure gradient. The Aeronautical Quarterly, Vol. 20 p. 25.

12. Glauert, M.B. 1956 : The wall jet. Journal of Fluid Mechanics, Vol. 1, Part 6, p. 625.

13. Goldstein, M.E. and Braun, W. 1969 : Injection of an attached inviscid jet at an oblique angle to a moving stream. NACA T.N. D 5501

14. Gosman, A.D. et al 1969 : Heat and Mass transfer in re-circulating flows. Academic Press.

15. Hanjalic and Launder, B.E. 1972 : A Reynolds Stress model of turbulence and its application to thin shear flows. Journal of Fluid Mechanics, 52, p. 609.

16. Irwin, H.P.A.H., 1973 : Measurements in a self pressuring plane wall jet in a positive pressure gradient.

Journal of Fluid Mechanics, Vol. 61 , p. 33.

17. Jacob et al, 1950 : Trans. ASME. p. 839, as reported in 30.

18. Hacker, S.C. and Whitelaw, J.H. 1968 : Some properties of the turbulent wall jet in a moving stream. Journal of Applied Mechanics, Vol. 35, Trans. ASME, Series E, p. 641.

19. Hacker, S.C. and Whitelaw, J.H. 1970 : The turbulence characteristics of two dimensional wall jet and wall Wake flows. Journal of Applied Mechanics, Vol. 38 Trans. ASME, Series E. p.239

20. Launder, B.E. and Spalding, D.B. 1971 : Turbulence models and their applications to the prediction of internal flows. Imperial College of Science and Technology, TM|TN|A|18.

21. Launder, B.E. and Spalding, D.B. 1972 : Mathematical models of turbulence - Academic Press.

22. Patankar, and Spalding, 1970 : Heat and Mass Transfer in Boundary Layer. Intertext Books.

23. Patel, V.C. 1965 : Calibration of the Preston tube and limitation on its use in a pressure gradient. Journal of Fluid Mechanics, Vol. 23, p. 185.

24. Phillips. As reported in 18.

25. Rouse, H. (Ed). 1959 : Advanced Mechanics of Fluids, John Wiley and Sons.

26. Rouse, H. Sino, T.T. and Nagaratnam, 1959 : Turbulence characteristics of a Hydraulic Jump. Trans. ASCE, Vol. 124, p. 926.

27. Rouse, H. 1960 : Repartition del' energie dans des zones de decollement. LA Houille Blanche No.3.

28. Runchal, A.K. 1969 : Predictions and experimental results for flow past a sudden enlargement in a circular pipe. Imperial College, Mech. Engg. Deptt. Rep. M F|TN|A|19.

29. Schwarz, W.H. and Cosart, W.P. 1961 : The two dimensional turbulent wall jet. Journal of Fluid Mechanics, Vol..10, Part 4, p. 31.

30. Sigalla, A. 1958 : Experimental data on a turbulent wall jets. Aircraft Engineering, p. 131.

31. Townsend, A, A.A. 1956, 1976 : The structure of turbulent shear flow, Cambridge.

32. Wygnaski and Newman, B.G. 1968 : The re-attachment of an inclined two dimensional wall jet to a flat surface in streaming flow. C.A.S.I. Transactions, Vol. 1, No.1.

33. Zerbe and Selna, 1946 : An empirical equation for the coefficient of heat transfer to a flat surface from a plane heated airjet directed tangentially to the surface, NACA, T.N. 1070.